# PREPARATION AND CHARACTERIZATION OF METAL SOAP NANOFILMS

**A Thesis Submitted to**
**the Graduate School of Engineering and Sciences of**
**İzmir Institute of Technology**
**in Partial Fulfillment of the Requirement for the Degree of**

**MASTER OF SCIENCE**

**in Chemical Engineering**

**by**
**Serdar ÖZTÜRK**

**July 2005**
**İZMİR**

We approve the thesis of **Serdar ÖZTÜRK**

**Date of Signature**

.....
**Prof.Dr. Devrim BALKÖSE**
Supervisor
Department of Chemical Engineering
İzmir Institute of Technology

**22 July 2005**

.....
**Assoc.Prof.Dr. Salih OKUR**
Co-Supervisor
Department of Physics
İzmir Institute of Technology

**22 July 2005**

.....
**Assoc.Prof.Dr. Serdar ÖZÇELİK**
Department of Chemistry
İzmir Institute of Technology

**22 July 2005**

.....
**Assoc.Prof.Dr. Günseli ÖZDEMİR**
Department of Chemical Engineering
Ege University

**22 July 2005**

.....
**Assist.Prof.Dr. Oğuz BAYRAKTAR**
Department of Chemical Engineering
İzmir Institute of Technology

**22 July 2005**

.....
**Prof.Dr. Devrim BALKÖSE**
Head of Department
İzmir Institute of Technology

.....
**Assoc.Prof. Dr. Semahat ÖZDEMİR**
Head of Graduate School

# ACKNOWLEDGEMENTS

This study is financially supported by a grant for major research project "Process development and industrial applications of metal soaps" from Turkish State Planning Organization (DPT), Project No: 2002K 120390. This support is gratefully acknowledged. I would like to thank and express my gratitude to Prof.Dr.Devrim Balköse and Assoc.Prof.Dr.Salih Okur for their supervision, guidance and support rendered at the all stages of my study. I am also grateful to Prof.Dr.Semra Ülkü for her permission and support to use Fourier Transform Infrared Spectrophotometer.

I am also indebted to Prof.Dr.Junzo Umemura from Kyoto university and Prof.Dr.Mike Petty from Durham university for their valuable technical suggestions and recommendations during the course of this research.

I wish to thank Hülya Eser for her help, encouragement and friendship throughout this project.

My thanks are also due to laboratory technician Şerife Şahin for laboratory works, Ayaz Allahverdiev for FTIR analysis and Filiz Özmıhçı for DSC analysis. I would like to express my thanks for the experts of IZTECH Center For Material Research (CMR).

I also appreciate deeply İlker Polatoğlu, Mert Atilhan, research assistants Kağan Oğuz and Savaş Ulucan in Physics Department, Mehmet Gönen, Yılmaz Yürekli and all other friends for their discussions, friendship and encouragements.

Finally, it is a pleasure to thank to my family and my friends for their help, appreciations and understandings throughout this study.

# ABSTRACT

In this study, the production of metal (zinc and calcium) stearate nanofilms by Langmuir-Blodgett (LB) film deposition process and their structural and electrical characterizations were investigated. The interaction of stearic acid monolayer with calcium, zinc cations as functions of pH, temperature, concentration of metal cation in the subphase and barrier speed was examined in detail. The effects of transfer surface pressure, the dipping speed, drying period, pH, concentration of metal cations in the subphase and temperature in the deposition of metal stearates onto glass substrates were optimized.

Metal stearate LB films were prepared and characterized by X Ray Diffraction technique. It was revealed that the zinc stearate arrangement may be identified as under the orthorhombic (R) subcell with chain tilt angle of $31^{o}$, which was confirmed by IR spectrum of zinc stearate. Atomic Force Microscopy and Scanning Electron Microscopy images showed that surface roughness on glass substrates was decreased by firstly chrome coating and then silver coating. Zinc stearate coated surfaces have large crystal size around 90 nm in agreement with XRD calculation and contained grains and defects. The results of LB film deposition processes, structural characterization of LB films and the water vapour adsorption experiments presented that $ZnSt_2$ LB films were easily formed and have good ordered structure in comparison to $CaSt_2$ LB films. Therefore $ZnSt_2$ LB films were chosen to study humidity sensor characteristics.

Conductivity of $ZnSt_2$ LB films was easily affected from environmental conditions. No hysteresis during adsorption and desorption of water vapor on conductivity-voltage measurements was observed for zinc stearate LB film.

As a result, zinc stearate LB films can be used as humidity sensor. By measuring conductivity in an humid atmosphere, humidity could be determined.

# ÖZET

Bu çalışmada, metal (çinko ve kalsiyum) stearat nanofilmlerinin Langmuir-Blodgett film tekniği ile üretilmesi, yapısal ve elektriksel karekterizasyonu yapılmıştır. Stearik asit tek katmanının kalsiyum ve çinko katyonları ile etkileşimi, pH, sıcaklık, altfazdaki metal katyon derişimi ve bariyer hızına bağlı olarak araştırılmıştır. Taşıyıcı yüzeylere metal stearat aktarılmasındaki etkin faktörler olan transfer yüzey basıncı, daldırma hızı, kurutma zamanı, pH, sıcaklık ve alt fazdaki metal katyon derişimi optimize edilmiştir.

Metal stearat LB filmleri hazırlanmış ve X-ışını kırınımı ile karakterize edilmiştir. Diyagramlar çinko stearatın ortorombik kristal yapıda olduğunu ve çinko stearat moleküllerinin hidrokarbon zincirlerinin $31^{o}$ sapma açısı yaptığını ortaya koymuştur. IR spektroskopisi ile de bunu desteklemektedir. Atomik kuvvet mikroskopisi ve Taramalı elektron microskopisi görüntüleri, cama ait yüzey pürüzlülüğünün ilk önce krom daha sonra gümüş kaplama yoluyla azaltıldığnı göstermiştir. Çinko stearat kaplı yüzeylerde gözlenen 90 nm büyüklüğündeki kristaller X-ışını kırınım diyagramlarından hesaplanan kristal büyüklüğüne yakındır. Bu yüzeyler topluluklar ve kusurlar içermektedir. $ZnSt_2$ LB filmlerinin $CaSt_2$ LB filmlerine göre kolayca ve düzenli bir yapıda üretilebildiğini LB film kaplama, karekterizasyon ve su buharı adsorplama deney sonuçları göstermiştir. Bu yüzden $ZnSt_2$ LB filmleri nem sensörü olarak karekteristikleri incelenmek üzere seçilmiştir.

Çinko stearat filmlerinde yapılan ölçümler, iletkenlik değerlerinin farklı çevre koşullarından kolayca etkilendiğini göstermiştir. Su buharı adsorpsiyonu ile iletkenliğin arttığı ve desorpsiyonu ile azaldığı gözlenmiş, adsorpsiyon ve desorpsiyon ile iletkenlikte histeriz gözlenmemiştir.

Sonuç olarak, çinko stearat LB filmlerinin nem sensörü olarak kullanılabileceği anlaşılmıştır. Nemli bir ortamda bilinen bir voltaj değeri uygulayarak ölçülen iletkenlik değerinden ortam nemi bulunabilecektir.

# TABLE OF CONTENTS

# LIST OF FIGURES

# LIST OF TABLES

# CHAPTER 1

# INTRODUCTION

Thin organic films which have a thickness of a few nanometers are used in many practical and commercial applications such as sensors, detectors, displays and electronic circuit components. A sophisticated thin film deposition technique can enable synthesis of organic molecules with desired structure and functionality almost without limitations. Hence, the production of electrically, optically and biologically active components on a nanometer scale can be achieved (Kondrashkina et al. 1996).

An organic thin film can be deposited on a solid substrate by various techniques such as thermal evaporation, sputtering, molecular beam epitaxy, adsorption from solution, self-assembly, Langmuir-Blodgett (LB) technique, etc. Among these, LB technique is one of the most promising deposition methods. In this study, LB film deposition process is chosen to prepare thin films of metal stearates as it offers the precise control of the monolayer thickness and homogeneous deposition of the monolayer over large areas. The monolayers can be deposited to almost any kind of solid substrate. It is possible to make multilayer structures with varying layer composition at desired molecular architecture (Ulman 1991).

Researchers from distinct fields such as physics, chemistry, electronic engineering, and biology, are interested in more and more in areas such as sensors and displays. These scientists are often dedicated to designing and synthesising novel functional molecular materials or device structures focused towards a particular application, but all depend to some extent on the methods available for processing the active sensing ingredient (the molecular material) into a usable form (the thin film). Hence, deposition processes such as the LB method, which offer control over the arrangement of molecules to form a thin film, are valuable for organic materials research area. In this point of view, Kusano tried to use cellulose LB films as humidity sensor and Petty showed the effect of humidity on electrical measurements. (Kusano et al. 1996, Petty 1996)

The LB technique is currently employed to fabricate organized molecular layered structures of a variety of functionalized molecules. Long chain fatty acid/salts have been extensively studied with LB systems both as Langmuir monolayers as well as

LB multilayers (Pignataro et al. 1999). Stearic acid and divalent metal stearates are mostly studied subgroups of these chemical materials (Sakai et al. 2002). Various properties of monolayers and LB films of these compounds such as composition, morphology, molecular structure etc. are investigated by Bukreeva (Bukreeva et al. 2003).

Fatty acid salts, whose films are interested in this study, are also called metal soaps. They are fabricated by the reaction of alkaline, alkaline earth, or transition metals with saturated, unsaturated straight chain or branched aliphatic carboxylic acids with 8-22 carbon atoms. These solid compounds produced by several chemical reaction pathways are commercially important compounds and used as waterproofing agents, driers in paints or inks, stabilizers for plastics, components of greases, fungicides, fuel additives, catalysts etc. (Blachford 1982). In addition to above applications mentioned, a number of other uses of polyvalent(divalent and trivalent) metal soaps have been suggested. Now, current interest in low dimensional compounds has led to a number of investigations on the potential application of metal soaps in this area, particularly as Langmuir-Blodgett (LB) multilayers (Peng et al. 2001).

According to the related studies Avila conducted, the monolayers composition and properties, its stability and molecular packing arrangement in films are significantly affected by many factors such as pH, temperature, addition of ions and dipping and barrier speeds. Various methods have been applied to clarify the structure of LB films; composition, morphology and molecular orientation and conformation such as FTIR, AFM, XRD, etc. The inhomogeneities and the defects are readily fixed using these techniques (Avila et al. 1999, Sigiyama et al. 1998, Hansma et al. 1991).

In this study, the production and characterization of metal stearate LB films has been undertaken. The monolayer formation, composition and structure of films and their dependence on formation conditions will be concerned investigating stearic acid, zinc stearate and calcium stearate LB films. The production of stearic acid and metal soap films was done by providing the required conditions; pH, metal concentration, etc., Identity of the composition and structural organisation of films on bare and silver coated glass was done by FTIR, AFM, XRD, SEM-EDX methods. Then, zinc stearate thin film was applied to a region between silver electrodes to study their electrical characteristics in the room, nitrogen and humid atmosphere.

# CHAPTER 2

# THIN FILM DEPOSITION TECHNIQUES

Recently, great attention has been paid to 'nanotechnology'. In order to develop a 'nano-device' using the nano-technology, it is necessary to control the structure of the materials at atomic or molecular scale.

A thin film is a two dimensional condensed matter structure (liquid or solid) such that one of its linear dimensions is very small in comparison with the other two dimensions. Usually, one classifies thin films as being smaller than 1 micrometer and thick films larger than 1 micrometer (Wagendristel 1994).

There are several ways to deposit a thin organic film onto a solid substrate. Essentially, they can be grouped as dry process which is vacuum processed (sputtering, thermal evaporation, molecular beam epitaxy) and wet process (spin coating, adsorption from solution, electrodeposition, self-assembly and Langmuir-Blodgett (LB) technique (Peterson 1990). The fabrication of ultra-thin films by the wet process is strongly required because the running cost is less expensive than the dry process and because it can be carried out at room temperature and normal pressure.

Sputtering is a dry coating process whereby thermally emitted electrons collide with inert gas atoms, which accelerate toward and impact a negatively charged electrode that is a target of the coating material. The impacting ions dislodge atoms of the target material, which are in turn projected to and deposited on the substrate to form the coating. This technique is used for depositing metallic, ceramic and organic films. Sputtered films have better step coverage and uniformity than evaporated films. However, they have disorganized structures whose mechanical properties and residual stresses are sensitive to sputtering conditions. Problems also arise from the inert gas used in the sputtering process, which can become trapped in the film and cause inconsistencies in the mechanical properties of the films (Wagendristel 1994).

Another way to place a material in a thin film on a substrate is to evaporate them from a hot source. The evaporation system uses a vacuum chamber, which is pumped down from $10^{-6}$ to $10^{-7}$ Torr. Polyimide and polyurethane films are the examples of thermal evaporation. Its advantages are solventless evaporation, good process control and low defect density. But expensive vacuum technology is required. As a general rule,

evaporated films are highly disordered, which causes a large residual stress and limits the thickness of the films (Stuart 1983).

Molecular Beam Epitaxy (MBE) is an Ultra-High-Vacuum (UHV) based technique for producing high quality epitaxial structures (metals, insulators and superconductors) with precise monolayer control. It consists essentially of atoms or clusters of atoms, which are produced by heating up a solid source. They then migrate in an UHV environment and impinge on a hot substrate surface, where they can diffuse and eventually incorporate into the growing film. Despite the conceptual simplicity, a great technological effort is required to produce systems that yield the desired quality in terms of material purity, uniformity and interface control (Rashid and Gunter 2004).

In spin coating, an excess amount of organic solution is placed on the substrate. The substrate is then rotated at high speed in order to spread the fluid by centrifugal force. Rotation is continued for some time, with fluid being spun off the edges of the substrate, until desired film thickness is achieved. If solvent evaporates too fast, bubbles can be seen. Film thickness is effected by concentration of solution and rotation speed. Spin cast films are also less dense and more susceptible to chemical attack than materials deposited by other means (Dreuth et al. 1998).

Another method; electrochemical deposition is especially used to prepare diamond-like carbon films from organic solutions. The deposition temperature is almost near room temperature. The apparatus is a simple electrolytic cell with DC source and has no need for vacuum equipment. The depositing liquids, source material, deposition system play important roles in the deposition. Depositing liquid must have enough conductivity. It must form a carbon atom-containing group on the substrate surface (Cao et al. 2000).

Layer-by-layer sequential adsorption process of polyelectrolytes, which fabricated monolayer or multilayer heterostructure ultra-thin films by dipping the substrate successively in each polyelectrolyte solution (polyanion or polycation), is another promising technique for the wet fabrication process for ultra-thin organic films. This technique utilized electrostatic attraction between the materials that had opposite electric charge and was able to fabricate ultra-thin film controlled at a molecular level (Ito et al. 2001).

Self-assembled monolayers are molecular assemblies that are formed spontaneously by the immersion of appopriate substrate into a solution of an active surfactant in organic solvent. There is a strong molecule-substrate interaction (Ulman

1996). Organosilicon and alkanethiol are possible applications. The major disadvantage afflicting this technique comes from it being a solution-based technique where side reactions and many molecule interactions can interfere with the deposition process. In addition the rates at which films are grown with this technique are relatively slow for practical uses (Ulman 1991).

The transfer of organized monolayers of amphiphilic molecules from the air-water interface to a substrate; commonly known as the Langmuir-Blodgett (LB) technique, with materials known as LB films, was the first of the molecular-scale materials technique (Gaines 1966).

LB technology is evaluated as a future component of "molecular engineering." The interest in this approach is primarily because the layered structure and molecular order present in the LB multilayers are expected to help in achieving better control over the size, shape and distribution of nanoclusters. Of course, as in all thin film techniques, limitations exist: It is time consuming and the structures can be thermally unstable (Rashid et al. 2004). This instability has been attributed to the weak intermolecular forces within the layers (Hasegawa et al. 1990). It might be thought that LB films are restricted to amphiphilic molecules capable of forming monolayers at a liquid-vapor interface. However, the usefulness of this technique has been recently extended to obtain uniform ultra-thin films of non-amphiphilic macromolecules such as polymers, various bio-molecules, fullerenes and other macro heterocyclic compounds (Schwartz 1997). The following sections give more details on LB films.

# CHAPTER 3

# STRUCTURES OF METAL SOAPS AND APPLICATION AREAS

Metallic soaps are understood to refer to the sparingly soluble or insoluble salts of saturated and unsaturated, straight-chain and branched, aliphatic carboxylic acids with 8-22 carbon atoms. They are reaction products of saturated or unsaturated fatty acids (carboxylic acids) with alkaline, alkaline earth or transition metals (Howe-Grant 1990). Metal soaps are also known as fatty acid salts (Peterson 1990).

Some commercially important metal soaps include those of aluminium, barium, cadmium, calcium, cobalt, copper, iron, lead, lithium, magnesium, manganese, potassium, nickel, zinc and zirconium. Significant application areas for metal soaps include lubricants and heat stabilizers in plastics as well as driers in paint, varnishes, printing inks. Other uses are as processing aids in rubber, fuel and lubricant additives, catalysts, gel thickeners, emulsifiers, water repellants and fungicides (Elvers 1990).

## 3.1. Composition of Metal Soaps and Their Properties

Metal soaps are composed of a metal and acid portion supplied as solutions in solvent or oil. They can be represented by the general formula $(RCOO)_x$ M where R is an aliphatic or alicylic radical and M is a metal with valence x. In the case of neutral soaps, x equals the valence of the metal M. Acid salts (the ratio of acid equivalents to metal equivalents is greater than one) contain free acid whereas neutral soaps contain no free acid. Basic salts are characterised by a higher metal to acid equivalent ratio than the normal metallic soap.

Metallic soap properties are determined by the nature of the organic acid, the type of metal and its concentration, presence of solvent, additives, and the method of production.

Fatty acids which can be used to produce metallic soaps include higher monocarboxylic acids having from about 12 to about 22 carbon atoms. Saturated or unsaturated, substituted or unsubstituted fatty acids are useful. Table 3.1. lists some common fatty acid used in the production of metal soaps. The melting points of saturated fatty acids increase gradually with their molecular weights.

Table 3.1. Structures and melting points of some common fatty acids.
(Source: Petty 1996)

| *Name* | *Carbons* | *Structure* | *Melting point (°C)* |
|---|---|---|---|
| Myristic acid | 14 | $C_{13}H_{27}COOH$ | 55 |
| Palmitic acid | 16 | $C_{15}H_{31}COOH$ | 63 |
| Stearic acid | 18 | $C_{17}H_{35}COOH$ | 71 |
| Arachidic acid | 20 | $C_{19}H_{39}COOH$ | 77 |

Alkaline, alkaline earth and transition metals or their compounds e.g., oxides, hydroxides, carbonates and sulfates and chlorides are used in metal soap production. Sodium and potassium are not in the above classification since the synthesized soaps by these metals are traditional soaps, which exhibit different properties than metallic soaps. They are soluble in water. Metallic soaps are sparingly soluble or insoluble. The selection of metal ion source and fatty acid depends on process type.

## 3.2. Production of Metal Soaps

The selection of a process and a solvent depends on the metal ion source, the desired final form of the product, acceptable purity, raw material availability and finally the fixed and overall manufacturing cost. The colour of metallic soaps depends on the type and amount of metal present. On the other hand, organic materials determine almost entirely the odour of metallic soaps in their manufacture.

Metallic soaps are prepared commercially by three general processes: Precipitation from aqueous solutions of metal salts and alkali soaps, fusion of metal oxides, hydroxides or salts with organic acids or esters and direct solutions of finely divided metals in heated organic acids (Gönen 2003).

In these processes, metal soaps are produced in the form of solids, pastes and liquids. However, in another area, the metal soap thin films are fabricated using monolayer formation in LB film deposition process.

# CHAPTER 4

# FUNDAMENTALS OF LANGMUIR MONOLAYERS

Insoluble monomolecular films on liquids (especially water) have been studied for many years. There is still great interest in such films, for both practical and scientific reasons.

## 4.1. Gas-Liquid Interface

The boundary between a liquid and a gas marks a transition between the composition and the properties of the two bulk phases. A surface layer exists with different properties from those of either bulk phase.

The molecules in a liquid have a certain degree of attraction to each other. The degree of this attraction, also called cohesion, is dependent on the properties of the substance. The interactions of a molecule in the bulk of a liquid are balanced by an equally attractive force in all directions. The molecules on the surface of a liquid experience an imbalance of forces i.e. a molecule at the air/water interface has a larger attraction towards the liquid phase than towards the air or gas phase. Therefore, there is a net attractive force towards the bulk and the air/water interface will spontaneously minimize its area and contract (Figure 4.1.).

The net effect of this situation is the presence of free energy at the surface. The excess energy is called surface free energy and can be quantified as a measurement of energy/area. It is also possible to describe this situation as having a line tension or surface tension which is quantified as a force/length measurement. The common units for surface tension are dynes/cm or mN/m. These units are equivalent.

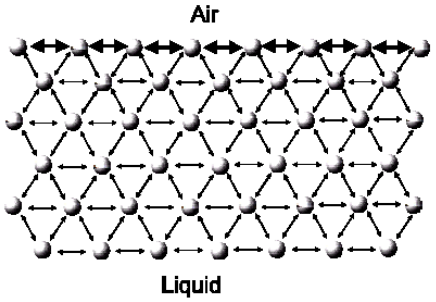


Figure 4.1. The interaction of molecules at an interface and in bulk.

At thermodynamic equilibrium, the surface tension of a planar interface, is given by the partial differential:

$$\gamma = \left( \delta G \big/ \delta \mathrm{A} \right)_{T,P,n_i} \tag{4.1}$$

where G is the Gibbs free energy of the system, A is the surface area, and the temperature T, pressure P, and composition $n_i$ are held constant. Polar liquids, such as water, have strong intermolecular interactions and thus high surface tensions. Any factor which decreases the strength of this interaction will lower surface tension.

The surface tension of water is 73 mN/m at 20$^{o}$C and atmospheric pressure. This is an exceptionally high value compared to the most other liquids and goes some way toward explaining water's preeminence as a subphase (Roberts 1990).

Surface tension is remaining constant for two phases in equilibrium if the temperature is constant, but changing with changing the temperature. An increase in the temperature of this system will lower surface tension.

## 4.2. Monolayer Materials

The molecules of most monolayer forming materials are composed of two parts: a hydrophilic (water soluble) and a hydrophobic (water insoluble) part. These molecules are amphiphiles, the most important types of which are soaps and phospholipids. Such compounds are also called surface active agents (surfactants).

The hydrophobic part in surfactants usually consists of hydrocarbon or fluorocarbon chains, while the hydrophilic part consists of a polar group (-OH, -COOH, $-NH^{3+}$, $-PO_4$ $-(CH_2)_2NH^{3+}$ etc.) (Figure 4.2.). In the absence of such a polar group, no monolayer is formed on water; long-chain hydrocarbons, such as decane ($C_{10}H_{22}$) or cetane ($C_{16}H_{36}$) merely float as drops or lenses on a water surface, without spreading (Gaines 1966).

Surfactants have a significant technological and biological importance. The amphiphilic nature of surfactants is responsible for their association behaviour in solution (micelles, bilayers, vesicles, etc.) and their accumulation at interfaces (air/water or oil/water).

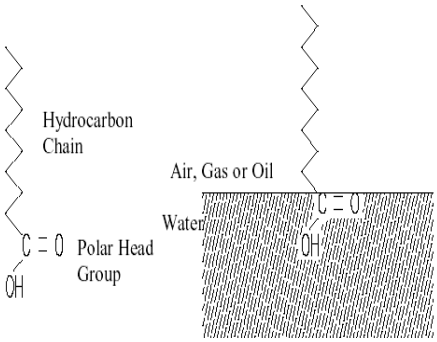


Figure 4.2. Components and the orientation of an amphiphile.

The association behaviour of surfactants in solution and their affinity for interfaces is determined by the physical and chemical properties of the hydrophobic and hydrophilic groups, respectively. The size and shape of the hydrocarbon moiety and the size, charge and hydration of the hydrophilic head group are of utmost importance in this respect. Depending on the balance between these properties a wide variety of self-assembled structures, both at interfaces and in bulk, have been observed. The driving force behind the association is the reduction of the free energy of the system. Therefore, when a surfactant comes in contact with water it accumulates at the air/water interface causing a decrease in the surface tension of water (Adamson 1990).

The hydrocarbon chain of the substance used for monolayer studies has to be long enough in order to be able to form an insoluble monolayer. A rule of thumb is that there should be more than 12 hydrocarbons or groups in the chain ($(CH_2)_n$, $n > 12$). The solubility of n-octadecanoic acid in water at 25$^oC$ has been estimated as 0.003 g/1000 g of water (Gaines 1966). If the chain is shorter, the amphiphile on the water surface tend to form micelles. These micelles are water soluble and in thermodynamic equilibrium with monolayer. Actually, the build-up of a monolayer at the interface is difficult at this condition. On the other hand, if the length of the chain is too long the amphiphile tends to crystallize on the water surface and consequently does not form a monolayer. Besides, they become insoluble to any solvents for spreading. It is difficult to determine the optimal length for the hydrocarbon chain because its film forming ability also depends on the polar part of the amphiphile. It is the balance between these two opposing character that results in the formation of an insoluble monolayer at the air/water interface. Any change in the nature of either the alkyl chain or the polar end group affects the monolayer properties. The absence of a polar group or a weakly polar head (e.g., $CH_2I$ or $CH_2Cl$) simply results in drops or lenses on the water surface. On

the other hand, if the dipole moment associated with the head group is large( e.g., $SO_3^-$), then the compound becomes too soluble in the aqueous subhase. Peculiarly shaped polar head, interactions between neighbouring polar groups and the large size of the head group affect the behaviour at the interface as well (Petty 1996).

Monolayer-forming materials can be fatty acids and related compounds, simple substituted aromatic compounds, dyes, porphyrins and phthalocyanine, fullerenes and charge-transfer complexes. They are applied to the subphase by first dissolving them in a solvent. The solvents should be capable of dissolving adequate quantity of the monolayer material, being chemically nonreactive to monolayer material, not dissolving in the subhase. Finally, the solvent must evaporate within a reasonable period so that no trace remains in the condensed monolayer. A solvent that evaporates too quickly may cause a problem that could prevent the accurate determination of the solution concentration. The solvent concentration can also affect the thickness of floating layers formed from compounds that do not form true monolayers at the air/water interface e.g., unsubstituted molecules, such as the phthalocyanines and fullerenes (Roberts 1990).

Some common solvents used in monolayer spreading are listed in Table 4.1. along with some of their properties; all these are relatively nonpolar.

Table 4.1. Properties of common spreading solvents.
(Source: Gaines 1966)

| *Solvent* | *Boiling point [$^oC$]* | *Water solubility at 25$^oC$ [kg/m$^3$]* |
|---|---|---|
| n-hexane | 69 | 0.01 |
| Cyclohexane | 81 | 0.07 |
| Chloroform | 62 | 8.0 |
| Benzene | 80 | 1.8 |

Sometimes, mixed solvents such as methanol-benzene are preferred to spread the chosen monolayer material which are not soluble in the relatively nonpolar volatile spreading solvents. This mixture may give sufficient solubility for some substances while at the same time not introducing serious water solubility problems.

## 4.3. Formation and Stability of Monolayers

Certain organic molecules such as amphiphilic substances orient themselves at the interface between a gaseous and a liquid phase (or between two liquid phases) to minimize their free energy. The resulting surface film is one molecule in thickness and is commonly called a monomolecular layer or simply a monolayer. The amphiphilic nature of the surfactants dictates the orientation of the molecules at the interface (air/water or oil/water) in such a way that the polar head group is immersed in the water and that the long hydrocarbon chain is pointing towards air, gas or oil. Srivastava and Verma showed that the measured thickness of unimolecular film and the chain length implies the monomolecular fatty acid spreadability on water surface (Srivasta and Verma 1996).

When a solution of an amphiphile (such as stearic acid seen in the Figure 4.3. in a water insoluble solvent (such as benzene) is placed on a water surface with a microsyringe, the solution spreads rapidly to cover the available area. Spreading continues until the surface pressure has risen to an equilibrium value. As the solvent evaporates, a monolayer is formed.

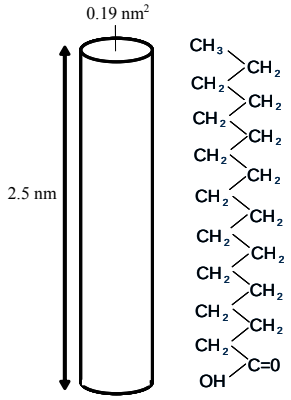


Figure 4.3. Chemical formula for n-octadecanoic acid (stearic acid). The approximate geometrical shape and dimensions of the molecule are shown on the right.

A floating monomolecular film may be in a metastable state rather than in true thermodynamic equilibrium. This state depends on some experimental parameters such as the compression speed, the temperature, pH and the nature of the substances (Schwartz 1997).

If the available surface area of the monolayer is reduced by a barrier system seen in Figure 4.4., the molecules start to exert a repulsive effect on each other. This two-dimensional analogue of a pressure is called surface pressure, and is given by the following relationship;

$$\pi = \gamma - \gamma_o \qquad (4.2)$$

where $\gamma$ is the surface tension in absence of a monolayer and $\gamma_o$ the surface tension with the monolayer present.

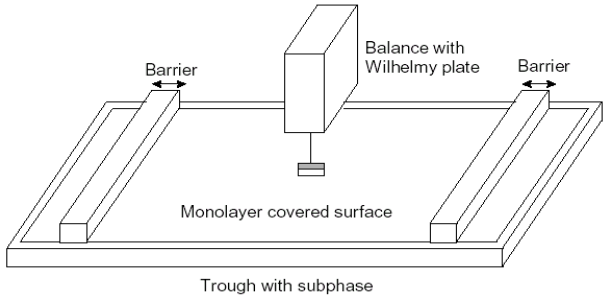


Figure 4.4. A Langmuir film balance with a Wilhelmy plate electrobalance measuring the surface pressure, and barriers for reducing the available surface area.

### 4.3.1. Surface Pressure Measurement

The surface pressure is measured by the Wilhelmy plate-method. This method is made by determining the force due to surface tension on a plate suspended so that it is partially immersed in the subphase (see Figure 4.5.). This force is then converted into surface tension (mN/m or dynes/cm) with the help of the dimensions of the plate.

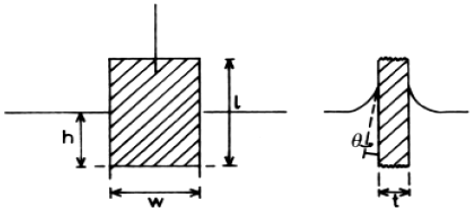


Figure 4.5. A Wilhelmy plate partially immersed in a water surface.

The plate is often very thin and made of platinum. Plates made of materials such as glass, quartz, mica and filter paper can also be used. The forces acting on the plate

consist of the gravity and surface tension downward, and buoyancy due to displaced water upward.

For a rectangular plate of dimensions $l_p$, $w_p$ and $t_p$, of material density $\rho_p$ immersed to a depth $h_l$ in a liquid of density $\rho_l$, the net downward force is given by;

$$F = (\rho_p g l_p w_p t_p) + 2\gamma(w_p t_p)(\cos\theta) - (\rho_l g h_l w_l t_l) \qquad (4.3)$$

where $\gamma$ is the liquid surface tension, $\theta$ is the contact angle of the liquid on the solid plate and g is the gravitational constant. When the plate is completely wetted by the liquid (i.e. $\cos\theta = 1$) the surface pressure can be then obtained from the following equation:

$$\Pi = -\Delta\gamma = -[\Delta F / 2(w_p + t_p)] = -\Delta F / 2w_p, \text{ if } w_p >> t_p \qquad (4.4)$$

The sensitivity can thus be increased by using a very thin plate.

## 4.3. Monolayer Phase Transitions

The most important indicator of the monolayer properties of an amphiphilic material is given by measuring the surface pressure as a function of the area of water surface available for each molecule. This is carried out at constant temperature and is known as a surface pressure-area ($\pi$-A) isotherm or simply "isotherm graph". Usually an isotherm is obtained by compressing the film at a constant rate while continuously monitoring the surface pressure. Depending on the material being studied, repeated compressions and expansions may be necessary to achieve a reproducible trace (Khomutov et al. 1997). A schematic $\pi$-A isotherm is shown in Figure 4.6.

A number of distinct regions is immediately apparent on examining the isotherm. These regions are called phases. The phase behaviour of the monolayer is mainly determined by the physical and chemical properties of the amphiphile, such as subphase temperature, pH and the subphase composition (Yazdanian et al. 1989). For example, various monolayer states exist depending on the length of the hydrocarbon chain length and the magnitude of other cohesive and repulsive forces existing between head groups. An increase in the chain length increases the attraction between molecules, condensing the $\pi$-A isotherm. On the other hand, if an ionizable amphiphile is used the ionisation of the head groups induces repulsive forces tending to oppose phase transitions.

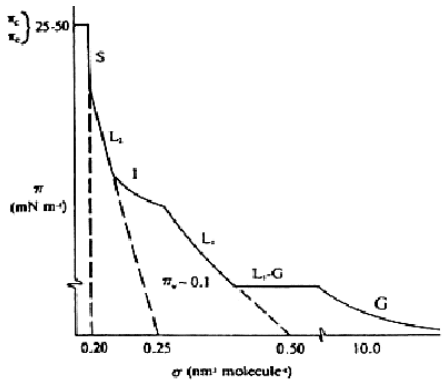


(a)

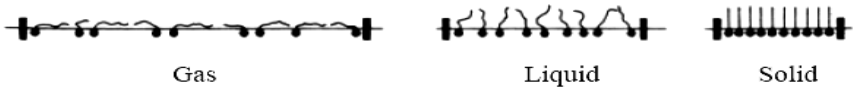


(b)

Figure 4.6. (a) Schematic π-A-isotherm, (b) Orientation of the molecules in different phases.

(Source: Roberts 1990)

Different terminologies were used to classify different monolayer phases of fatty acids in the literature. Generally, the monolayers exist in the gaseous state (G) at which molecules are floating about in the surface layer far enough apart so that they exert little force on one another (Adamson 1990). For an ideal two-dimensonal gaseous phase, the molecules have negligible size compared to the interface area, and thus they obey the following equation;

$$\pi \times \mathrm{A} = k \times T \qquad (4.5)$$

which is a two dimensional ideal gas equation, where A is the area per molecule, π is the surface pressure, k is the Boltzman constant and T is the absolute temperature.

As barriers close towards each other, the intermolecular distance decreases, molecules are compressed, surface pressure increases, monolayer phase changes from gaseous phase to the liquid-expanded state ($L_1$). Hühnerfuss reported that in the case of stearic acid, the first transition occurs around ~24 $Å^2$. Upon further compression, the $L_1$ phase undergoes a transition to the liquid-condensed state ($L_2$). In the liquid phase, the monolayer is coherent, except that the molecules occupy a larger area than in the condensed phase. LS (super-liquid), S (solid) and CS (close-packed solid) are other defined phases at compressed layers respectively. Again they observed transition to LS

phase for stearic acid when the area per molecule is around ~20 $Å^2$. In this condensed phase, the molecules are closely packed and uniformly oriented. These various monolayer states are related to different interactions and arrangements of the polar groups and hydrocarbon chains (Hühnerfuss et al. 1996).

Sakai and Umemura showed that for the stearic acid monolayer, the liquid-condensed $L_2$ phase and the super-liquid LS phase (more correctly solid phase) are observed while there was only an LS phase in the zinc stearate monolayer. Dhanabalan and coworkers have reported that at a pH value of 4.9, the isotherm exhibited a well defined liquid condensed region, indicating the presence of a mixture of acid and zinc arachidate. However, at subphase above 6.4, the liquid condensed region completely disappeared and a steep rise in surface pressure is noticed (Sakai and Umemura 2002, Dhanabalan et al. 1998).

Monolayer compressibilities and surface compressional moduli can be calculated from π-A data according to the following equation (Gaines 1966),

$$C_S^{-1} = (-1/A) \times \left( \frac{\partial A}{\partial \Pi} \right) \tag{4.6}$$

where $A$ is the area per molecule at the indicated surface pressure π. The data is expressed in terms of the reciprocal of isothermal compressibility, surface compressional moduli ($C_S^{-1}$).

π-A isotherm can be helpful to characterize the monolayer composition whether formed layer is acid or salt. Sometimes, the parameter $\chi_\pi$ determining the fraction of acid conversed into the salt is used in the literature:

$$X_\pi = (A_a - A_m) / (A_a - A_S) \tag{4.7}$$

where $A_a$, $A_s$, and $A_m$ are the values of area per molecule for the monolayers of acid, salt, and for mixed monolayer, respectively, obtained by the extrapolation of the linear parts of compression isotherms corresponding to the liquid condensed state to their intersections with the abscissa axis. Bukreeva obtained the $A_s$= 20.5, $A_m$ = 21.9 and $A_a$ = 25 $Å^2$ for stearic acid molecule although this $A_a$ is much larger than the generally accepted value (Bukreeva et al. 2003).

If the monolayer is further compressed after reaching the S state, it collapses into three-dimensional structures. The collapse is generally seen as a rapid decrease in the surface pressure or as a horizontal break in the isotherm if the monolayer is in a

liquid state. This collapse pressure is a function of temperature, pH of the subphase, and rate of barrier (Avila et al. 1999).

The forces acting on a monolayer at this point are quite high (Roberts 1990). For example, a surface pressure of 100 mN/m acting on a layer of molecules 2.5 nm high corresponds to a three-dimensional pressure of about 400 atmosphere (Petty 1996). When collapse occurs, molecules are forced out of the monolayer as illustrated in Figure 4.7.

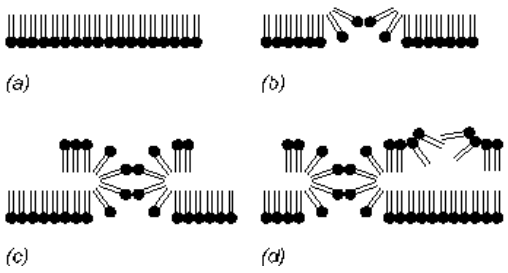


Figure 4.7. The collapse of a monolayer.

Vollhardt studied the collapse process by nucleation and further growth of the nuclei formed. They considered the hypothesis of the formation of cylindrical or hemispherical geometry nuclei in which the growth occurs from the base or from the nucleus periphery. The general equation for the different kinds of nucleation is described by Vollhardt:

$$\left[\ln\left\{\frac{1}{1-(A_o-A)/(A_o-A_\infty)}\right\}\right]^{1/X} = K_S{}^{1/X}\times(t-t_i)=\mu \qquad (4.8)$$

where $A_o$ is the initial area of the monolayer when t = 0 ; A is the monolayer area in a time t; $A_\infty$ is the monolayer area for t = ∞ ; $K_S$ is the specific constant for each kind of nucleation; and $t_i$ is the induction time (Vollhardt et al. 1992).

The parameter 1/x allows the determination of the particular mechanism of nucleation involved in the process, by the best fitting of the experimental data using the x values of Table 4.2.

Table 4.2. Time exponent specification for the several nucleation mechanisms included in the Vollhardt model.

(Source: Avila et al. 1999)

| *Type* | *Nuclei geometry* | *Growth* | *Nucleation* | *Exponent x* |
|---|---|---|---|---|
| A | Hemispherical | Edges | Instantaneous | 3/2 |
| B | Hemispherical | Edges | Progressive | 5/2 |
| C | Hemispherical | Basal area | Instantaneous | 3 |
| D | Hemispherical | Basal area | Progressive | 4 |

In monolayer studies, there are some parameters like metal cation presence and pH those affecting monolayer behaviour. The increase in the number of multivalent metal cations bound with acidic groups of Langmuir monolayer is possible via the increase in pH value and/or metal cation concentration in the subphase. At high enough pH values depending on the metal cation nature, the fatty acid Langmuir monolayer is condensed and converted completely to the salt form that is manifested by the characteristic compression isotherm without $L_2$ / LS phase transition.

Figure 4.8. shows the effect of the incorporation of calcium ions on the pressure versus area isotherms for n-heneicosanoic acid (Shih et al. 1992). At the lowest pressure pH (2.1), the isotherm is identical to that observed at the same temperature without ions in the subphase. However, as the pH is increased, the structure in the isotherms corresponding to the phase transitions is lost. At the highest pH (10.4), the surface pressure versus area curve for the salt monolayer is featureless. The formation of the salt monolayer appears to convert the floating monolayer into a more condensed solid as the head groups are drawn closer together and the tails move closer to the vertical.

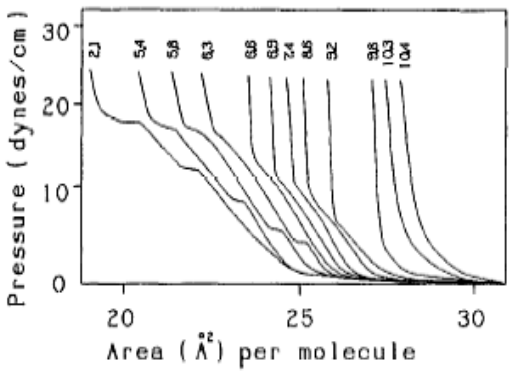


Figure 4.8. π-A isotherms at different pH values.
(Source: Shih et al. 1992)

On the other hand, temperature is another factor on phase behaviour. An increase in temperature increases the surface pressure of the phase transition. Nieto-Suarez reported that as the temperature rises, the collapse occurs at a lower surface pressures for ethyl palmitate monolayers. They also found that a strong temperature dependence on transition region, which becomes gradually smaller and shifts to higher surface pressures with increasing temperature (Figure 4.9.) (Suarez et al. 2004).

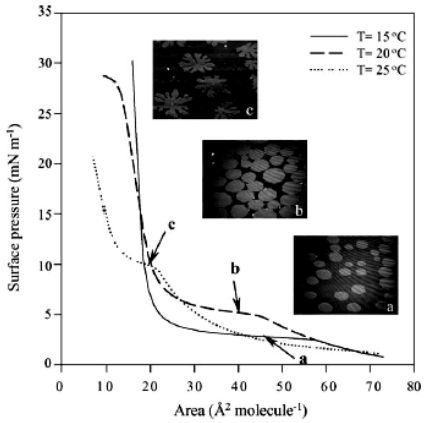


Figure 4.9. *π–A* isotherms recorded on water subphases (15, 20 and 25°C) and BAM images taken at the points indicated by arrows.
(Source: Nieto-Suarez et al. 2004)

The temperature and surface pressures must be carefully controlled so that the floating monolayer is well within a single phase region in its phase diagram.

# CHAPTER 5

# FILM DEPOSITION AND CHARACTERIZATION OF LANGMUIR-BLODGETT FILMS

The surface pressure and temperature of the monolayer are controlled to providing that organic film is in a condensed and stable state. For fatty acid type materials, deposition generally proceeds from either the $L_2'$, LS or S phase with surface pressures in the range of 20 to 40 mN/m and temperatures between 15$^o$C and 20$^o$C. However, it is also possible to start from one of the other monolayer states. The molecular organization in the resulting LB film depends on these initial conditions.

Table 5.1. lists conditions for the succesful transfer of long-chain fatty acids and their cadmium salts.

Table 5.1. Typical conditions for the deposition on glass slides of monolayers of some cadmium salts of long-chain fatty acids.

(Source: Petty 1996)

| *Fatty Acid* | *Formula* | *Subphase pH* | *Temperature [$^o$C]* |
|---|---|---|---|
| n-octadecanoic (stearic) | $C_{17}H_{35}COOH$ | 5.4-5.8 | 18-20 |
| n-nonadecanoic | $C_{18}H_{37}COOH$ | 5.6-6.0 | 20 |
| n-eicosanoic (arachidic) | $C_{19}H_{39}COOH$ | 5.5-6.0 | 18-22 |
| n-heneicosanoic | $C_{20}H_{41}COOH$ | 5.6-5.7 | 25 |
| n-docosanoic (behenic) | $C_{21}H_{43}COOH$ | 6.0 | 29 |

## 5.1. Deposition Principles

Langmuir film balance can be used for building up highly organised multilayers of the used amphiphile. This is accomplished by successive dipping of a solid substrate up and down through the monolayer while simultaneously keeping the surface pressure constant by a computer controlled feedback system between the electrobalance measuring the surface pressure and the barrier moving mechanism. Consequently, the

floating monolayer is transferred to the solid substrate. In this way, multilayer structures of hundreds of layers can be produced. These multilayer structures are commonly called Langmuir-Blodgett or simply LB films. The deposition process is schematically shown in Figure 5.1.

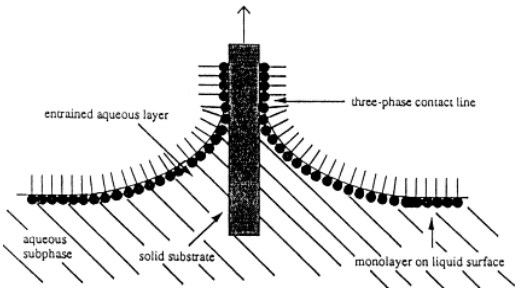


(a)

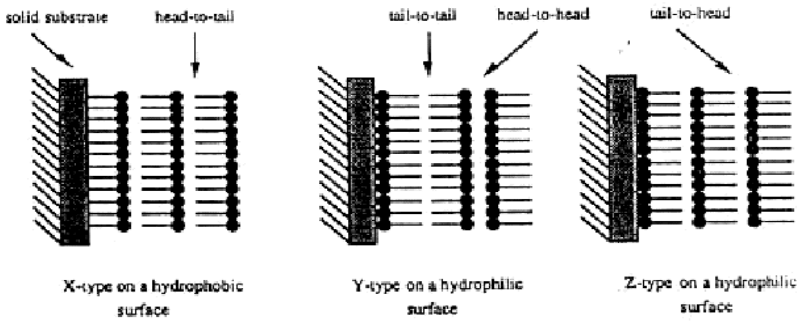


(b)

Figure 5.1. (a) Deposition of a floating monolayer on a solid substrate,
(b) Deposition types of LB films.
(Source: Petty 1996)

There are several parameters that affect the type of LB film produced. These are the nature of the spread film, the subphase composition, pH and temperature, the surface pressure during the deposition and the deposition speed, the type and nature of the solid substrate and the time the solid substrate is stored in air or in the subphase between the deposition cycles (Leonard et al. 1995).

The LB deposition is traditionally carried out in the "solid" phase. The surface pressure is then high enough to ensure sufficient cohesion in the monolayer, so that the monolayer does not fall apart during transfer to the solid substrate. This also ensures the build up of homogeneous multilayers.

The surface pressure value that gives the best results depends on the nature of the monolayer and is usually established empirically. However, amphiphiles can seldom

be successfully deposited at surface pressures lower than 10 mN/m, and at surface pressures above 40 mN/m collapse and film rigidity often pose problems (Petty 1996).

Deposition speed is another significant factor in deposition process. Especially, on withdrawal through the floating monolayer, it is important not to raise the substrate faster than the rate at which water drains from the solid. This drainage is not due to gravity but is a result of the adhesion between the monolayer being transferred and the material on the substrate which acts along the line of contact and so drives out the water film. It is normal to transfer the initial monolayer onto a solid substrate relatively slow: speeds of 10 μm/s to a few mm/s are typical. The upper limit is set by the rate of drainage of the water between the substrate and the film being deposited (Peng et al. 2001).

The quantity and the quality of the deposited monolayer on a solid support is measured by so called transfer ratio, τ. This is defined as the ratio between the decrease in monolayer area during a deposition stroke, $A_L$, and the area of the coated solid substrate, $A_S$ given as following;

$$\tau = A_L / A_S \qquad (5.1)$$

For ideal transfer, τ is close to 1. Transfer ratios significantly far from unity suggest poor film homogeneity. LB multilayers can be produced by successive deposition of monolayers on the same substrate shown in Figure 5.1. The most common one is the Y-type multilayer, which is produced when the monolayer deposition to the solid substrate is in both up and down directions. For strong hydrophilic head groups (-COOH, $PO_3H_2$, etc.), this is the most stable deposition mode, since the interactions between adjacent monolayers are either hydrophobic-hydrophobic, or hydrophilic-hydrophilic.

When the monolayer deposition is only in the up direction, multilayer structure is called; Z-type or only in down direction; X-type. Intermediate structures are sometimes observed for some LB multilayers and they are often referred as XY-type multilayers.

## 5.2. The Effect of Substrate Properties

Condensed monolayers can be transferred to a variety of surfaces. The adhesion of the first layer to the underlying substrate is particularly critical and determines the quality of subsequent layers.

Many different types of substrate materials with a fairly well defined surfaces can be used. Substrates can, however be divided into two categories with distinctly different behaviour towards deposition of the first layer. For hydrophilic substrates (the category which includes all metals and semiconductors with a native oxide layer and glass as normally prepared) no monolayer is deposited as the substrate is initially immersed, so that the eventual number of layers when the substrate finally emerges into the air is odd. On the other hand, hydrophobic substrates (including silicon and other semiconductors when oxide-free, metal like silver, gold, and silanised glass) take up a monolayer on the first downstroke hence the final number of layers is even. In both cases, it is essential that the surface properties are uniform.

Glass is a popular choice because glass slides are readily available and films deposited on them can subsequently be examined optically. For a wider transparent range, it is possible to use fused silica or quartz. When a conductive substrate is required to allow electrical measurement of film characteristics, it is often to use by vacuum-deposition techniques to fabricate aluminium, chromium, tin, lead, silver, gold or platinum thin films on a glass slide (Peterson 1990).

For electron microscopy, LB films have been deposited on thin polymer substrates or the anodisation layer of aluminium. Inexpensive and extremely smooth semiconductor wafers, particularly silicon have been great interested in recent studies due to their conductivity and infrared transparency (Bukreeva et al. 2003).

Viswanathan studied the pH effect on mica and silicon oxide substrate. They observed that during the deposition onto a silicon oxide substrate, there is a thin layer of water present between the film and the substrate, but much less water presence was observed for mica at pH 5.5 (Viswanathan et al. 1992).

There are many parameters associated with substrate surface that can influence deposition. Its exact chemical composition may affect ion exchange in the first layer deposited. Dote and Mowery found very different absorbate-surface bonding and orientation of stearic acid monolayers on gold and aluminium substrate. Acid is chemisorbed onto aluminium oxide substrate, the acidic proton is dissociated from the

acid to form the metal carboxylate. On gold, the acid is physisorbed and both the carboxylic acid and carboxylate are present (Dote and Mowery 1988).

The physical structure of the substrate surface ( e.g., whether it contains gaps or voids) may also be important in determining the quality of the deposited layer. If the substrate is very irregular, then it is possible that the LB film can follow the undulations. For surface roughness on the nanometre scale, it is more likely that, at the moment of deposition, the monolayer will bridge over voids, suppported by a layer of water. When this layer has drained or dried, the film will collapse.

## 5.3. Subphase and Containment

The water subphase itself must be of the highest purity available. The quantity of monolayer-forming material is used in the microgram range; the subphase volume can be hundreds of millilitres. Therefore p.p.b impurities, if they are surface active, can cause a problem. A deionizing water system can produce water of high specific resistance ($1.8 \times 10^6$ Ωm) and total organic contamination in the p.p.b. level. Taylor and coworkers showed that trace surface active impurities is undetectable in π-A measurements. In contrast, surface conductance measurement is sensitive to presence of impurities (Taylor et al. 1989).

The requirements of a trough material are relatively straightforward: the material must be inert and must not release impurities into the subphase; it should preferably be hydrophobic to enable easy cleaning; it should withstand organic solvents as well as inorganic acids. For example, polytetrafluoroethylene (PTFE) trough is hydrophobic, and resists almost all chemicals (Gaines 1966). Therefore, in our study, PTFE was chosen as a trough in our LB system.

## 5.4. Defects in Film Structures

There have been direct and indirect observations of defects at molecular length scales, dislocations, disclinations, and grain boundaries. Namely, defects are present at all length scales. Molecular scale defects such as lattice dislocations and domain boundaries have been directly observed as well as steps, pinholes, and crystallites at larger length scales.

Various types of gross inhomogeneities can occur in LB films if the substrate surface properties are not uniform, or if the monolayer undergoes a phase change on the

water surface to a solid, non-ductile state. However, with normal precautions, this does not occur and the resulting films have essentially uniform thickness. There can also be other, more subtle, inhomogeneities. All LB films so far investigated display local crystalline packing of the molecules (even the preformed polymers have close-packed aliphatic chains). Since this short-range order has never been observed to extend over the whole trough, some types of orientational inhomogeneity might occur. In fact, continuous changes of orientation occur at almost all points of the monolayer indicating the presence of internal stresses.

Li and Leonard both reported that crystal defects in LB films originate from the monolayer and are conserved upon deposition (Li et al. 2000, Leonard et al. 1995).

One-dimensional discontinuities of orientation, usually called grain boundaries, can also occur (Peterson 1990). Smectic-organised films also have zero-dimensional inhomogeneities called disclinations. These well known and characteristic structures of liquid crystals are points where the orientational ordering interaction is frustrated. Figure 5.2 shows a locally HCP lattice of tilted molecules with two disclinations of opposite signs joined by a twin boundary. Twin boundaries and disclinations have been identified as dominant causes of defect conduction in mono- and multilayers of fatty acids and soaps (Petty 1996).

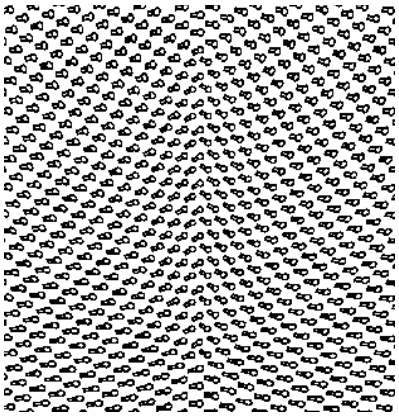

Figure 5.2. A hexatic lattice of tilted molecules.
(Source: Peterson 1990)

According to the study done by Wolthaus defects in LB monolayers are covered up by subsequent monolayers. Figure 5.3. shows a typical AFM image of the dipping line separating a single from a triple monolayer of cadmium palmitate ($C_{16}$) on mica. Defects in the first monolayer (left to the dipping line) reaching the dipping line are

covered up by the bilayer of the second and third monolayers (right) without showing any deflection in the area of the hole (Wolthaus et al. 1994).

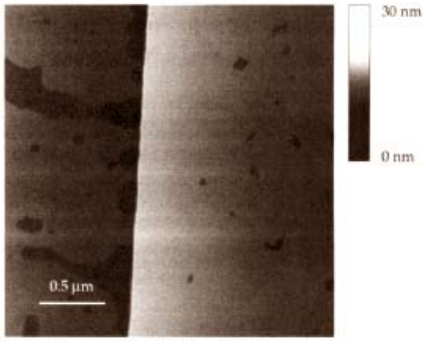


Figure 5.3. AFM image of cadmium palmitate ($C_{16}$) with different layer thicknesses on mica.

(Source: Wolthaus et al. 1994)

Other types of defect also occur in LB films. These include pin-holes and regions containing collapsed monolayer (normally observed as striations in the LB film). Using AFM, Hansma observed holes about 3 nm deep in $CdAd_2$ monolayers deposited on mica at pH = 5.7. They noted that the number of holes and fragility of the film increased dramatically after aging for several months (Hansma et al. 1991).

These inhomogeneities are not an inescapable fact of life. It is possible to process the monolayers on the water surface so as to improve the ordering of the deposited film and in particular to achieve significant reductions in the density of disclinations. Careful precaution is necessary as well in all the steps of the LB deposition procedure (Schwartz 1997).

# CHAPTER 6

# METAL SOAP LB FILMS

Monolayers and Langmuir-Blodgett films of fatty acids and their salts have been investigated for a long time. These films have attracted much interest due to their high stability on the surfaces of liquid and solid substrates and the controlled cationic composition. They are also characterized by high degree of organization and easy preparation (Peng et al. 2001).

Generally, commercial metal stearates are formed by metal ions and stearate anions through ionic bonds. These substances are only soluble in polar solvents with high dielectric constants. Polar solvents weaken the force of attraction between oppositely charged ions in crystals. However, the most important property of metallic soaps is that there is no good solvent for them. They are sparingly soluble or insoluble in water. Based on this property, they are widely used in waterproofing materials formulation. They are partly bound with Van Der Waals forces among hydrocarbon chains as well. Furthermore, they are bound with Coulombic attraction among (not between) metallic and stearate ions. Therefore, nonpolar solvents such as benzene can not dissolve metal stearates.

## 6.1. Preparation of Metal Soap LB Films

To produce LB films of metal soaps, using fatty acid monolayer on the water surface, the metal cations are added into the subphase in the form of water soluble metal salts. These metal salts can be any of $-SO_4^{2-}$, $-Cl^-$, etc. at a concentration in the level of $10^{-4}$ M. Metal incorporation is generally due to chemistry occurring between the species in solution and the headgroups of the molecules in the monolayer on the subphase surface.

The reactions of monolayers differ from those in the bulk solution because of both the concentration and orientation of molecules at the air-liquid interface. Monolayer forming molecules are oriented, their reactive groups may be less accessible to reagents than they would be in a homogeneous bulk phase. Reagents, also, may be preferentially, concentrated at or repelled from an interface.

Monolayers of neutral molecules such as long chain fatty acids at a pH of 4 or less bear no electrical charge. At such a low pH value, the acidic headgrous do not dissociate and neither the cations do affect the Langmuir monolayer, nor they are incorporated into an LB film. However, on making the subphase more alkaline, ionization of the polar head groups occurs to form hydrogen ions in the subphase and carboxylate ions in the film, i.e.,

$$C_nH_{2n+1}COOH \leftrightarrow C_nH_{2n+1}COO^- + H^+ \qquad (6.1)$$

The ionization of weak electrolytes, such as carboxylic acids or amines, is strongly dependent on pH that pH at which half of the molecules of an acid are ionized is known as the $pK_A$ of the acid. Charges associated with ionized monolayers is neutralized by counterions in (or added to) the aqueous subphase. At sufficiently high pH, the amphiphile is completely deprotonated and converted to the soap. In the intermediate pH range, the relative fractions of acid and soap in the Langmuir monolayer are a function of pH.

The combination of counter-ions from solution with ionized fatty acids to form soaps can be considered as a monolayer reaction. In a subphase containing cadmium chloride, the following reaction takes place;

$$2C_nH_{2n+1}COO^- + CdCl_2 \leftrightarrow (C_nH_{2n+1}COO)^-Cd^{2+} + 2HCl \qquad (6.2)$$

The equilibrium conditions for such reactions can be outlined in principle, but the details are not yet well understood. These reactions may be diffusion limited, and/or occur slowly. The floating monolayer is a mixture of the fatty acid and salt.

The variation in the pH necessary for conversion to soap has generally been interpreted as due to differences in the competitive reactions between the metal ion and the proton with the carboxylate group. In the review by Peng, to obtain a 100% combination of the carboxylate anions with divalent cations in the film, the pH value required for lead should be $\geq 4$, for cadmium $\geq 6.5$, for manganese $\geq 7.0$, for calcium $\geq 7.5$ and for barium $\geq 9$ (Peng et al. 2001).

There is a critical pH-value dependent on the metal cation type and a critical concentration in the subphase at which complete ionization of the monolayer fatty acid molecules due to cation binding is just achieved. Further increase in pH value above the critical point can result in overstoichiometric incorporation of metal cations into

multilayer LB films deposited from such subphase and hydrolysis, hydration of the ions. Hence the formation of hydroxide complexes can be proposed to explain such effects. Over a range of pH values, the complex pattern of hydrolysis for $Zn^{2+}$ in solution leads to changes in the composition and stability of spread arachidic acid monolayers (Dhanabalan et al. 1998). Avila found that the stability of the calcium stearate monolayers increased at high pH values due to the presence of divalent cations in the water subphase as well (Avila et al. 1999).

When fatty acid LB films with transition and multivalent metal cations are formed, the increase in pH value of the subphase containing multivalent metal cations often leads to the worsening of Langmuir monolayer processability making the formation of highly-ordered LB films problematic (Khomutov et al. 1997, 2002).

Studies with LB films have shown that different cations under the same conditions give films with different structure and properties. Such differences between metal ions in aqueous solution related to the ionic size, degree of hydration, and Lewis acid/base character. Those differences can also be attributed to the different character of interactions of metal cations with fatty acid monolayer: non-specific screening of surface electrostatic charges and if divalent cations are considered, 1:2 binding stoichiometry for alkaline earth cations ($Ba^{2+}$, $Ca^{2+}$, $Mg^{2+}$), and specific complexation with covalent binding character for transition metal cations ($Pb^{2+}$, $Cd^{2+}$) (Yazdanian et al. 1989). Moreover, the nature of the anions present in the subphase affect the uptake of cation by the monolayer as shown in Bagg's study in the case of calcium uptake of stearic acid as shown in Figure 6.1 (Bagg et al. 1964).

The interaction of the carboxylic groups of the fatty acid monolayer with metal ions depends on the physical and chemical properties of the ions. Metal cations can bind to the carboxylate group in several ways. The first one is ionic binding. The second is the unidentate type, where a metal atom covalently binds to one of the carboxylate oxygen. The third is the chelate bidentate type, where a metal atom binds covalently to both oxygen atoms of the carboxylate group. The fourth is the bridging bidentate type, where two different metal atoms bind covalently to each of the oxygen atoms of the carboxylate group (Sakai and Umemura 2002).

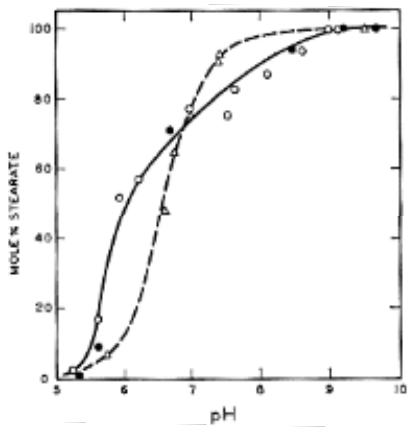


Figure 6.1. Composition of stearic acid-calcium stearate monohydrate films (plated and skimmed) from $1\times10^{-3}$ M bicarbonate (○), ammonium (●), and phosphate (Δ) substrates.

(Source: Bagg et al. 1964)

The structures of the central portions of multilayer LB films of fatty acids and their salts are similar to the structures of their bulk phases. The bulk phases have a lamellar structure, where the arrangement of the molecules is illustrated in Figure 6.2.

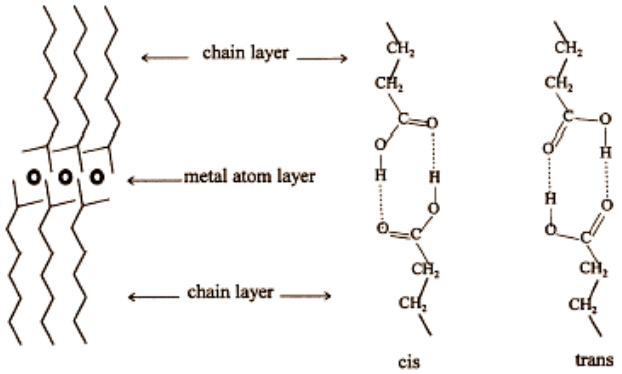


Figure 6.2. The molecules arranged in: (a) a lamella in a metal soap film; (b) a lamella in a fatty acid film showing two kinds of dimers; in cis and trans conformation.

(Source: Peng et al. 2001)

In multilayer LB films, the basic structure is similar to that observed in the bulk crystals: a lamellar structure where each lamella is a bilayer consisting of two monolayers in a head-to-head arrangement irrespective of the deposition type. With fatty acids, the two monolayers are bound together by hydrogen bonding forming

dimers, with the chains tilting at an angle to the normal of the plane of the head groups. With the salts of divalent cations, a lamella consists of two layers of long-chain carboxyl anions combining with one layer of cations. The chains may either be tilted or parallel to the normal of the plane of the head groups. The correlation length in the film plane is approximately 100-200 Å, but only approximately two bilayers in the direction of the normal. (Peng et al. 2001).

Rajagopal and friends investigated $CdAd_2$, $CaAd_2$, $PbAd_2$, $BaAd_2$ and $ZnAd_2$ in their study and showed that an increase in the electronegativity of the counterion leads to an increase in the covalent character of the bond between the cation and the carboxyl group. This increase in the covalent character of the bond gives films with the hydrocarbon chains more or less perpendicular to the substrate (Rajagopal et al. 1998).

There is also a special case for metal incorporation stemming from substrate effect. In Figure 6.3., a schematic drawing of the one monolayer LB film incorporated with evaporated Ag islands (Umemura et al. 1987). The Ag islands come between the polar groups of stearic acid monolayer and Ge plate and react with stearic acid, forming silver stearate.

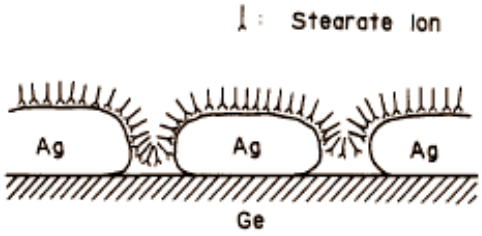


Figure 6.3. Schematic drawing of the one monolayer LB film incorporated with evaporated Ag islands.
(Source: Umemura et al. 1987)

## 6.2. LB Multilayer Films of Fatty Acid and Metal Soaps

### *Structures of Single-Monolayer LB Films of Fatty Acids and Their Salts*

Generally, at room temperature in single monolayer LB films of fatty acid and salts, the acyl chains are in the trans conformation and oriented with their long axes normal to the substrate. The molecules are hexagonally packed and this in-plane packing shows long-range bond orientational order and short-range positional order regardless of the deposition conditions and irrespective of the substrate whether

crystalline $CaF_2$ or amorphous glass slides: often called hexatic-B packing and corresponding to the smectic BH structure (Peng et al. 2001). This structure is obtained independent of the phase of the parent floating monolayer. The film has been removed from contact with the floating monolayer and dried. However, while the LB monolayer is kept in contact with the parent monolayer it retains the structure of that monolayer, probably because of a thin water film between the monolayer and the substrate. Occasionally, orientational and rarely strain epitaxy may be observed when there is strong interaction between the monolayer head-group and the substrate. There is also some evidence that larger features such as domain size may be preserved during LB deposition.

### *Structures of LB Multilayer Films of Fatty Acids and Their Salts*

In LB films, all the monolayers are parallel to each other and to the substrate. However, the intralayer and interlayer positional correlation lengths in the LB films are only $10^2$-$10^3$ Å: much smaller than those of single crystals of their bulk phases. Therefore, an LB film is more like a stack of highly-oriented quasi-2D powder layers rather than a large crystal.

The transition from the hexagonal in-plane structure in monolayer films to the centred rectangular structure in multilayer films as the number of layers is increased has been reported many times to occur in the first three layers, or to take up to nine layers.

### *Polymorphism in LB Films of Fatty Acids*

Long chain fatty acid type compounds exhibit polymorphism, they can exist in variety of crystallographic states, depending on the packing arrangements of the main and subcells. Different packing arrangements of the $C_2H_4$ repeat units define the crystallographic nature of the subcell or sublattice. There are three possible close-packed strutures with similar packing densities: orthorhombic (R), monoclinic (M) and Triclinic (T). LB films of fatty acid salts invariably consist of upright molecules with a R(001) packing. However, several different structures for fatty acid multilayers have been identified, depending on the precise deposition parameters. For 22-tricosenoic acid, the R(001) structure is found over a wide range of dipping conditions.

### *Chain Tilt and Orientation*

In practice, it is found that the tilt angle of the alkyl chains in fatty acid materials varies inversely with the deposition pressure; the greater the pressure, the smaller the angle of tilt from the substrate normal. The structure of these LB layers of tilted molecules may therefore be quite complex, since it is consisting of regions of crystallinity in which grains are inclined to the subphase with a distribution of tilt azimuths and permeated by holes.

Films of acids show some chain tilt indicating monoclinic structures and occasionally polymorphism different tilt angles, etc., but studies of the salts with divalent cations report that the chains are either normal to the substrate or tilted, depending on the cation.

Umemura and Sakai studied that in the stearic acid monolayer, the orientation angle decreased from $20^{o}$ to almost $0^{o}$ upon monolayer compression. On the other hand, they found that in the cadmium stearate monolayer, the orientation angle (near $0^{o}$) did not change upon monolayer compression, though it was widely scattered at large surface areas because of the presence of a rigid crystalline island (Umemura and Sakai 1997).

### *Epitaxial Growth in Multilayers*

It is possible that in the multilayer films, sometimes, if there is a strong coupling between the monolayer and the surface of the substrate, the orientation of the monolayer structure may be correlated to that on the surface of the substrate. This is known as epitaxial growth during the LB deposition.

During LB film deposition, the first monolayer on the solid substrate is an example of heterogeneous crystal growth. For subsequent layers, transferring onto existing film, the deposition will be homogeneous.

For fatty acids, evidence from electron diffraction shows that each monolayer has the same local orientation of its molecular lattice as that of the underlying monolayers; however, this does not necessarily mean that translational order also extends from layer to layer (Peterson 1990).

### *Superstructure in LB Films of Fatty Acid Salts*

Some multilayer films show evidence of superstructures. This feature seems to depend strongly on the nature of the cation and on the pH of the subphase. Dupres

reported that divalent ions can be divided into two categories: those that induce the classical S phase for the fatty acid molecules and those that lead to superstructures, i.e., an ordered inorganic lattice in addition to the organic lattice. The first kind of cations includes nickel, barium, cobalt, and copper, whereas manganese and magnesium belong to the second category. In previous experiments, performed with chloride salts of cadmium and lead in the subphase of arachidic and heneicosanoic acid Langmuir monolayers at low temperature and pH between 7 and 9, superlattice structures were also evidenced. In the case of zinc and calcium dissolved in the aqueous subphase of heneicosanoic acid Langmuir monolayers, no superlattice structure has been observed (Dupres et al. 2003).

Sigiyama and coworkers gave a structural model for superstructures as in Figure 6.4. where white circles denote acid molecules and hatched circles denote the alkyl chains composing salt molecules. This model is based on the molecular arrangements changing with pH, i.e. variation of the salts forming ratio. The 2×2 model is composed of the acid and the salt alkyl chains alternatively. A local salt forming ratio in this model is to be 50 %. The 3×1 model is composed of an arachidic acid alkyl chain existing at intervals of two salt chains. Salt forming ratio is 66.7 % in this case. In both models, the coordination of arachidic acid molecules and Ba ions is assumed to be two second-neighboring acid molecules are bonded to a Ba ion (Sigiyama et al. 1998).

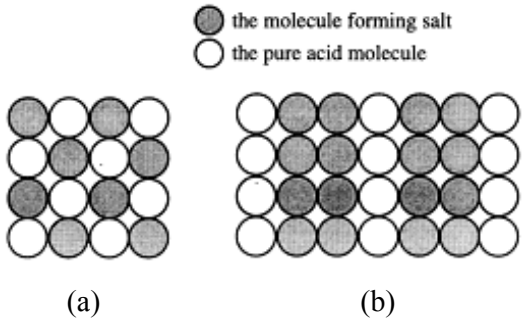


Figure 6.4. Schematic structural models for each superstructure, (a) 2×2 and (b) 3×1. (Source: Sigiyama et al. 1998)

## *Thermal Behaviour of Fatty Acid and Salt LB Films*

LB films of fatty acid soaps are mechanically soft and melting at fairly low temperatures. The thermal stability of the films has been extensively investigated. They melt at around 100$^{o}$C and desorb from the substrate at around 150$^{o}$C.

Umemura studied the thickness and temperature dependence of molecular structure in stearic acid and metal stearate LB films. 1-, 3-, 9- and 21-layer LB films of stearic acid, $CdSt_2$ and $CaSt_2$ were fabricated on silver coated glass slides. FTIR, RAS of these LB films were recorded at various temperatures from 31 to 72$^oC$ for stearic acid and 31-140$^oC$ for metal stearates (Umemura et al. 1993, 1994) .

They reported that spectra of stearic acid at 31$^oC$ exhibited characteristic features of high perpendicular orientation of the hydrocarbon chain. In the 1- and 3-monolayer LB films, the trans isomer of stearic acid was prominent, but the cis isomer took its place in the 21-monolayer LB film. FT-IR, RAS measurements at elevated temperatures indicated that the chain melting temperature increases and approaches to the bulk melting point with an increase in the number of monolayers, except for the 1-monolayer LB film which had a higher melting temperature than the 3-monolayer film owing to the strong interaction with silver subsrate. At room temperature, the hydrocarbon chains in these metal stearate LB films were in a well-ordered state with a high degree of perpendicular orientation to the substrate. However, they become disordered at elevated tempearatures. These order-disorder phase transition temperatures were dependent on thickness. In the $CaSt_2$ LB films (103-129$^oC$), the effect of dehydration was inferred.

## 6.3. Characterization of Fatty Acid and Metal Soap LB Films

This section describes the related techniques that can be used extensively to investigate LB film structure and outline some important results.

### *Fourier Transform Infrared Spectroscopy (FTIR)*

This technique has the advantage of being easy to use, nondestructive against samples, and sensitive to changes in the molecular conformation. It has been a very important tool in LB film research. Three varieties are often used, transmission, grazing-incidence reflection, and attenuated total reflection (ATR).

In transmission FTIR, the LB film is simply inserted into the IR beam, and the observed band intensities give information about relative amounts of and the conformation of various chemical groups - as in solution-phase FTIR.

In addition, grazing incidence and ATR can also give information about the orientation of molecular groups on the substrate. Grazing-incidence reflection is performed on highly reflective metal substrates. Grazing incidence IR is sensitive only

to the component of a dipole moment perpendicular to the substrate. This can be exploited to obtain information regarding molecular orientation. ATR involves the multiple internal reflection of the IR beam inside the LB film on substrate itself.

Hasegawa studied the thermal stability of metal stearates. Figure 6.5. shows a series of RA spectra of 9 layer LB film of $CdSt_2$ obtained at various temperatures on silver evaporated glass slide.They interpreted that the introduction of disordered conformation into the alkyl chains and a break-up of the Cd lattice (Hasegawa et al. 1990).

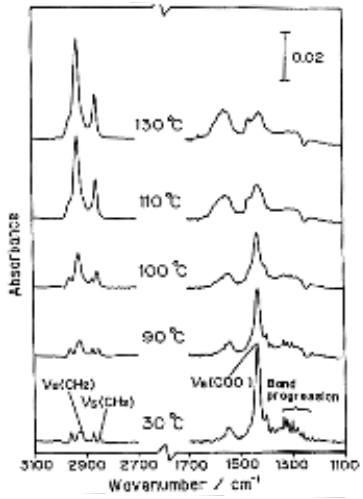


Figure 6.5. Infrared RA spectra of 9 layer LB film of $CdSt_2$ at elevated temperatures. (Source: Hasegawa et al. 1990)

## *X-ray Scattering*

The X-ray scattering techniques include diffraction and reflectivity measurements to analyze the structures of floating monolayers and LB films. X-ray diffraction (XRD) technique gives information about laterally averaged film structure in the surface normal direction. The information about the laterally averaged electron density profile in the monolayer can be obtained by scattering in this geometry and it is called X-ray reflectivity (Schwartz and Daniel 1997).

X-ray scattering can also be used to obtain information about intralayer structure. For these experiments, the transferred wave vector should be essentially in the surface plane and the technique is known as Grazing incidence X-ray diffraction (GIXD). GIXD experiments can determine not only the type of molecular packing within the layer, but also give information about the molecular orientation, i.e. tilt angle.

It has been most frequently used in studying the microscopic molecular structure of LB films such as the in-plane positional ordering, lattice structure, and molecular orientation in layers of fatty acid. In Figure 6.6., Dhanabalan studied that X-ray diffraction of $ZnAd_2$ multilayers deposited at different subphase pH, revealed a strong dependence of the layered structure and molecular packing on the subphase pH (Dhanabalan et al. 1998) .

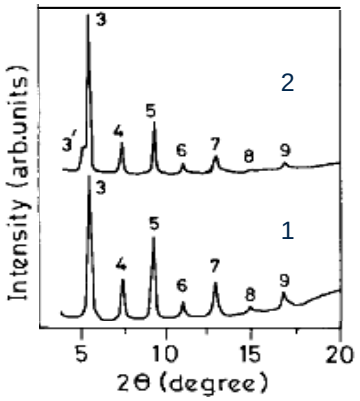


Figure 6.6. XRD patterns for $ZnAd_2$ multilayers deposited at subphase pH values; 1) 6.6, 2) 7.18.

(Source: Dhanabalan et al. 1998)

The monolayer thicknesses for fatty acid salts as a function of the number of carbon atoms in the molecule, obtained from X-ray experiments are plotted in Figure 6.7 according to the data taken by Srivastava (et al. 1966). The X-ray data are in close aggreement with those calculated from the lengths of the molecules, inferring that the hydrocarbon chains in transferred monolayers are oriented almost at right angles to the subphase surface.

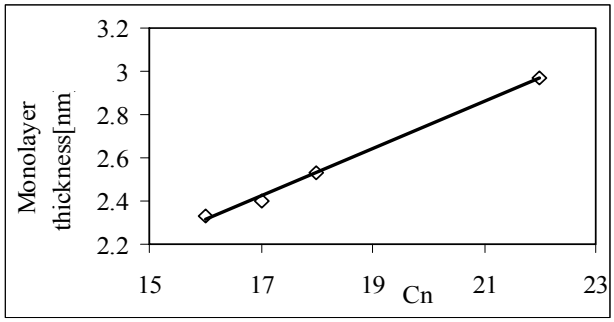


Figure 6.7. Monolayer thickness versus number of carbon atoms in the molecule for barium salts of long-chain fatty acids.

(Source: Srivastava et al. 1966)

*Scanning Probe Microscopy (SPM)*

SPM techniques have become very important in LB research in recent years. Scanning tunneling microscopy (STM) has extremely high lateral resolution but is limited to monolayers on conducting (or semiconducting) substrates. Atomic force microscopy (AFM) is ideally suited for LB film characterization and has recently provided an explosion of information about surface structure (molecular arrangements of LB films) and identification of local defects and inhomogeneities in ordered surfaces. Surface roughness and topographical survey of multilayers are investigated by this technique because of its surface sensitivity. These techniques can give information ranging from molecular resolution crystallography to surface morphology at length scales up to about 100 μm on films with any number of layers. SPM give complementary real-space information relative to scattering and diffraction measurements.

According to Sigiyama's study, high magnification image of (a) arachidic acid, (b) a cobalt arachidate and c) a manganase arachidate bilayer LB films are shown in Figure 6.8 (Sigiyama et al. 1998).

In their study, for arachidic acid and $CoAd_2$, well-ordered molecular arrangements were observed. On the other hand, only an unclear arrangement was partially observed for $MnAd_2$. These facts indicated that the $MnAd_2$ film was unstable and the packing of the molecules was loose.

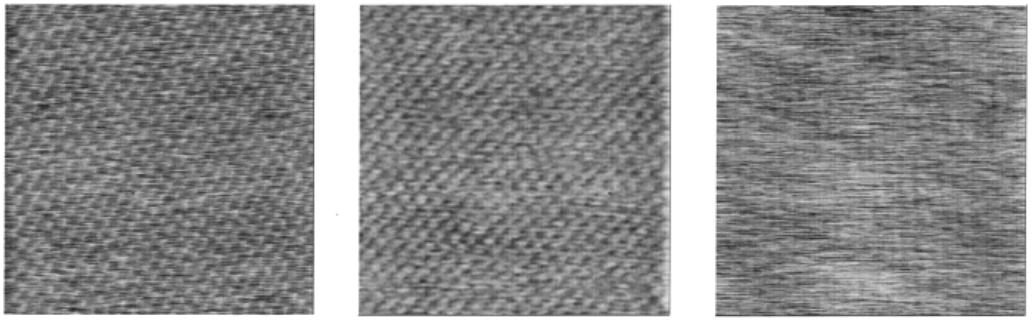


Figure 6.8. 10×10 $nm^2$ AFM images of (a) an arachidic acid, (b) $CoAd_2$ and (c) $MnAd_2$. (Source: Sigiyama et al. 1998)

## *Scanning Electron Microscopy(SEM)*

Scanning electron microscopy also gives information about the film morphology and growth mechanism in self-aggregated films and topographic examination in LB films. With Energy Dispersive X-ray, it enables us to get information about surface composition (C, O, ions etc.). The LB film formed by stearic acid monolayer on $GdCl_3$ subphase is shown in Figure 6.9. (Khomutov et al. 2002).

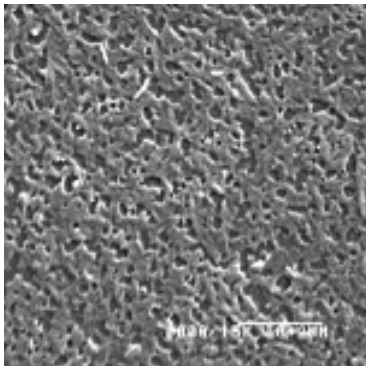

Figure 6.9. 20 layer of Gadolinium stearate LB film formed at pH 5.0.
(Source: Khomutov et al. 2002)

## *Quartz Crystal Microbalance(QCM)*

The masses of LB films are determined from the monolayer deposited on quartz oscillator plate by using Quartz Crystal Microbalance technique. It is basically a mass sensing device with the ability to measure very small mass changes on a quartz crystal resonator in real-time. It measures mass changes as small as a fraction of a monolayer or single layer of atoms.

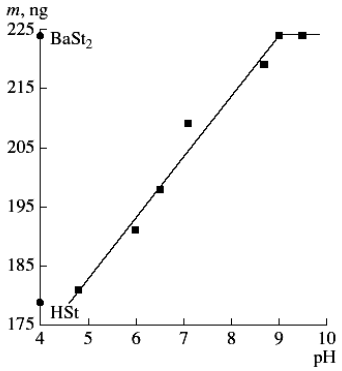


Figure 6.10. Dependence of the mass m of $BaSt_2$ on pH.
(Source: Bukreeva et al. 2003)

Figure 6.10. shows the results of QCM method applied by Bukreeva (Bukreeva et al. 2003). The masses of StAc and $BaSt_2$ monolayers calculated with occupied area by a molecule in the monolayer during transfer were plotted on the ordinate axis.

# CHAPTER 7

# ELECTRICAL PROPERTIES OF LB FILMS

LB films generally show electrically insulating behaviour. Electrical investigations have generally fallen into three main categories, namely conductivity studies, photoelectrical measurements and enhanced semiconductor studies. Besides these, growing interest has evolved recently in pyroelectric and piezoelectric effects in LB films and the utilization of certain electrical characteristics to yield novel sensor devices. Many of these sensors involve changes in conduction due to the presence of gas molecules such as $NO_2$.

The electrical conduction of an LB multilayer is a very complicated process which depends on several factors such as molecular structure, film structure, degree of intermolecular charge transfer, defect density and so on. Several problems are being encountered, such as the limited number of organic molecules with predominant functions, imperfections in LB films, difficulty in controlling molecular deposition precisely, etc. Because of these problems research on the electronic applications of LB films is being hampered. Selectivity is another serious problem for gas sensors which will not be solved using LB film techniques (Moriizumi 1987).

Çapan and coworkers investigated pyroelectric activity using copolysiloxane/eicosylamine alternate layer LB films incorporating different metallic cations such as $Cd^{2+}$, $Ba^{2+}$, and $Mn^{2+}$. They reported that addition of these ions within the LB film multilayers causes a significant increase in the pyroelectric effect and increases the thermal stability of the LB films (Figure 7.1.) (Çapan et al. 2004).

Peterson suggested that the electrical conductivity is often governed primarily by the nature and density of defects within the LB film. Because many LB films contain highly ordered arrays of molecules, it may be expected to observe some anisotropy in conductivity with certain materials. Tredgold and Winter concluded the same expression for measuring tunnelling currents in stearic acid LB films. Tredgold and coworkers also showed that tunnelling currents through cadmium stearate films are dependent on the crystallite size and number of grain boundaries present (Peterson 1990, Tredgold et al. 1981, 1984).

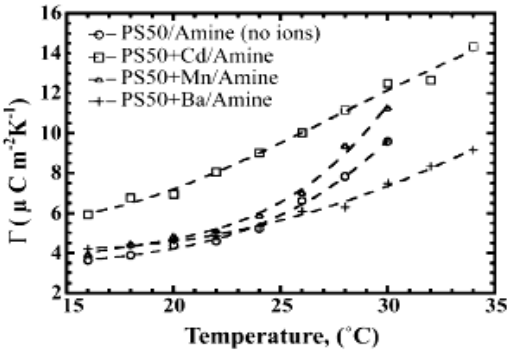


Figure. 7.1. The pyroelectric activity of PS50/eicosylamine alternate layer LB films prepared using a subphase containing either $CdCl_2$, $MnCl_2$ or $BaCl_2$.
(Source: Çapan et al. 2004)

The majority of researchers have attempted to identify LB materials which show a change of electrical conductivity when exposed to low levels of gases. These chemiresistors are simple devices to produce and often show enormous conductivity changes although their recovery time is often slow.

A study on gas sensor using electrical properties of fatty acid Langmuir–Blodgett films was done by Kim and other researchers (Kim et al. 1998). They attempted to investigate the electrical properties of stearic acid LB films to develop a gas sensor. In Figure 7.2.a, their electrode structure for I-V measurement is seen.

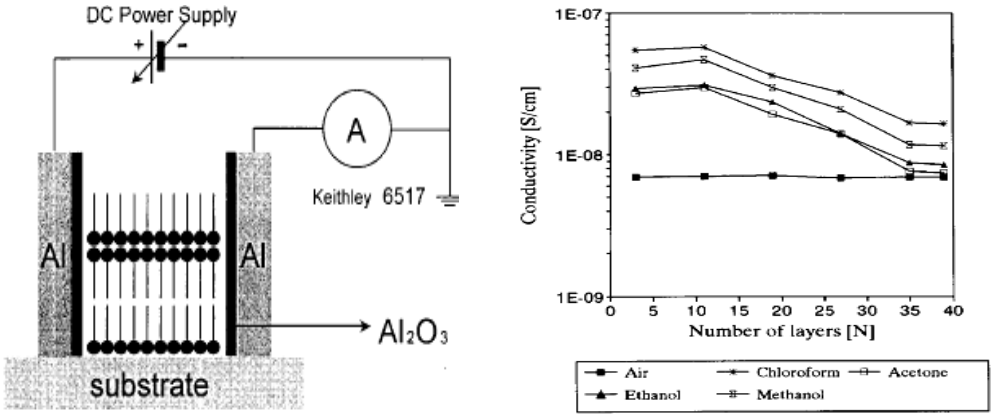


(a) (b)

Figure 7.2. (a) Electrode design for LB films and I–V measurement circuit,
(b) Conductivity change properties of injected organic gases.
(Source: Kim et al. 1998)

The results of this study were as follows: (1) the thickness of the electrode is about 1000 Å by I–V characteristics for in-plane; (2) in the J(current density)–V(Voltage) characteristics, the orders of other current density are acetone < ethanol < methanol < chloroform at the same voltage (15 V); (3) if a change of conductivity is observed by organic gases injection, this phenomenon can be explained by the penetration of organic gases into LB films (Figure 7.2.b).

There is more applied LB film research than ever before with scientists placing their emphasis on the potential use of these molecular assemblies as sensors, non-linear optics materials or electroluminescent emitters. Interest to these fascinating organic assemblies will continue to grow.

# CHAPTER 8

# WATER SORPTION PROPERTIES OF LB FILMS

Langmuir-Blodgett (LB) films, with extremely small and variable thickness might allow to be used in membrane applications to generate large, controllable fluxes. The real challenge, then, is to create LB films which exhibit interesting and valuable selectivity characteristics. Such characteristics could be useful in sensor applications as well as in membrane technology.

Even simple fatty acids are the most well studied LB multilayers, are capable of imparting selectivity. These films are highly anisotropic with distinct hydrophilic, polar "head" group regions and lipophilic, nonpolar "tail" regions. This dual nature gives rise to contrasting sorption characteristics for polar and nonpolar sorbents; a similar phenomenon has been explored in detail for micellar systems which share some of the same anisotropic structural features as LB multilayers (Girard et al. 2002).

Marshbanks and his friends studied the Langmuir-Blodgett (LB) films of calcium stearate using FTIR before, during, and after contact with water and aqueous solutions of hydrochloric acid. The films retain from 1.5 to 3 wt % water of hydration, and they absorb at least 8 wt % (possibly up to 16 wt %) water, probably in voids, when contacted with bulk liquid water. Conversion of calcium stearate to stearic acid caused film dehydration, recrystallization, and an increase in trans conformations (Marshbanks et al. 1994).

Israelachvili found that increased vapor humidity leads to increased water penetration, mainly into the head group-substrate interface region. This effect is greater for ionic head group, for more hydrophilic head group, for more hydrated head groups or surface counterions, and for more loosely packed chains (lower coverage). It results in the swelling of monolayers, an increased lateral mobility and overturning of molecules within the monolayer, increased monolayer fluidity (sometimes leading to a melting transition), to a decreased monolayer-substrate adhesion, and to an increased adhesion between two monolayer-covered surfaces (due to the exposure of the polar groups of the overturned or flip-flopped molecules) (Israelachvili et al. 1992).

Kusano and his friends investigated the characteristics of cellulose LB film humidity sensors using the QCM method on palmitoyl cellulose LB films under fixed

relative humidity. Figure 8.1. shows the dependence of the number of sorbed water molecules $N_{H_2O}$ on the number of layers in the film. At each fixed point of relative humidity p, the number of sorbed water molecules increases with the number of layers (Kusano et al. 1997).

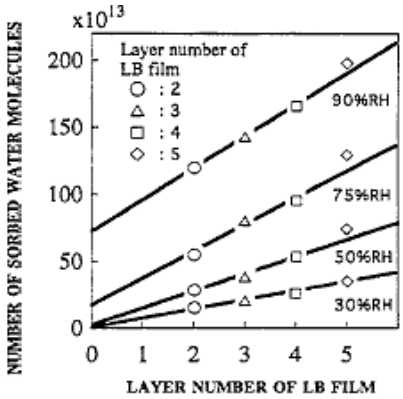


Figure 8.1. Dependence of number of sorbed water molecules on the number of layers in the LB film.

(Source: Kusano et al. 1997)

They reported that the increased number of sorbed water molecules with the number of monolayers in the films revealed the presence of two distinct mechanisms; in the low relative humidity region; Freundlich (linear dependence) and in the high relative humidity region; Polanyi (free condensation of water molecules onto film surface).

Girard and coworkers investigated the relationship between the mass uptake and the swelling of arachidic acid Langmuir–Blodgett films exposed to water vapor using QCM (Figure 8.2.).

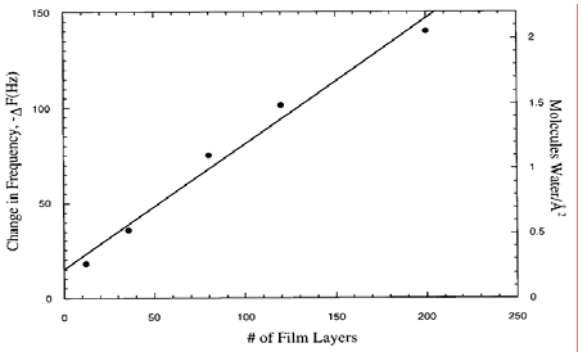


Figure. 8.2. Equilibrium mass uptake of water vapor at $P/P_o$ = 0.6 by arachidic acid LB films of increasing thickness.

(Source: Girard et al. 1999)

They observed that the degree of film swelling is less than that predicted if the water taken up exhibits the molar volume of bulk liquid water. They attribute this difference to a number of factors, including the filling of voids or defects as well as the nonbulk nature of sorbed water. They stated that confinement may also play a role, perhaps by reducing the solubility of water in the film (Girard et al. 1999).

# CHAPTER 9

# MATERIALS AND METHODS

This chapter deals with the materials used in the experiments, the equipments, and the experimental methods applied. It also focuses on the characterization methods.

The experiments done in this study can be grouped under four categories;

- Substrate and equipment preparation,
  - Substrate and equipment (trough, barrier etc.) cleaning
  - Metal film coating on substrate
- Preparation of monolayer and deposition of LB films,
- Characterization of produced LB films ( FTIR, AFM, electrical characterization, etc.)

## 9.1. Materials

Ultrapure water was used to prepare water subphase mixture. It was deionized to 18.3 MΩ cm resistivity using Labconco water purification system and Elix 5 Millipore Milli-Q-Gradient Millipore system.

The glass substrates were purchased from Nima, Marienfeld and Matsunami. In some experiments, besides bare glass slides, metal coated glass slides were also used. For this purpose, silver wire (Alfa Aesar, 0.5 mm diameter, annealed, 99.9 % metals basis) and chromium wire were evaporated thermally in vacuum chamber (Leybold Univex 300).

The chemicals used during the experiments are given in Table 9.1. The chemicals in these tables were used for different purposes as stated near them. They were used as received without further purification. The purity of the organic amphiphile (stearic acid), organic solvent (benzene) the inorganic bases and metal salts added to the water subphase under study is of great importance in film production. Therefore, in the experiments, it was tried to use chemicals with highest purity available.

Table 9.1. Chemicals used for production of LB films.

| Chemicals | | Specifications |
|---|---|---|
| Stearic acid (StAc) | Monolayer Material | >99.5 %, Fluka, 99 %, Nacalai, > 95 %, Sigma |
| Benzene | Monolayer-Solvent | >99.5 %, Riedel-deHaen, |
| Acetone | Cleaning Solvent | >99.8 %, Merck |
| 2-propanol | | 99.5 %, Riedel-Aldrich |
| Ethanol | | 99.5%, Panreac |
| Zinc chloride | Subphase Solution | >99.9 %, Wako, 98-100.5 %, Merck, >96 %, Sigma |
| Calciumchloride-dihydrate | | >99.9 %, Wako |
| Calcium chloride | | >96 %, Sigma |
| Borax | Buffer Solutions for subphase | >99 %, Sigma |
| Potassium phosphate-monobasic | | 99 %, Sigma |
| Sodium phosphate-dibasic | | 99 %, Sigma |
| Sodium bicarbonate | | 99.5 %, Sigma |
| Sodium carbonate | | 99.5 %, Merck-Riedel |
| Sodium hydroxide | pH adjustment | >98 %, Sigma |

## 9.2. Substrate and Equipment Preparation

The nature and surface quality of a substrate are of a vital importance in achieving a film of the required uniformity. The glass substrates were cleaned according to two main procedure. Transsonic 660/H Elma 300W ultrasonic bath cleaner was used through all cleaning process to remove hydophobic and hydrophilic contamination on substrates. RBS 35 concentrate cleaning solution was provided from Fluka.

→ Procedure I:

- RBS 35$^{o}$ concentrate cleaning solution (%5): 30 min, 30$^{o}$C
- Acetone: 15 min, 30$^{o}$C
- Ethanol: 15 min, 30$^{o}$C
- Deionized water: 20 minutes × 5 times, 30$^{o}$C

→ Procedure II:

- Acetone: 15 min, 30$^{o}$C
- 2-propanol: 15 min, 30$^{o}$C
- Ethanol: 15 min, 30$^{o}$C
- NaOH (1M) : 15 min, 30$^{o}$C
- Deionized water: 20 minutes × 5 times, 30$^{o}$C

After cleaning stage, the cleaned glass slides were kept in deionized water.

For metal coated glass substrates, silver wire was cut into small pieces and put onto heated tungsten boat of chamber "Leybold Univex 300 Metal Thermal evaporator", as shown in Figure 9.1.


Figure 9.1. LEYBOLD UNIVEX 300 high vacuum device.

This chamber have 300 mm diameter and can reach up to $10^{-6}$ torr base pressure. The glass substrates were subjected to silver and chromium evaporation from a tungsten boat in vacuum chamber at around $5\times10^{-6}$ Torr evaporation pressure for different time periods, at defined current values (for chrome, 70 A; and for silver 140-150 A). The thickness of coated silver and chromium is around 70-80 nm and 10 nm around respectively. After metal coating process, surface becomes available for electrical characterization as well.

Another important issue is the treatment of the trough and barriers between experiments; in other words, the cleaning procedures. Any surface in the trough should be free of surface-active materials. For this reason, acetone and ethanol were preferred to clean barrier and teflon trough and then they were rinsed with large amounts of pure deionized water.

## 9.3. Monolayer Formation

To form the monolayers and Langmuir-Blodgett films and study their properties, Teflon Langmuir trough with automated surface balance in KSV 3000 LB device was used.

The aqueous subphase solutions were prepared first. Different concentration ranges from $1\times10^{-5}$ M to $1\times10^{-3}$ M of metal salts ($CaCl_2$ and $ZnCl_2$) were studied and the effect of concentration on monolayer formation was investigated. Adjusted concentrations of phosphate, carbonate or borax buffers and 1 M NaOH were mixed for half an hour to make the subphase pH around 9-10 which is required for calcium chloride subphase. For Zinc chloride subphase, addition of phosphate buffer or 1 M NaOH made the subphase solution neutral (6-7). pH measurements were done by Metrohm pH 744 model device.

Surface cleaning prior to monolayer spreading was done by simply "washing" the subphase surface with benzene. Benzene solution of StAc was prepared as stock solution and stored at $4^oC$ in the refrigerator. The concentration was 0.92 mg/ml. The solutions were spread by Hamilton microliter syringe at required amount (50-100 μl) onto the subphase solution by distributing the droplets over the entire trough area.

In monolayer formation, temperature, pH, the concentration of subphase solution and monolayer material amount were changed to reach the optimum conditions. Studied parameters are given in Table 9.2. pH of subphase solutions was adjusted by buffer solutions ($Na_2CO_3$-$NaHCO_3$, $KH_2PO_4$-$Na_2HPO_4$, $Na_2B_4O_7$) at differing concentrations and NaOH (1 M) and HCl (1 M) solutions.

Surface pressure relaxation with time studies were done at constant surface area of LB film and moreover surface area shrinkage with time experiments were also conducted at constant surface pressure.

## 9.4. Deposition of LB Films

Films were fabricated using a commercial deposition system (KSV 3000 LB device, Figure 9.2.). The trough has a working area of $425\times150$ $mm^2$ and 1.3 lt water volume capacity. It is enclosed in a chamber and continuous air flow was maintained in the chamber. The two barriers are hyrophilic polyacetal and trough is hydrophobic polytetrafluoroethylene (Teflon). The trough has a dipping well in the middle. Surface pressure is measured by platinium Wilhelmy plate. The resolution for the surface

pressure measurement is 0.004 mN/m, according to the instrument specifications. Barrier and dipping speeds can be controlled. Aluminium thermo regulated base plate provides required temperature for subphase. Temperature and pH are monitored using sensors touching to the subphase surface. The software controlled operation make robust deposition of monolayers onto the substrates.

Table 9.2. Experiment conditions through metal stearate LB films production process.

| ***Subphase*** | | *Pure water* | *Ionic subphase ( $ZnCl_2$ )* | *Ionic subphase ( $CaCl_2$ )* |
|---|---|---|---|---|
| Temperature ( $^oC$ ) | | 15±0.5, 20±0.5 | 15±0.5, 20±0.5, 25±0.5 | 15±0.5, 20±0.5 |
| Monolayer concentration ( mg/ml ) | | 0.92 | 0.92 | 0.92 |
| Spreading solvent | | Benzene | Benzene | Benzene |
| Spreading quantity ( μl ) | | 60, 100, 110 | 60, 70, 100 | 50, 60, 100 |
| Surface pressure ( mN/m ) | | 23, 25, 30, 35 | 8, 10, 12, 15, 20, 25, 30 | 10, 15, 20, 25, 28, 30, 35 |
| Barrier rate ( mm/min) | | 3, 5, 10 | 3 | 3 |
| Dipping speed ( mm/min) | | 1, 2, 3, | 1, 2, 10 | 1, 2, 3, |
| Substrate type | | Glass (Nima, Marienfeld, Matsunami) | Glass (Nima, Matsunami, Marienfeld), Silver coated glass (Nima, Marienfeld), | Glass (Nima, Matsunami, Marienfeld), Silver coated glass (Nima, Marienfeld), |
| Ionic concentration (M) | | - | $1\times10^{-5}$, $1\times10^{-4}$, $5\times10^{-4}$, $1\times10^{-3}$, $1.5\times10^{-3}$ | $1\times10^{-5}$, $1\times10^{-4}$, $5\times10^{-4}$, $1\times10^{-3}$, $1.5\times10^{-3}$ |
| pH | | 5.6, 5.7, 6.1, 6.2, 6.3, 6.5, 6.7 | 6.1, 6.2, 6.3, 6.5, 6.7, 6.8 | 9.5, 9.8, 9.9, 10.2 |
| Buffer Solutions concentration | $Na_2CO_3$ – $NaHCO_3$ | - | - | $1\times10^{-3}$ M-$1\times10^{-3}$ M |
| | $KH_2PO_4$-$Na_2HPO_4$ | - | $1\times10^{-4}$ M-$1\times10^{-4}$ M | $1.5\times10^{-4}$ M-$1\times10^{-4}$ M |
| | $Na_2B_4O_7$ | - | - | $1\times10^{-4}$ M, $3\times10^{-4}$ M |
| NaOH (1 M)-pH adjustment | | - / + | + | + |

The spread monolayer solutions were allowed to evaporate along at least 30 minutes before compressing the monolayer to desired surface pressure value. Using KSV 3000 LB device, after the solvent evaporation, the monolayer were compressed using a couple of movable barrier with compression rates of 3 to 10 mm/min while the surface pressure was recorded using the Wilhelmy platinium plate. Once surface transfer pressure was reached, the monolayers were allowed to stabilize for 5 minutes before conventional dipping began at a given speed.

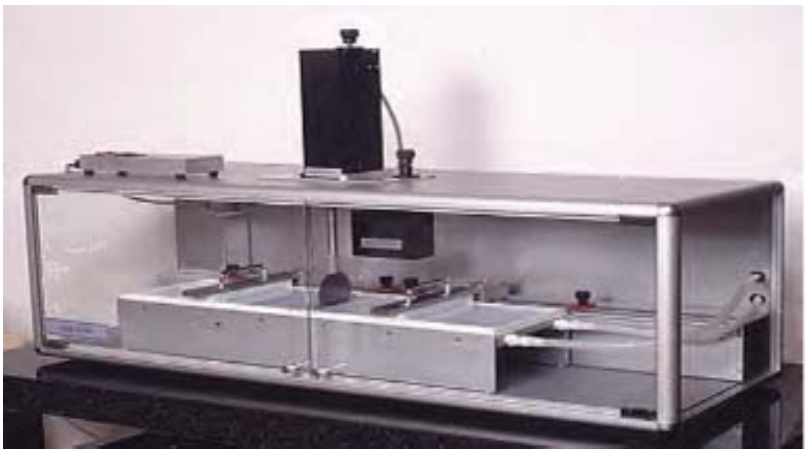

Figure 9.2. KSV 3000 model Langmuir-Blodgett device.

Monolayers were deposited by vertical dipping method onto bare glass slide and/or silver coated glass slide at (15-25) ±0.5 $^{o}$C and at a constant surface pressure in the range of 5-35 mN/m. Y type deposition (Figure 5.1) were applied for monolayer fabrication. Thus it is possible to prepare only odd-numbered monolayer films in the usual way. The substrate dipping speed (up and down motion through the monolayer) were in the range of 1-10 mm/min. Barrier rate and dipping speeds play essential role to be able to produce high quality films. Therefore these parameters and surface pressure were optimized during the experiments (Table 9.2.). Moreover, temperature effect was also investigated. Throughout the experiments, calculated transfer ratios were recorded as well.

After deposition of the first monolayer, the glass slide was kept dry in a desiccator with $P_2O_5$ for at least 15 h. Typically, required number of layers of studied compound monolayers were transferred after this period. For multilayer transfer, the substrate was dried between each cycle for a given period of time (20 minutes). The produced LB films were finally stored in a $P_2O_5$ dessicator prior to characterization.

## 9.5. Characterization of LB Films

Contact angle measurements were performed on the bare and coated glass surfaces by KRÜSS-G10 contact angle measurement device. Surface hydrophobicity and hydrophilicity were measured.

Intralayer structure of the exposed samples were determined by using X-ray powder Diffractometer (Phillips X'Pert Pro) using Grazing Incidence attachment at 20$^{o}$C. The instrument was operated with Cu-K$\alpha$ radiation with Ni filter adjusted to 45 kV and 40 mA. The scan was performed in the 2-70° 2θ range with the help of Grazing Incidence attachment. Using this technique, lattice structure, d-spacings and tilting angles were defined with Bragg's law. Crystal size was calculated according to Scherrer equation from diffraction patterns.

The infrared spectra of LB films, specimen / KBr pellets were taken by using transmission mode, horizontal ATR spectroscopy (Pike Technologies) 80 degree specular reflectance accessories, in the reflection-absorption mode with Excalibur DIGILAB FTS 3000 MX type Fourier Transform Infrared Spectrophotometer at 20$^{o}$C with a resolution of 4 cm$^{-1}$. DTGS type detector was used for all measurements. First, background and then LB films spectrums were collected with 50 scans. All spectra reported in this study were results of substraction of the curves measured in background spectra from those measured sample spectra. This method gave information about the functional groups in produced thin LB films. The purity of stearic acid, benzene and $ZnCl_2$ prior to usage were investigated as well preparing KBr pellets. For benzene spectrum, a small amount of benzene was dropped onto KBr pellet. IR spectra of skimmed LB films from the water surface were taken after mixing with KBr.

DSC runs were carried out up to 200$^{o}$C at 10 $^{o}$C/min heating rate under 40 ml/min nitrogen purge stream flowrate with 2.5 mg of sample using Shimadzu DSC50.

To study water vapor adsorption and desorption behaviour of stearic acid, calcium and zinc stearate, ACS environmental chamber (Angelantoni Industries) was used. One gram of each compound was dried at different temperatures; stearic acid at 50$^{o}$C, calcium and zinc stearate at 85$^{o}$C to avoid melting. Then, dried substances were put into humid atmosphere at desired relative humidity in the range of 20% to 60% at 25$^{o}$C and to get adsorption and desorption characteristics. The weight of substances was taken per one minute after one hour equilibriation period. By means of computer controlled Sartorius GP 603S balance, all data was taken robustly till 30 minutes.

By Multimode SPM, Nanoscope IV, Digital Instrument device, AFM measurements were performed in contact and tapping modes. In these modes, oxide-sharpened silicon nitride probes and etched Si probes were used. Before using the instrument, glass slides were cut to a suitable area (< (1 cm×1 cm)). With piezotube, sample was fitted in x, y and z direction. Height or phase image data taken with tapping mode was obtained by using AFM in two-dimensional and three-dimensional. This mode was applied to observe topography of surfaces (glass, metal coated glasses and LB films) revealing various structures. The channel width of electrical measurement set-up for in plane measurement was also measured with contact mode. Every image has been measured at room temperature in the air.

Scanning Electron microscope (Phillips XL-30S FEG) was used to see the morphology of films at 20$^{o}$C with 5 kV and 15 kV respectively. The samples were coated with gold and palladium metals by using sputtering technique.

The electrical characteristics of metal stearate LB films were investigated as well. I-V measurements were conducted with controlled set-up in two ways; through plane and in plane. For both these DC experiments, the voltage supply was Keithley 230 Programmable Voltage source and the current was measured by means of a Keithley 485 Auto ranging Picoammeter. The measurement interval was 5 sec. The films were in direct contact with two silver electrodes.

Figure 9.3. shows I-V measurement set-up and representative electrode structure for through plane measurements. These measurements were done in the room conditions at 20$^{o}$C and 45% RH. The electrode structure was prepared by means of aluminium mask. Bottom silver electrode length is 50 mm and 0.5 mm width and there are 2 contacts with 2 mm diagonal length, top silver electrodes length are 15 mm and 0.5 mm width and there are 12 contacts with 2 mm diagonal length contacts. Voltage source and current device were connected to the circuit in series. Voltage was given to point 0 and the current values taken from 1, 2 and 3 connection points respectively. The nine layer of $ZnSt_2$ LB films conductivity was measured by this method.

The second arrangement was in plane as it is seen in Figure 9.4. The system of interdigitated electrodes improved the sensitivity of the measurements. The channels were made in silver layer by using a steel needle and the width of these channels were around 60-70 μm measured with AFM contact mode and required numbers of LB layer were deposited. Total length of the channels measured with a calliper was around 36 cm. The measurements were done at 20$^{o}$C and 40% RH.

A serial circuit was formed with voltage source and picoammeter. The currents were measured from the points 4, 5 and 6 respectively when the voltage was given to point 1. Another current value read from point 6 when voltage was applied to 2. The thirteen layer of $ZnSt_2$ LB films conductivity was measured by this method.

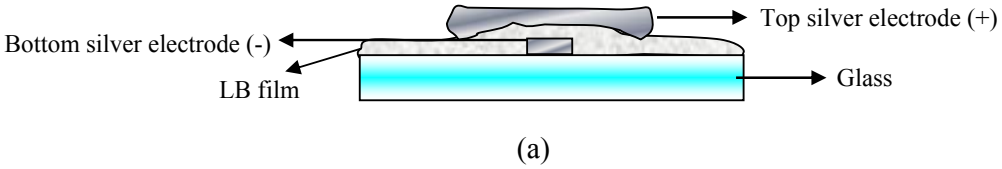


(a)

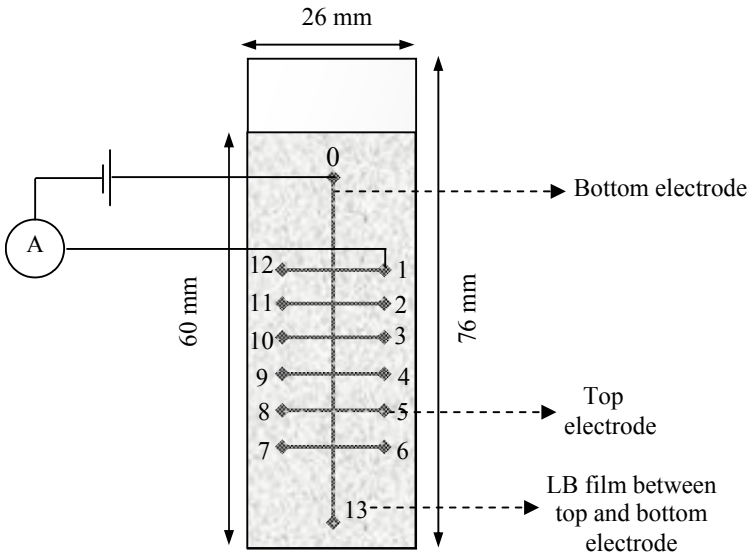


(b)

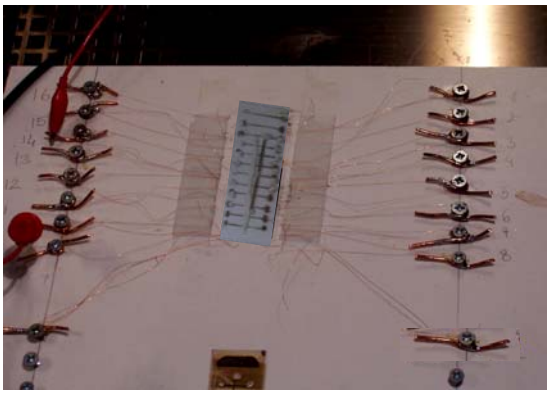

(c)

Figure 9.3. Through plane arrangement, (a) Side and (b) Top view representative pictures, (c) picture of I-V measurement set-up.

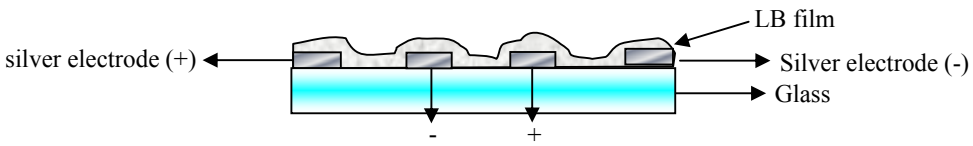


(a)

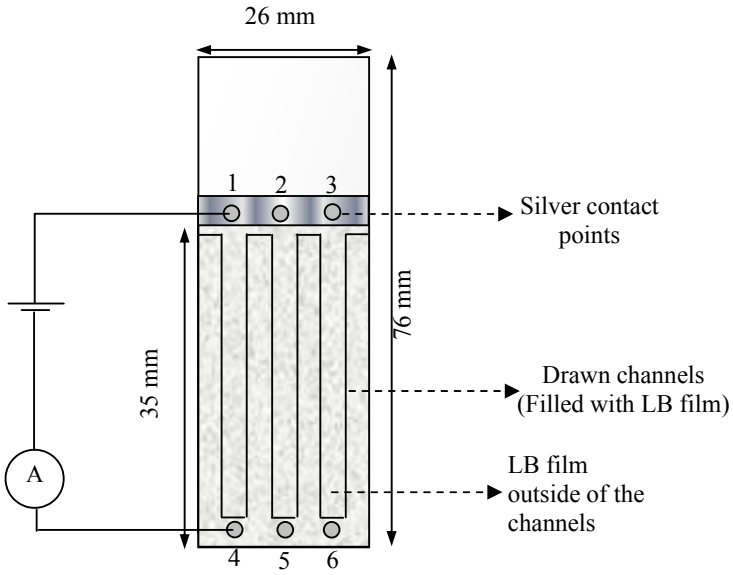


(b)

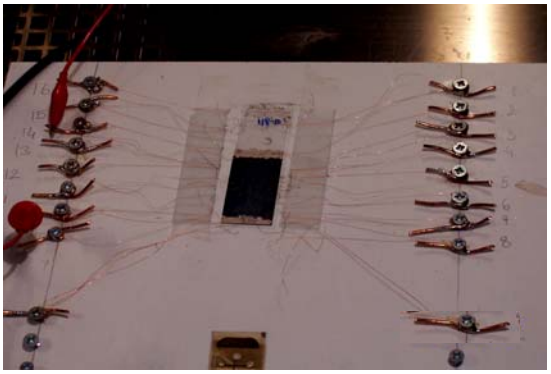

(c)

Figure 9.4. In plane arrangement, (a) Side and (b) Top view representative pictures, (c) picture of I-V measurement set-up.

For both arrangements, after coating with LB film, electrical contacts to the top and bottom electrodes were made by using an air-drying silver paste (Figures 9.3., 9.4.). In plane measurements were done under nitrogen and humid atmosphere as well (Figure 9.5.).

(a) (b)

Figure 9.5. Electrical measurement set-up (a) in the glove box under nitrogen and (b) in the environmental chamber under humid atmospheres.

815-PGB “LA PETITE” glove box was used to provide nitrogen atmosphere for measurements. ACS environmental chamber (Angelantoni Industries) was used to obtain humid atmosphere (at 25$^{o}$C and desired relative humidity; 20% to 60%).

# CHAPTER 10

# RESULTS AND DISCUSSION

## 10.1. Raw Materials Characterization

The purity of stearic acid under study is of great importance. Any contaminant in the stearic acid may be incorporated in the monolayers, even if it is soluble in the water. The same purity criteria should be implemented for organic solvent benzene used to prepare the spreading solution, and the inorganic acids, bases and salts added to the water subphase.

In this respect, infrared spectra of stearic acid, benzene, various $ZnCl_2$ compounds and DSC curves of stearic acid samples, $ZnSt_2$ and $CaSt_2$ were taken in below figures.

### 10.1.1. IR Spectra of Substances

Figure 10.1. illustrates the IR spectrum of stearic acid-KBr pellet prepared in the ratio of 2 mg / 200 mg. The StAc molecule has a well defined infrared absorption peak near 1705 $cm^{-1}$ due to the stretching vibration of the C=O in the carboxylic acid group COOH and the band near 1300 $cm^{-1}$ due to the C-H-O stretching and deformation vibrations. The bands around 2916 and 2848 $cm^{-1}$ are due to the antisymmetric and symmetric methylene stretching vibrations. Around 1475 $cm^{-1}$ a band is observed representing the methylene bending mode. This spectrum shows that stearic acid does not contain organic impurity.

On the other hand, benzene was used as monolayer spreading material. Figure 10.2. gives IR spectrum of benzene. The aromatic C-H stretch appears at 3100-3000 $cm^{-1}$. There are aromatic C=C stretch bands (for the carbon-carbon bonds in the aromatic ring) at about 1500 $cm^{-1}$. Two bands are caused by bending motions involving carbon-hydrogen bonds. The bands for C-H bends appear at approximately 1000 $cm^{-1}$ for the in-plane bends. In the C-H bending or ring breathing mode region, the spectrum of benzene shows bands at 1820 and 1960 $cm^{-1}$, corresponding to the C-H out-of-plane bending vibrations.

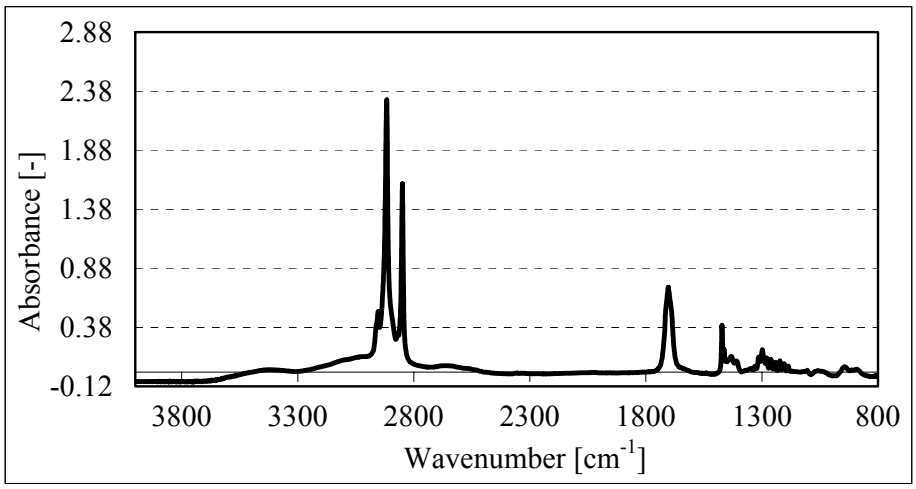


Figure 10.1. IR spectrum of pure StAc (99.5%).

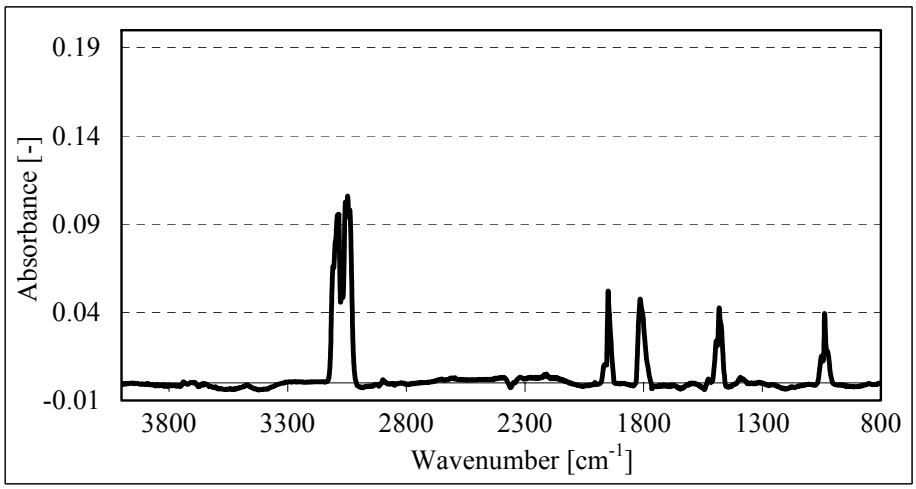


Figure 10.2. IR spectrum of benzene drop in KBr pellet.

The IR spectra of different $ZnCl_2$ compounds (99.9%, 98-100.5%, >97%) used in the experiments was shown in Figure 10.3. The water bands in the region of at about 1607 $cm^{-1}$ (OH stretching and HOH bending modes), 3594 and 3522 $cm^{-1}$ double peak are clearly seen. $ZnCl_2$ is a hygroscopic material and it should have absorbed water vapour from air during preparation.

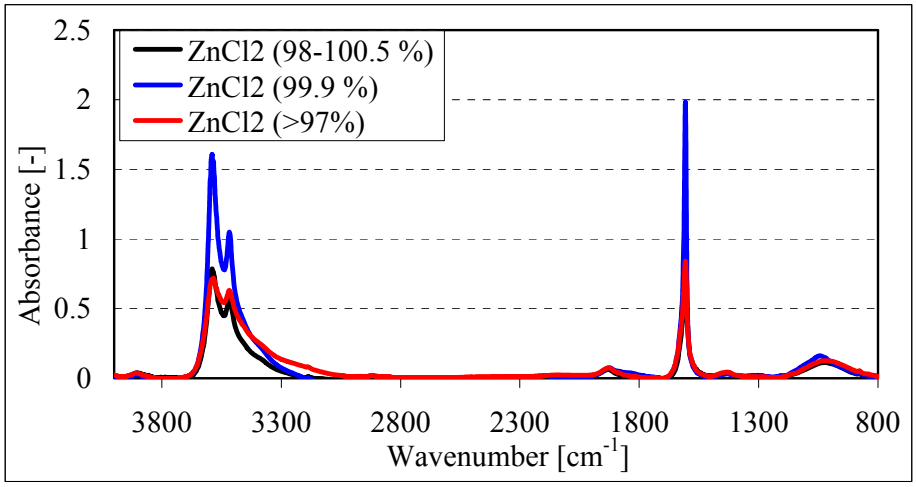


Figure 10.3. IR spectra of three different $ZnCl_2$ (96%, 98-100.5%, 99.9%).

### 10.1.2. DSC Analysis

DSC curves of stearic acid samples, $ZnSt_2$ and $CaSt_2$ are shown in Figure 10.4. and 10.5. respectively. There is no significant differences between the shapes of the stearic acid curves and peak minimum temperatures corresponding to melting point of stearic acids and the heat of melting determined from the peak area are summarized in Table 10.1.

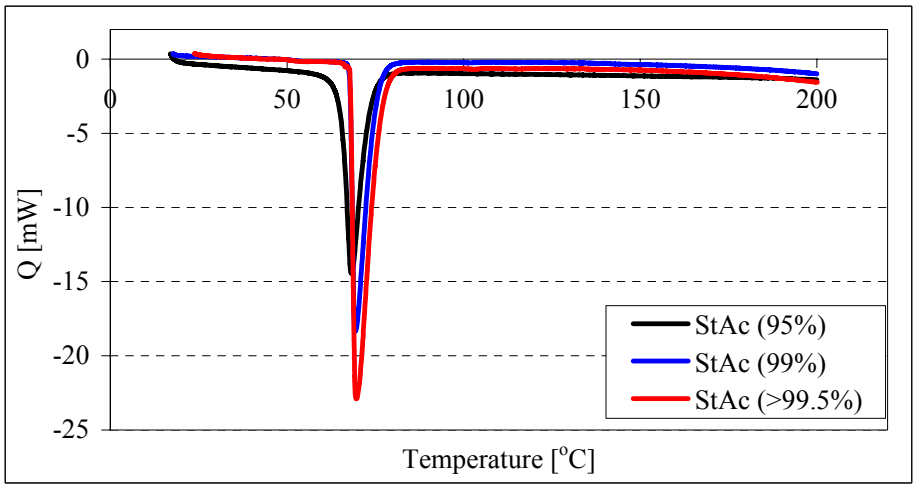


Figure 10.4. DSC curves of stearic acid samples (95%, 99%, 99.5%) between 25°C and 200°C.

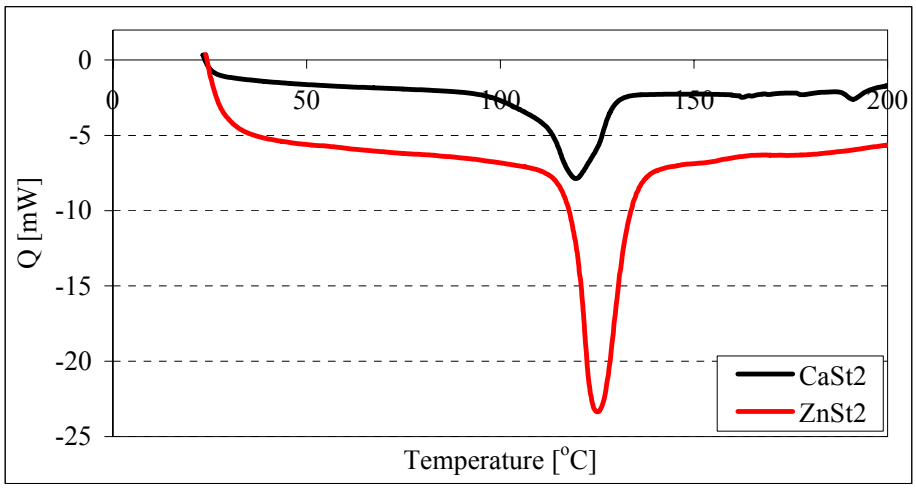


Figure 10.5. DSC curves of $ZnSt_2$ and $CaSt_2$ between 25°C and 200°C.

$ZnSt_2$ and $CaSt_2$ optical solid-liquid phase transition were observed at higher temperatures than stearic acid as it is seen in Table 10.1. Heat of fusion per kg for both compounds is also reported in the table as well. There was not any peak corresponding to impurity that might be present for all curves taken. Expected sharp peaks at defined points were observed.

Table 10.1. DSC Peak Minimum Temperatures and corresponding heat of fusions.

| *Sample* | *Melting Temp. (°C)* | *Heat of fusion (kj/kg)* |
|---|---|---|
| StAc (99.5%) | 70 | 210 |
| StAc (99%) | 69 | 206 |
| StAc (95%) | 68 | 198 |
| $ZnSt_2$ | 125 | 117 |
| $CaSt_2$ | 119 | 183 |

$ZnSt_2$ melted at higher temperature (125°C) and had lower heat of fusion than $CaSt_2$. StAc which is at highest purity melts at a bit higher temperature, around 70°C and takes more heat than other two type during melting.

## 10.2. Monolayer Studies

There have been considerable advances in developing new experimental techniques to obtain information about the microstructure on the molecular level of monolayers. Surface pressure measurements have been the main source of understanding of insoluble monolayers.

### 10.2.1. Stearic Acid Surface Pressure/Area Isotherm

It is known that the shape of the isotherm depends on the amphiphilic substance and also on the nature and temperature of the subphase. Stearic acid monolayer was compressed at a velocity 3 mm/min to 53 mN/m surface pressure. There are typical phases of stearic acid; liquid-condensed ($L_2$) or super-liquid (LS) phases were observed in the isotherm at 293 K and pH 5.6 respectively (Figure 10.6.). The passage from $L_2$ phase to LS phase nearly appears at around 23 mN/m. These results are repeatedly reproduced. The collapse pressure ($\pi_C$) was around 53 mN/m. This is in agreement with the study done by Avila (Avila et al. 1999).

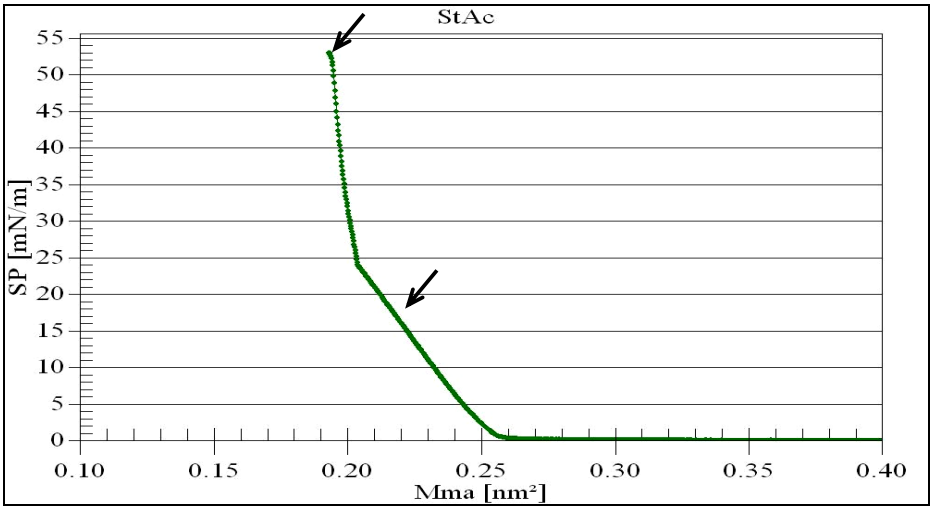


Figure 10.6. The typical π-A isotherm of stearic acid on the water surface at pH 5.6 and 20°C.

In all experiments conducted, the greatest uncertainty in measuring molecular areas in isotherms was in determining the amount of material delivered to form the film. The concentration of sperading solution was determined initally and freshly prepared, but evaporation of a volatile solvent sometimes led to suprisingly changes.

### 10.2.2. Surface Pressure Relaxation of Stearic Acid Monolayer

Figure 10.7. shows the surface pressure relaxations of monolayers of stearic acid compressed to the surface pressure areas of 0.22 ($L_2$) phase and 0.19 $nm^2$/molecule (LS) phase. At the surface area of 0.22 $nm^2$/molecule shown by arrow in Figure 10.6., the surface pressure slightly decreases from 16 to 12.1 mN/m after 100 min. At 0.19 $nm^2$/molecule shown by arrow in Figure 10.6., on the other hand, the pressure sharply decreases from initial value of 53 mN/m in ca. 20 min and finally reaches 12.2 mN/m. During the compression of this film, there has been no surface pressure drop as observed in the collapse process of the monolayer (Gaines 1966). Since the solution to the subphase water or evaporation of stearic acid is very slow at room temperature, the magnitudes of these relaxations are much larger than that expected from loss by solution or evaporation.

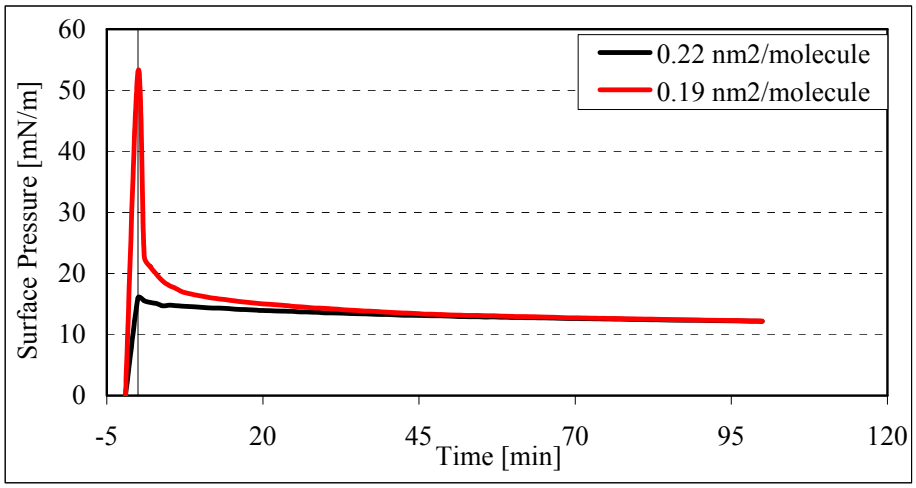


Figure 10.7. Surface pressure relaxation curves of stearic acid compressed to area of 0.22 and 0.19 $nm^2$/molecule.

Here it is seen that after compressed Langmuir film of stearic acid to a target surface area with a moderate speed and then the surface pressure was recorded with time lapse, to examine the effect of surface pressure relaxation. A fast decrease of area at the beginning, and after some time, a constant area is probably a rearrangement of molecules in the monolayer takes place (promotion of crystallization within the two dimensional space) or collapse of monolayer.

The plausible mechanism of the second type relaxation is the collapse of the monolayer such that some molecules in the compressed monolayer slip out upward to

form molecules with disordered chain by gaining the free space. Then, the surface pressure could decrease owing to the decrease in number of molecules in the two dimensional monolayer spaces. In other words, the compression energy in excess is released by the monolayer collapse during pressure relaxation. The evidence of such collapse is provided by the FT-IR/RES experiments done by Umemura (Umemura et al. 1996). The another mechanism that the holes in the L film are gradually filled with surrounding molecules might be partly responsible for the gain of the free space in this case.

### 10.2.3. Nucleation Modelling of Stearic Acid Monolayer

The collapse process by nucleation and further growth of the nuclei formed for the stearic acid monolayer on a Milli-Q water subphase was evaluated in detail by applying the mathematical model developed by Vollhardt (Vollhardt et al. 1992). Experimental data for change of area with time at 25 mN/m constant surface pressure were used for this purpose (Figure 10.8).

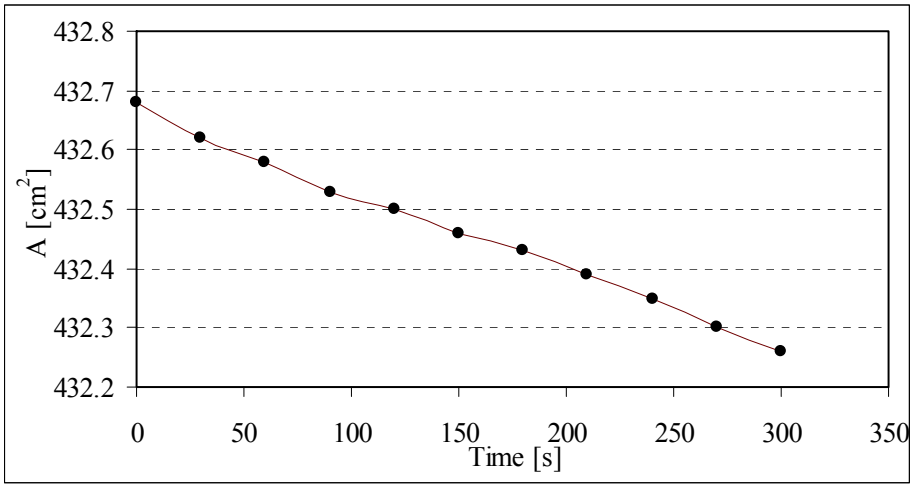


Figure 10.8. Area change vs time for stearic acid monolayer at 25 mN/m and 20$^{o}$C.

If this experimental data can be adjusted to the conditions of one of the theoretical mechanisms of nucleation and growth, μ vs. time linearity is obtained (Figure 10.9.). For the stearic acid monolayer on a Milli-Q water subphase (pH 6.7), keeping the surface pressure 25 mN/m constant, the values of $t_i$ and $K_s$ are obtained by linear regression of the μ versus t curve (Equation 4.8). According to the equation, specific constant, $K_s$ is $3.32\times10^{-4}$ and $-t_i$ is found as 8.73 s.

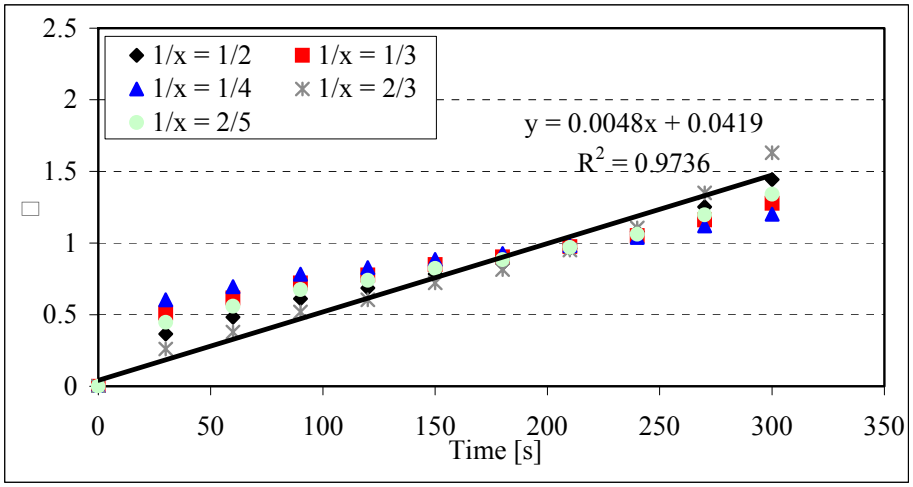


Figure 10.9. Mechanism of nucleation type A at 20°C and pH 6.7.

In Figure 10.9., the straight line which exhibits a better fit to the experimental data corresponds to 1/x = 2/3 (type A, Table 4.2). This fitting occurs when the mechanism of nucleation is instantaneous with hemispherical nuclei formed and growth through the edges.

Figure 10.10. Schematic presentation of the overlap of hemispherical centers growing on a monolayer (instantaneous nucleation).
(Source: Vollhardt et al. 1992)

Vollhardt found similar results for octadecanoic acid layer area relaxation at 30 mN/m and T = 35°C and represented this behavior as in Figure 10.10. (Vollhardt et al. 1992). For the instantaneous nucleation, a state of homodispersity was formed by the freely growing regions as well as by regions in which two or three centers overlap.

### 10.2.4. Temperature Effect on Stearic Acid Monolayer Behaviour

Stearic acid isotherms in Figure 10.11. taken at different temperatures are similar in shape. While temperature decreases from 20°C to 15°C, Langmuir film condensed and this decrease shifted the isotherm to progressively smaller areas at low

surface pressures. Thus, the area per stearic acid molecule where condensed liquid phase starts became lower at 15°C than molecular area at 20°C. After compressing both monolayers at different temperatures, they eventually coincides at higher pressures.

The surface compression ($C_S^{-1}$) moduli of stearic acid monolayers at studied temperatures were calculated according to Equation 4.6 and found their high dependency on temperature. The surface compression modulus decreased with decrease in temperature (Table 10.2.).

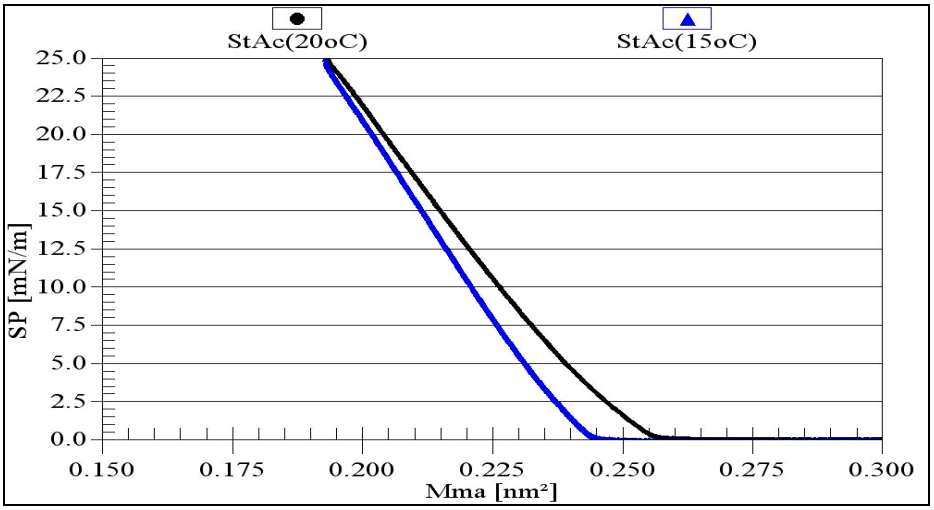


Figure 10.11. Stearic acid isotherms taken at pH 6.5 and different temperatures (15°C and 20°C).

Table 10.2. Surface compression modulus of StAc layers at the $L_2$ phase.

| *T(°C)* | *pH* | *$C_S^{-1}$(mN/m)* |
|---|---|---|
| 15 | 6.5 | 95 |
| 20 | 6.1 | 112 |
| 20 | 6.2 | 93 |
| 20 | 6.3 | 86 |
| 20 | 6.5 | 75 |

Higher $C_S^{-1}$ value (95 mN/m) at 15°C than the value 75 mN/m at 20°C means that more densely packing of stearic acid molecules occur on the surface and cohesion is higher at this temperature.

### 10.2.5. pH Effect on Stearic Acid Monolayer Behaviour

The obtained data from stearic acid isotherms showed that for the stearic acid monolayers at pH 6.1 adjusted with 1 M NaOH in solution, transition from gas phase to liquid expanded phase appears at lower molecular area than higher pH values (Figure 10.12.).

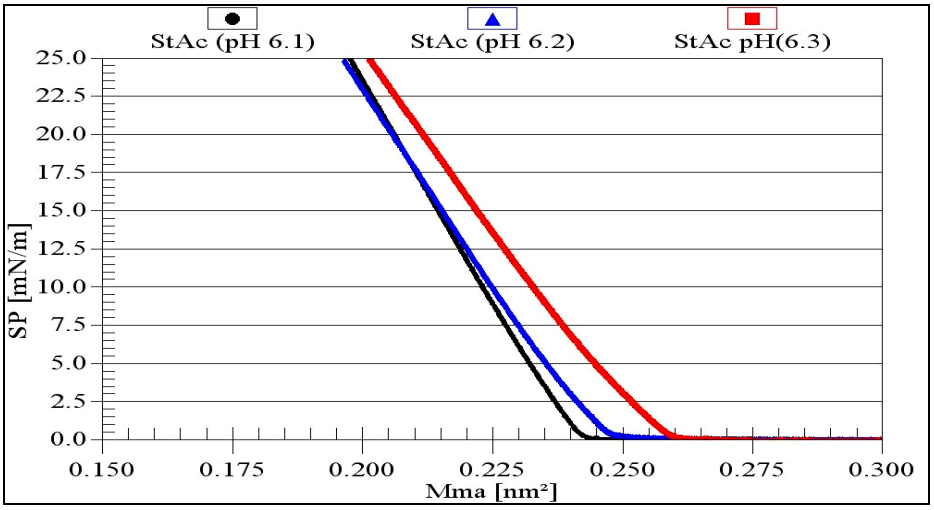


Figure 10.12. Stearic acid isotherms taken at different pH media (6.1, 6.2 and 6.3) at 20°C.

It can be said that acidic or basic property of subphase influences the packing density of molecules. Surface compression moduli corresponding to studied pH values are given in Table 10.2. as well. It is clearly seen that with increasing pH at the same temperature, surface compression moduli of StAc layers decreases. With highest pH value, the packing of stearic acid molecules occur loosely and the attraction force between them is lower. pH dependency also indicates that the nature of the instability i.e. the relaxation processes below and above the critical pH is caused by different factors. Here, it can be concluded that pH values near to the $pK_A$ (5.6) value (Petty 1996), are more proper to study considering ordered structure. In this pH range, deposition of stearic acid molecules onto glass surfaces is more suitable to obtain good transfer ratios. On the other hand, there are controversial $pK_A$ values of stearic acid. Kanicky and Shah reported it as 10.1 from titration of water soluble potassium stearate (Kanicky and Shah 2002). They observed a two step titration curve for this process and they took the first step as the basis of $pK_A$. Nevertheless, complete crystallization of stearic acid at lower pH values was reported by the same authors.

### 10.2.6. Compression Speed Effect on Stearic Acid Monolayer Behaviour

The degree of mobility and arrangement of stearic acid molecules in the monolayer are determined by the extent of monolayer compression. Hence, the compression of molecules is one of the essential step which require special attention for obtaining a monolayer without defect. Figure 10.13. presents the isotherms of monolayers of stearic acid at pH 5.7 and 20$^{o}$C taken with different compression speeds from 3 mm/min to 10 mm/min.

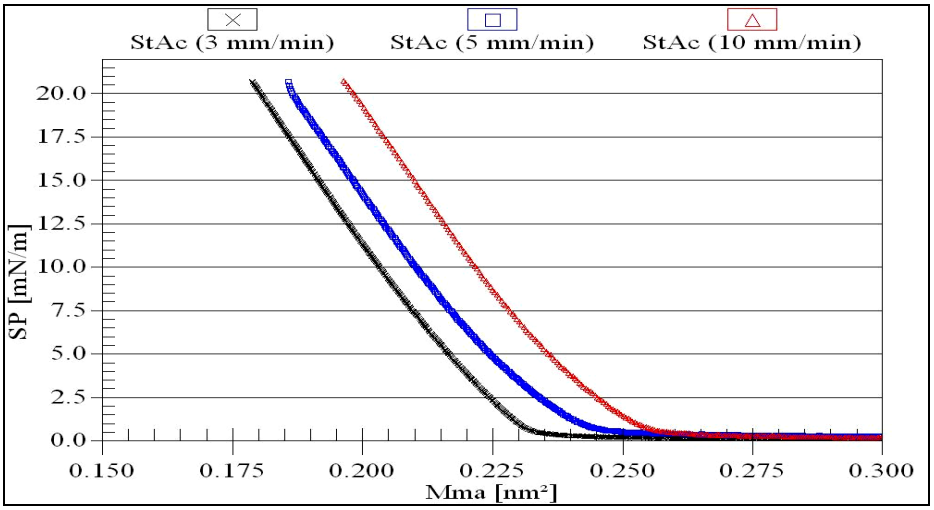


Figure 10.13. π-A isotherms of stearic acid monolayers at different compression speeds.

As shown in Figure 10.13., there is a change with the decrease in barrier speed from 10 mm/min to 3 mm/min and isotherm curves are found to shift towards lower mean molecular areas with further decrease in compression speed. The change of mean molecular area with compression speed may usually be related to the compression of a meta-stable monolayer under non-equilibrium conditions. Under such conditions, the molecules still either undergo reorganization on the water surface or dissolve into subphase water during compression process. The decrease of the effective mean molecular area with decrease of barrier speeds essentially reflects the increase of time duration of the compression process. In this point of view, it can be explicated that monolayer compression rate could change the collapse behaviour as well.

### 10.2.7. Metal Soaps (Calcium and Zinc stearates) Surface Pressure/Area isotherms

It should be known that the properties of a floating stearic acid Langmuir monolayer are substantially dependent on the ionic content of the water subphase. The initial presence of metal cations in the aqueous subphase causes definite changes in the behaviour of the monolayer that depend on the nature of the cation, the cationic charge and the pH value of subphase.

Stearic acid monolayer isotherms were recorded from pure deionized water subphase. However, the formation of $CaSt_2$ and $ZnSt_2$ Langmuir layers, it is necessary to study at subphases containing these metal cations.

The expected $pK_A$ for n-octadecanoic acid on a water surface is 5.6 (Gaines 1966). Ionization itself depends on the pH of the solution. If proton is rich (low pH), stearic acid does not dissociate. If proton is poor (high pH), stearic acid must dissociate into ions. If buffers are used such as $Na_2B_4O_7$, formation of RCOO-Na is possible in the solution phase, but it is completely soluble (ionizable). Instead, the divalent cations binds to form insoluble (tight bound) monolayer since the monovalent cation soaps are not so stable as divalent cation soaps.

At high enough pH values dependent on the metal cation nature, the stearic acid monolayer is condensed and converted completely to the salt form what is manifested by the characteristic compression isotherm without $L_2$/LS phase transition. The critical pH value dependent on the metal cation type and concentration in the subphase correlates as a rule with the state of maximal monolayer condensation and stability.

The pH values of the subphase at which molecules of stearic acid are converted into $CaSt_2$ layer is around 9-10 and into $ZnSt_2$ layers, around 6-7 (pH range calculations for studied cations are given in Appendix A). The phosphate, carbonate and borax buffers were used to obtain higher and stable pH media because on exposure to the atmosphere, water absorbs carbondioxide and its pH decreases over a period of a few hours. Buffers can be any kind. As it is stated in Bragg's study, presence of different anions in the subphase may lead to different $CaSt_2$ conversions depending on pH range (Bragg et al. 1964). However, the studied pH range suits maximum calcium stearate pH range.

In $ZnSt_2$ experiments, pHs were always lower than 8.5. It is in neutral region to prevent $Zn(OH)_2$ precipitation. For $CaSt_2$ experiments, pHs were generally between 9-

10. $Ca(OH)_2$ only precipitates at pH 13, thus there were no problem in studying this pH range as well.

Figure 10.14. shows the characteristic compression isotherms of StAc monolayer and $1\times10^{-3}$ M zinc and calcium chloride containing aqueous subphase at 20°C. In the stearic acid monolayer, the liquid condensed $L_2$ phase and the super-liquid LS phase (more correctly solid phase) were observed while there was only an LS phase in zinc stearate and calcium stearate monolayers.

The isotherms of all the stearates exhibit similar behaviour (Hasmonay et al. 1980), like the curves in Figure 10.14., and is characterized by a very steep slope after a transition plateau which corresponds to the coexistence of "islets" of condensed matter with a very dilute homogeneous phase.

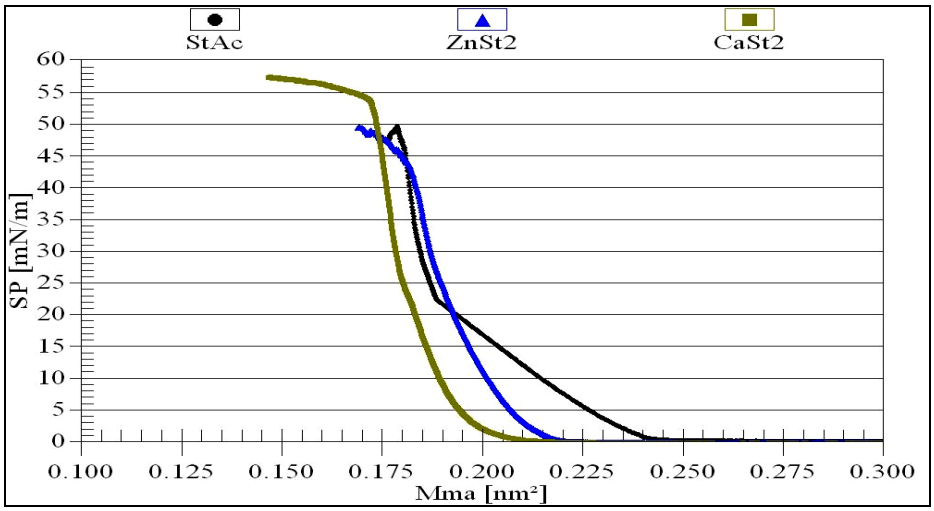


Figure 10.14. Monolayer behaviour of StAc, $CaSt_2$ and $ZnSt_2$ Langmuir monolayer isotherms taken at 20°C and different pH media (StAc, 5.6; $ZnSt_2$, 6.6 and $CaSt_2$, 9.5).

On the subphase surfaces containing a divalent cation $Zn^{2+}$ or $Ca^{2+}$, transition pressure ($\pi_t$) decreased. The slope of the metal stearate isotherms are bigger and monotonously smooth without any noticeable phase transitions. The isotherm of zinc stearate and calcium stearate are similar and the common features of curves of $ZnSt_2$ and $CaSt_2$ are the general decrease in the monolayer compressibility and the collapse behaviour.

Two main types of isotherms shape have been recorded: terminated by a "spike" or a "plateau" in the region of the maximum surface pressure attained. The "spike" at

$\pi_C$ has been interpreted as being due to the growth of "organized" trilayers (stabilized by head group hydrogen bonding). The "plateau" at $\pi_C$ has been associated with the irregular fracture of the ionized monolayers.

For the same low compression rate like here (3 mm/min), the plateau at $\pi_C$ reflects the greater resistance of the monolayer toward transformation into a 3D phase. The limit of the monolayer stability is characterised by the magnitude of $\pi_C$. StAc and $ZnSt_2$ layers collapse at approximately around 50 mN/m and $CaSt_2$ layer collapse at 53 mN/m. The magnitude of $\pi_C$ for each substance reflects the limit of the monolayer stability with respect to transformations into a 3D phase. Just after collapse, it is clear that a bimolecular film started to form and yielding a trilayer and on the aqueous surface, whitish streaks indicating collapsed material was observed.

It was revealed that StAc and $ZnSt_2$ had a more sparse molecule packing in the monolayers than $CaSt_2$ monolayers. With addition of metal cations, the area per molecule decreased even at gaseous phase. This comparison confirms the well known phenomenon that both cations exert a strong condensing effect, yielding solid type monolayers. In these conditions, these cations stabilize the floating monolayer by diminishing the repulsion forces between the head groups of stearic acid molecules. As it is seen from Figure 10.14., the interaction of stearic acid with zinc and calcium was different depending on the interaction.

Table 10.3. gives the ionic size and electronegativities of the calcium and zinc metal ions. It is seen that $Ca^{2+}$ has lower electronegativity and higher ionic size. If the electronegativity of $Ca^{2+}$ ions are compared with oxygen electronegativity (3.5), the big difference (larger than 2) can give information about the ionic bond between these atoms. However, electronegativity difference for $Zn^{2+}$ and oxygen is not enough to give such a interpretation.

Moreover, although $CaSt_2$ contains calcium ions with higher molecular size, the attraction force between molecules in $CaSt_2$ layer is bigger and gives smaller area per molecule. As the electronegativity of the metal ion decreases, the bonding between the metal ion and the fatty acid carboxylate ion tends to acquire stronger ionic character (Rajagopal et al. 1998). Zinc ions have higher electronegativity and this leads to an increase in the covalent character of the bond between the cation and the carboxyl groups.

Table 10.3. Transition points in π-A isotherm and area per molecule values.

| *Material* | *Liquid-solid transition* | | *Ionic radius of cations (Å)* | *Eletronegativity of cations* |
|---|---|---|---|---|
| | *Surface pressure (mN/m)* | *Area per molecule ($Å^2$)* | | |
| Stearic acid | 23 | 0.19 | - | - |
| Calcium stearate | 2 | 0.195 | 0.099 | 1.0 |
| Zinc stearate | 2 | 0.205 | 0.074 | 1.6 |

The limiting area per molecule, appears to be governed by the tendency for covalent bonding, with a smaller area per molecule associated with covalent bonding and with a higher area per molecule associated with ionic bonding. The simplest relation to describe this event is the relation between the limiting area per molecule and the Pauling electronegativity of metal counterion. Although Zinc has higher electronegativity, Table 10.3. shows that the area per molecule of zinc stearate monolayers is bigger. Therefore, it is large to be correlated with its electronegativity as in the case of zinc fatty acid salts LB films in the study of Dutta. For calcium ions, the same interpretation due to low moleculear area instead of high one might be done in conformity with the measured area per molecules values reported in the literature (Dutta et al. 2001).

Rajagopal also reported that this higher covalent character of the bond gives films with the hydrocarbon chains perpendicular to the substrate and maximum area per molecule and belonged to $BaAd_2$ with the lowest electronegativity. However, they studied at neutral pH region. Therefore some arachidic acid layers might not be converted completely to metal-arachidate layers (Rajagopal et al. 1998).

## 10.2.8. Nucleation Modelling of Metal Stearates

A similar procedure done for stearic acid was followed for determination of the nucleation and growth mechanism for stearic acid monolayer on a subphase containing $5\times10^{-4}$ M $CaCl_2.2H_2O$ at pH 9.52 and $ZnCl_2$ at 6.7 for a constant pressure of 10 mN/m. Experimental data for change of area with time were recorded at 10 mN/m constant surface pressure (Figure 10.15. and 10.17.). Figure 10.16. and 10.18. illustrate the nucleation modelling results for $Ca^{2+}$ and $Zn^{2+}$ ions. The straight line which is more adjustable to the experimental data corresponds to 1/x = 2/5 and to a progressive

nucleation mechanim (type B) as described in Table 4.2. This mechanism means that hemisperical nuclei formed and grow from the edges (Figure 10.19.). Similar result was obtained for a $ZnCl_2$ subphase.

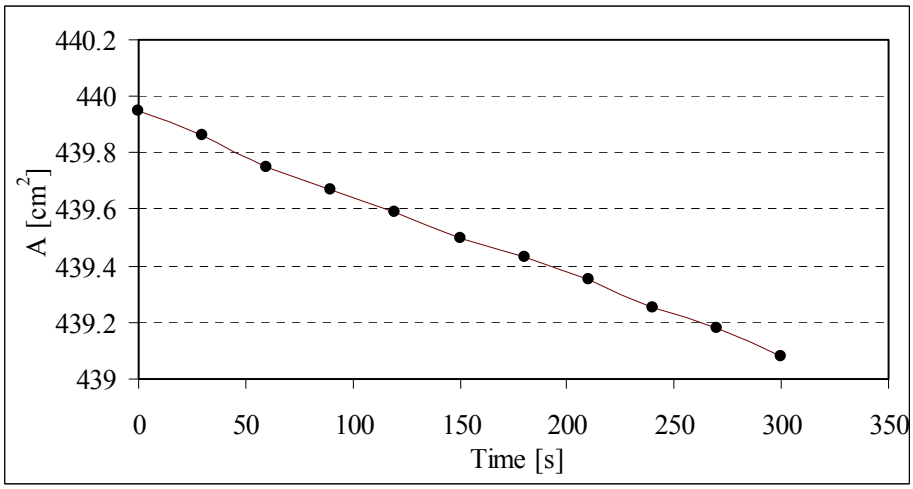


Figure 10.15. Area change vs time for $CaSt_2$ monolayer at 10 mN/m and 20°C.

By means of equation 4.8 and using linear equations obtained from Figure 10.16. and 10.18., $K_s$ and $t_i$ values can be calculated for both $ZnSt_2$ and $CaSt_2$ layers. $K_s$ values are $1\times10^{-6}$ and $1.1\times10^{-6}$ and $-t_i$ values are 53.6 and 49.9 respectively. The results of negative induction time ($t_i$) obtained from the plot of μ versus t showed that the induction time for the nuclei growth of the stearic acid monolayer on a Milli-Q water subphase is shorter than the induction time in the presence of ions. Thus, the nucleation process in its intial phase is faster in the presence of the ions especially for $CaSt_2$ monolayer.

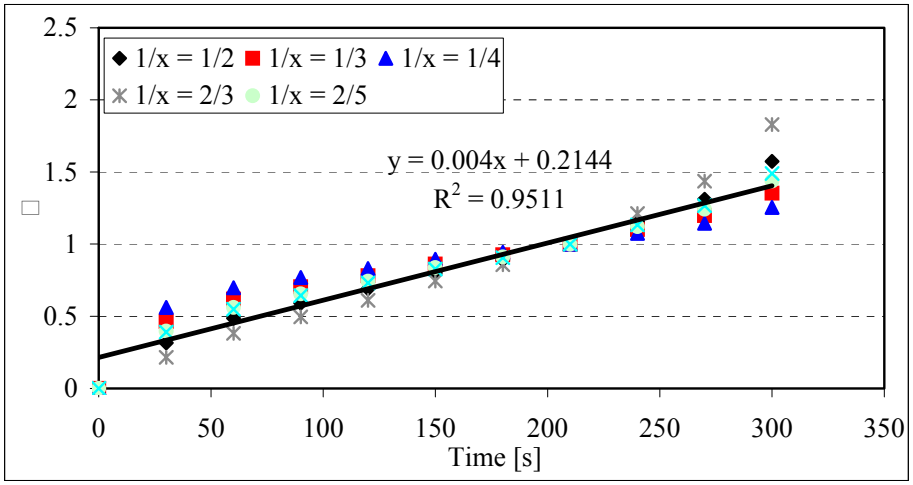


Figure 10.16. Mechanism of nucleation type B at 20°C and pH 9.5 for $CaSt_2$ monolayer.

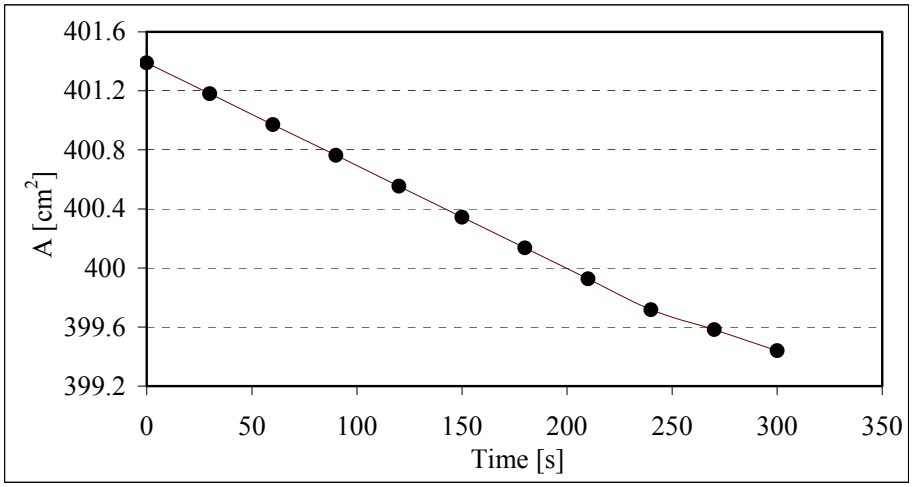


Figure 10.17. Area change vs time for $ZnSt_2$ monolayer at 10 mN/m and 20°C.

The progressive growth from the edges in the presence of electrolytes may be attributed to the tendency of the monolayer molecules to a preferential association with the ions in the solution, which contributes to the growth from the edges of the nuclei. In the absence of electrolytes, however, the growth of the centers may be related to the incorporation of neighbouring molecules through the edge of the centers instantaneously.

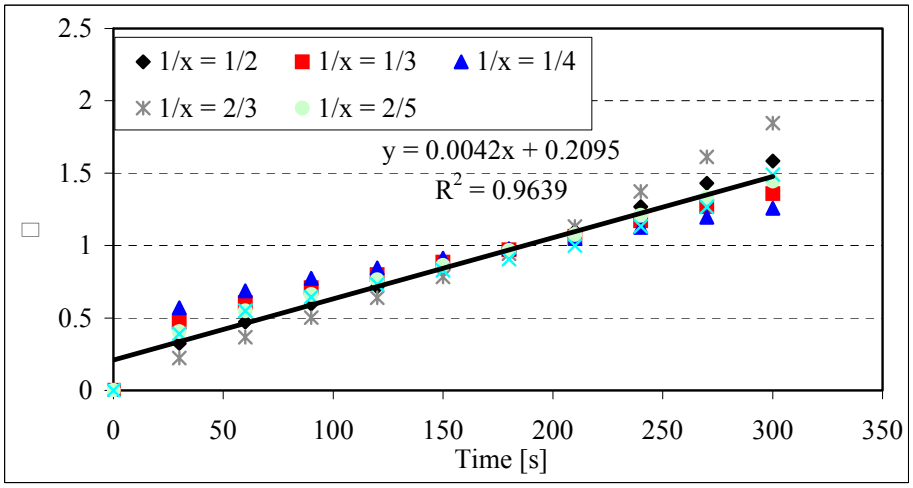


Figure 10.18. Mechanism of nucleation type B at 20°C and pH 6.7 for $ZnSt_2$ monolayer.

Figure 10.19. Schematic presentation of the overlap of hemispherical centers growing on a monolayer (progressive nucleation).
(Source: Vollhardt et al. 1992)

The instantaneous nucleation was defined as a state of homodispersity formed by the freely growing regions as well as by regions in which two or three centers overlap before. For the progressive nucleation, polydispersity of the centers is expected due to their different lifetimes. Consequently, the size of the freely growing and overlapping regions is different. In the shaded regions, two centers overlap, and in the dark regions, three centers overlap.

## 10.2.9. Concentration Effect on Metal Stearate Monolayer Behaviour

The effective lateral diffusion of stearic acid molecules in the monolayer apparently hinders the formation of some extended structure attached to the monolayer surface and consisting of stearic acid molecules and ionic or polar components of the aqueous phase. In spite of this fact, monolayer compression and the corresponding effective reduction and restriction of surface lateral diffusion of stearic acid molecules results in the stabilization of negative charges in the monolayer and can create conditions for realization of the effect of discreteness of surface charges.

The metal concentration in the subphase can also affect the phase transition behaviour of compressed stearic acid layer by forming metal stearates. In Figure 10.20., for $CaSt_2$ layers at pH 9.5 and 20$^{o}$C, this behaviour is easily seen. When the concentration of $CaCl_2$ is lower such as $1\times10^{-5}$ M, it is possible that the product may change from Ca-stearate rich acid salt to stearic acid rich acid salt. Acid salt is a compound between acid and its metal salt.

If metal concentration increases from $1\times10^{-5}$ to $5\times10^{-4}$ and then to $1\times10^{-3}$ M, transition from gas to solid phase occurs more sharply and at lower surface area per molecule. This results in condensed and more organized structure. The effect of concentration on monolayer composition can be explained as added amount of $CaCl_2$ are distributed evenly in the bulk solution and only part of them near surface reacts with

monolayer. The advantage of using higher metal cation concentration is to assure the formation of complete metal stearate.

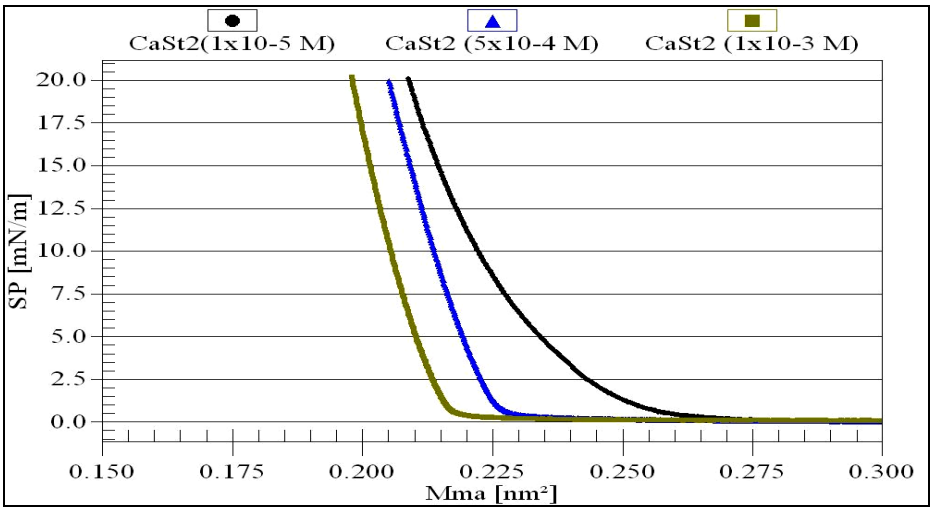


Figure 10.20. π-A isotherms of $CaSt_2$ taken at chosen $CaCl_2$ concentrations.

As a result of electrostatic interactions, the conditions for effective localization of ordered calcium complexes in the aqueous phase in the vicinity of the charged surface of the monolayer (especially for polar calcium complexes with $OH^-$ and $Cl^-$) could be created. The possible achievement of geometric and stereochemical matching and the complementarity of surface charges, calcium complexes and site symmetry of ions in the crystal lattice of clusters under a definite extent of monolayer compression apparently initiate the nucleation and formation of clusters discovered on the monolayer surface.

## 10.2.10. Temperature Effect on Metal Stearate Monolayer Behaviour

Surface pressure/area isotherms of zinc stearate monolayers recorded at three different temperatures of the aqueous subphase (pH 6.1) are presented in Figure 10.21. It is seen that moderate tempearture variations may influence monolayer isotherms.

The decrease in temperature leads to less thermal motion, tending to condense the film and transition from gas phase to condensed liquid phase occurs at lower molecular area (Roberts 1990). This is not suprising that the monolayer at lower temperature is in more ordered structure than the one at higher temperature as in the case of three dimensional world.

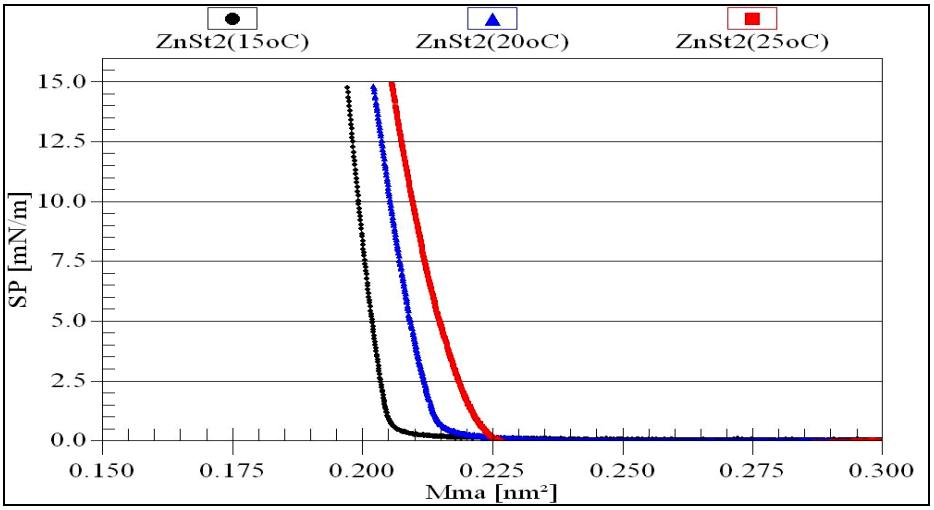


Figure 10.21. π-A isotherms recorded on $ZnCl_2$ aqueous subphases ($5\times10^{-4}$ M) at different temperatures (15°C, 20°C, 25°C).

If surface compression ($C_S^{-1}$) values of $ZnSt_2$ are calculated according to Equation 4.6, both surface compression values strongly decreases with temperature (Table 10.4.). Since high $C_S^{-1}$ values are characteristic of films showing a high degree of cohesion, it becomes evident that with lowering temperature, stearate molecules were more densely packed. Therefore, an increase of surface area in the LC phase can be expected on increasing the temperature, since the interactions between stearate molecules at the interface lesser.

Table 10.4. Surface compression modulus values of $ZnSt_2$ layers at the LC phase.

| *T(°C)* | *pH* | *$C_S^{-1}$(mN/m)* |
|---|---|---|
| 15 | 6.1 | 424 |
| 20 | 6.1 | 340 |
| 20 | 6.2 | 272 |
| 20 | 6.5 | 228 |
| 20 | 6.8 | 171 |
| 25 | 6.1 | 285 |

Small vaues of $C_S^{-1}$ data corresponding to the LC region at higher temperatures for $ZnSt_2$ monolayers can be explained by the phenomenon that the formation of complexes is easier at a higher temperature. The higher molecular energy results in the decrease of intermolecular interactions at the interface, which facilitates the approach of

cations toward the monolayer and hydration water can be expelled from the monolayer as the temperature rises because of higher thermal agitation.

### 10.2.11. Influence of pH on Metal Stearate Monolayer Behaviour

The quality of LB films can be related to the pH dependent complexation of cations with the fatty acid monolayer. The limiting monomolecular area ($A_o$) was dependent of the pH values irrespective of metal stearate type as it is seen in Figures 10.22., 10.23. and 10.24. It increased with increasing pH at 20°C but decreased at 15°C.

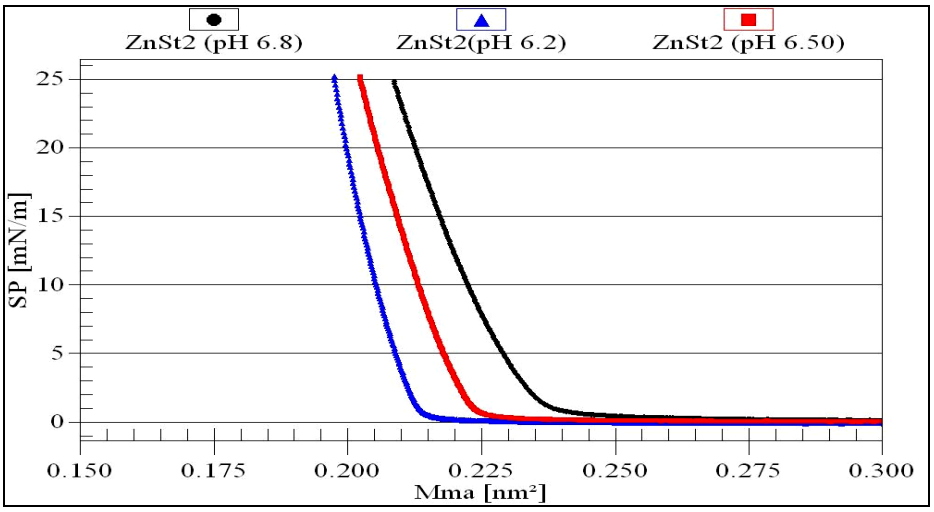


Figure 10.22. π-A isotherms of $ZnSt_2$ at different pH media (6.2, 6.5 and 6.8).

The subphases at $1\times10^{-3}$ M $ZnCl_2$ concentration and 20°C with different pH values affect the $ZnSt_2$ monolayer isotherms (Figure 10.22.). However, the slopes of curves are different. The curve with highest slope belongs to the subphase at pH value of 6.2, the area per molecule at solid phase region is the smallest. Hence, complete condensation was observed at this area. This pH may be the critical pH for zinc stearate formation. For above pH values; 6.5 and 6.8 collapsed layers may be observed. For higher pH values, the stability of the monolayer is reduced.

It may be possible that as the pH is raised, aqueous ions undergo hydrolysis and specific soluble hydroxide complexes may be formed. It is difficult to predict what particular hydroxide species of zinc forms directly under the organic monolayer since the concentration and pH at the interface are unknown. However, it may be the interaction with a particular species of zinc hydroxide complex though it is known that

these complexes is dominant at high concentration of $Zn^{2+}_{(aq)}$ and pH range bigger than 8.5. Hence, the process of hydrolysis may explain the fact that the monolayer goes a series of structures as the pH is raised.

Surface compression moduli were calculated at each subphase pH value and listed in Table 10.4. At high pH value at 20°C, surface compression modulus of zinc stearate layer is lowest. This result emphasizes the significance of studying at lower pH values close to 6 to obtain more ordered zinc stearate layer structure and get better transfer ratios onto substrates.

$CaSt_2$ monolayer isotherms behaved differently at different temperatures; 20°C and 15°C respectively (Figure 10.23. and 10.24.). The subphases were $5\times10^{-4}$ M $CaCl_2$ concentration with different pH values. In the experiments done at 20°C, the average area per molecule at 10 mN/m surface pressure is not constant with increasing pH. The area at pH 9.5, appears to be reduced by as much as 6 %. This could be related to the presence of 3D crystal formation at high pH. The ions repel each other at pH 9.9.

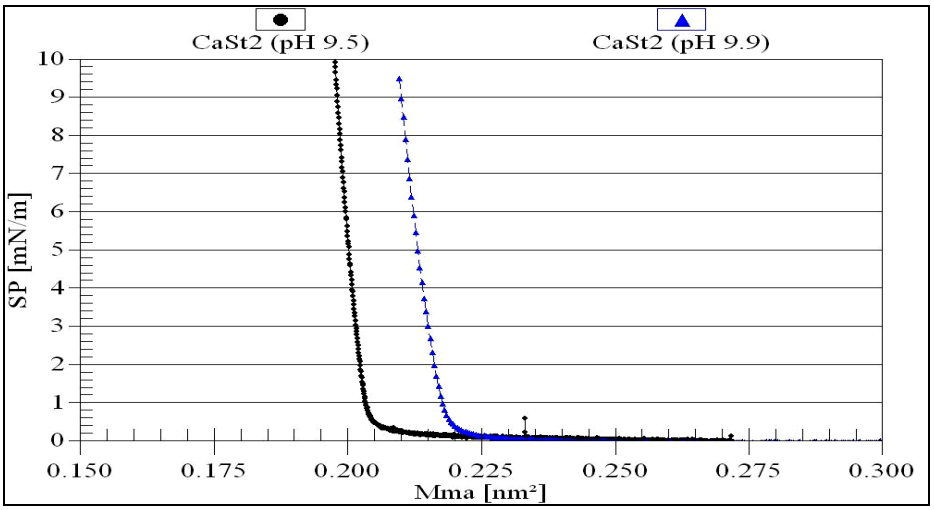


Figure 10.23. π-A isotherms of $CaSt_2$ taken at T = 20°C and different pH media (9.5, 9.9).

The behaviour of calcium stearate monolayer film shows significant difference at 15°C subphase temperature. The limiting area of calcium stearate decreased with pH increase. It is obvious that there is an interaction between the positively charged $Ca^{2+}$ ions and the negatively charged surface of the stearic acid monolayer, and this interaction increases with decreasing the subphase temperature. The calcium stearate forms the more stable and better packed monolayer at the air/water interface when

temperature is low although pH is high. The low temperature and high pH made unknown interaction between molecules led to formation of different complexes.

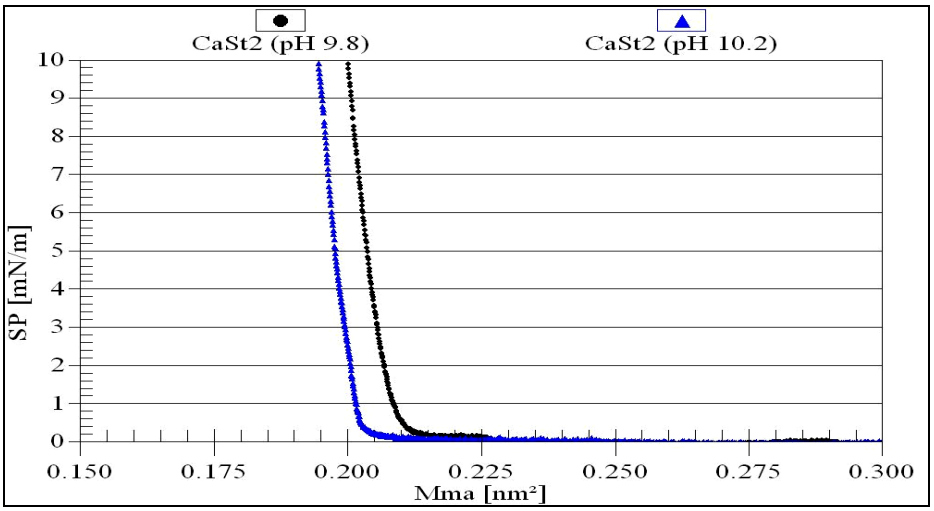


Figure 10.24. π-A isotherms of $CaSt_2$ taken at T = 15°C and different pH media (9.8, 10.2).

The substantial changes in monolayer properties in different pH regions for calcium stearate are possibly caused by the changes in the character of intermolecular interactions in the monolayer, when the physical state of the monolayer is determined not only by the interactions between individual molecules of stearic acid or calcium stearate but also by the principal role played by interactions between new calcium-containing structures formed under the surface of the monolayer. These interactions were influenced by both temperature and pH.

## 10.3. Deposition of Stearic Acid and Metal Soaps

It is important to understand the deposition characteristics of a new LB film material in order that its properties at the macroscopic level may be accounted for by the arrangement of its molecules within each monolayer and that of the layers themselves. There are many characrization tools which have been utilized when studying LB films.

### *Transfer Ratio*

The calculation of transfer ratio; measurement of area loss from floating monolayer represents the most straightforward method characterising its deposition.

This method allowed us to measure the transfer ratio of the floating monolayer as the thickness of the solid LB film is built up layer by layer.

### 10.3.1. Stearic Acid Deposition

In stearic acid isotherm, most proper transfer phase was LS. Therefore it is better to transfer stearic acid layer above 22-23 mN/m which is the transition point to LS phase. More ordered and regular structure was obtained in this way. During stearic acid LB film production, pH and substrate type were also important.

#### 10.3.1.1. pH Effect on Stearic Acid Deposition

Figure 10.25. shows the deposition results of StAc monolayers onto bare glass slides taken at 20$^{o}$C and 25 mN/m surface pressure at different pH values. It can be said that more proper pH value which is close to unity is 6.1. In this pH value, the distribution of deposition values taken at each second through the substrate surface is in narrower area. At lower pH values close to 6.1. is more ordered structure might be obtained as explained in monolayer studies.

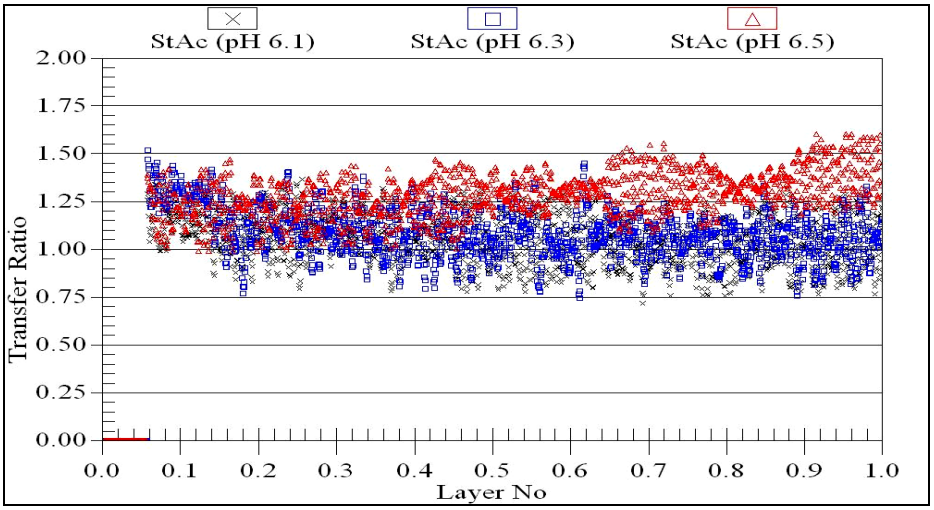


Figure 10.25. pH dependency of StAc layer transfer.

Besides these, the stearic acid molecules can self-aggregate into two dimensional crystalline domains, even at zero pressure shown by Li (Li et al. 2001). This results in the inhomogeneity of the monolayer and the structure defects in LB films originate from the monolayer and are conserved upon deposition.

### 10.3.1.2. Substrate Effect on Stearic Acid Deposition

In deposition of stearic acid layers onto silver coated glass surfaces, prolonged exposure of the cleaned metal surface to the subphase liquid changes the deposition from reactive to nonreactive. Presumably, this results from oxidation and roughening of metal in the aqueous solution. Thus, on surface there are some hydrophilic and hydrophobic local areas were formed. This variety on surface directly affected the deposition as seen in Figure 10.26. Here, StAc monolayer transferred at pH 6.5 and 25 mN/m surface pressure.

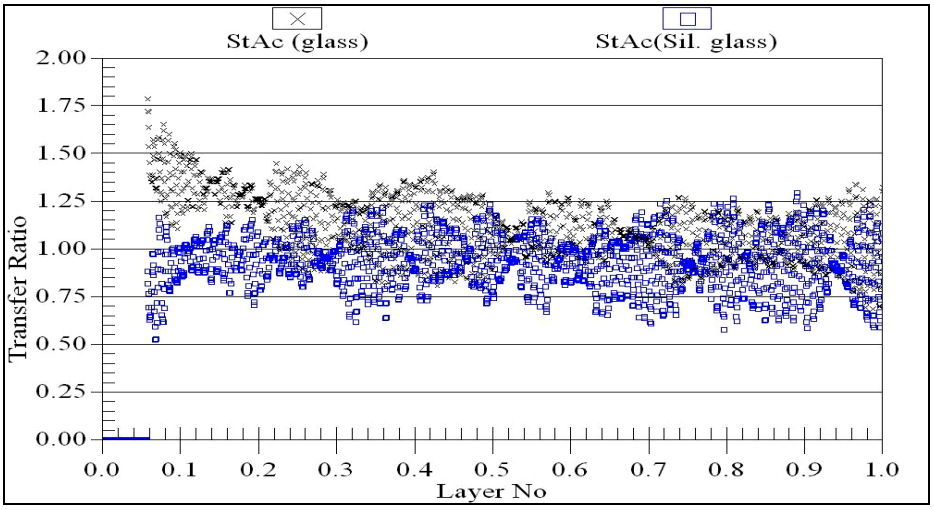


Figure 10.26. The effect of different surfaces onto deposition of StAc layers at 20$^{o}$C.

Due to uncompleted formation of oxide layers caused lower transfer ratios. For both cases, piror to coating contact angles were measured and seen that they show hydrophilic behaviour. Because glass is hydrophilic due to SiOH groups on the surface and AgO layer showed hydrophilic property although pure silver layer behaves as hydrophobic surface. However, it could not be possible to search every part of the surface and in some areas on silver surface, this oxidation was not completed and that surface behaved as hydrophobic. Besides, while using silver coated glasses, one surface of the glass is glass surface and another surface is silver. This can result in different transfer ratio for both sides and thus total transfer ratio.

### 10.3.2. Metal Soap (Calcium and Zinc stearate) Deposition

In metal stearate isotherms, direct passage from gas (G) phase to LS phase without $L_2$ phase was oberved at even low surface pressures. Hence, there would be no problem to choose lower surface pressures to deposit LB films. However, there are several factors affected on this deposition as given in following sections.

#### 10.3.2.1. Substrate Effect on Metal Stearate Deposition

The influence of molecule-substrate interactions on the final quality of LB films was studied with three types of glass substrates; Marinfeld, Nima and Matsunami for two types of compounds; calcium and zinc stearates. The transfer of $CaSt_2$ layers at 30 mN/m transfer surface pressure onto different glass surfaces shows the effect of substrate surface on deposition (Figure 10.27.). The subphase $CaCl_2$ concentration is $1\times10^{-3}$ M. In LB film deposition, the first layer may be different from subsequent layers since the molecules interact with the bare substrate instead of headgroups or tails of the previous layer.

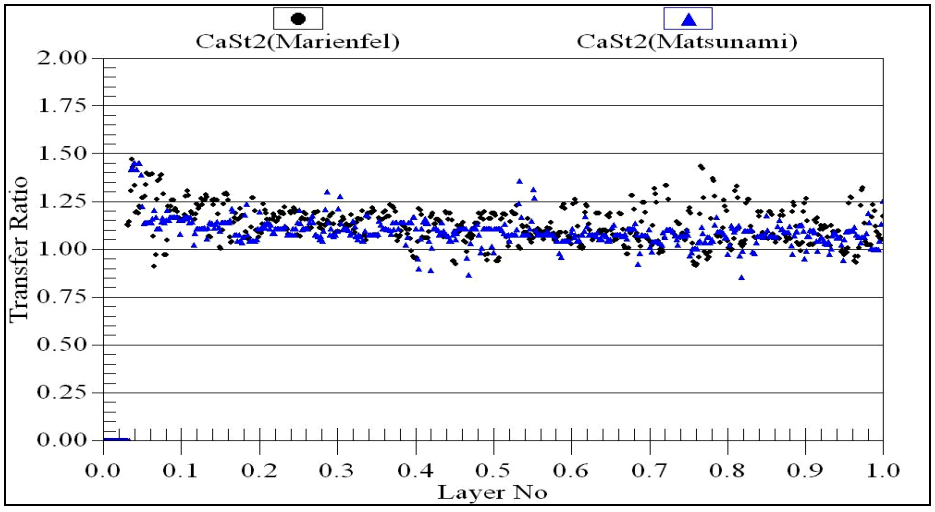


Figure 10.27. The substrate type dependency of $CaSt_2$ monolayer transfer at pH 9.5 and 20°C.

AFM images belong to the different substrate surfaces in Figure 10.28. show the difference between two kinds of substrate and the importance of substrate on film quality. Although, both LB films were deposited at dipping speed of 3 mm/min, the surface hydrophilicity and roughness affected transfer ratio. The maximum withdrawal

rate for fully–drained deposition has been given by Peng to depend on the nature of the hydrophilic substrate (Peng et al. 2001).

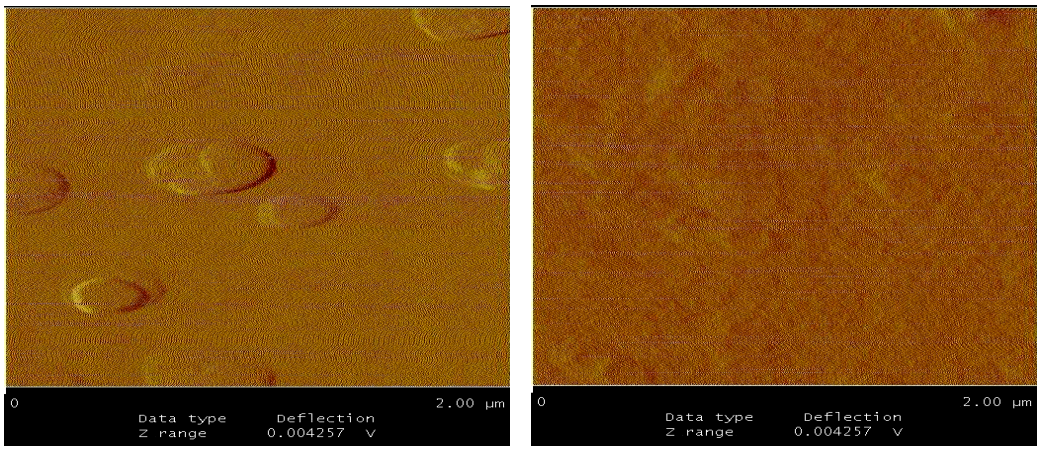


(a) (b)

Figure 10.28. The morphologies of used glass surfaces at 10 µm (a) Matsunami, (b) Marienfeld.

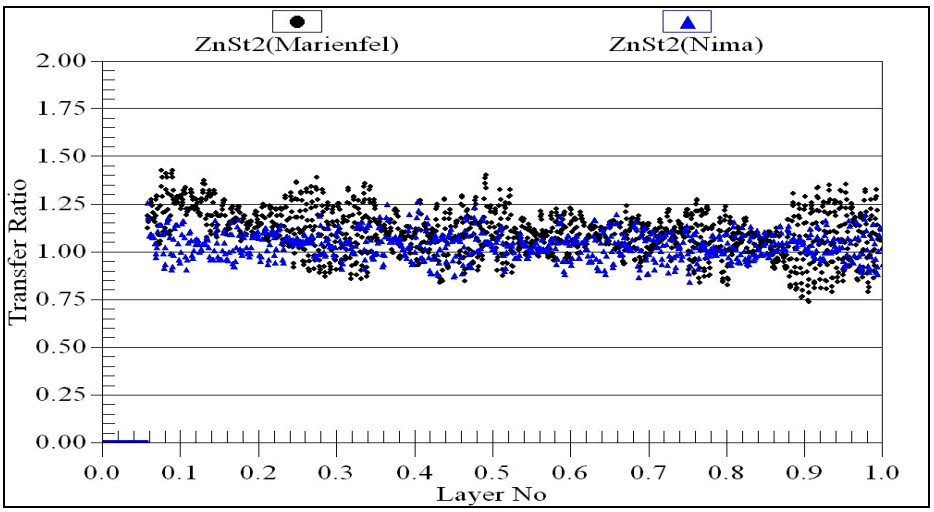


Figure 10.29. The substrate type dependency of $ZnSt_2$ monolayer transfer at pH 6.5 and 15°C.

The same results were obtained from $ZnSt_2$ layer transfer onto different substrates at 15 mN/m transfer surface pressure (Figure 10.29.). The subphase $ZnCl_2$ concentration is $1\times10^{-3}$ M. The calculated transfer ratios above 1.0 might result from high roughness of the substrate on molecular level or from low stability of the Langmuir film.

### 10.3.2.2. Concentration Effect on Metal Stearate Deposition

A significant role in LB film formation is played by the metal salt concentration in the aqueous subphase and its anionic composition. The increase in $CaCl_2.2H_2O$ solution concentration makes the deposition of calcium stearate layer difficult as it is presented in Figure 10.30. Although transfer was performed at the same pH and temperature, transfer ratios are higher for $1.5\times10^{-3}$ M $CaCl_2$. $2H_2O$ at 30 mN/m surface pressure.

The increase in calcium concentration in the bulk phase may thus cause the formation of rather extended structures attached to the monolayer surface, resulting in significant changes in the shape of π-A isotherm as seen in Figure 10.20. and the monolayer properties. Hence, the obtained transfer ratios are directly affected from these changes.

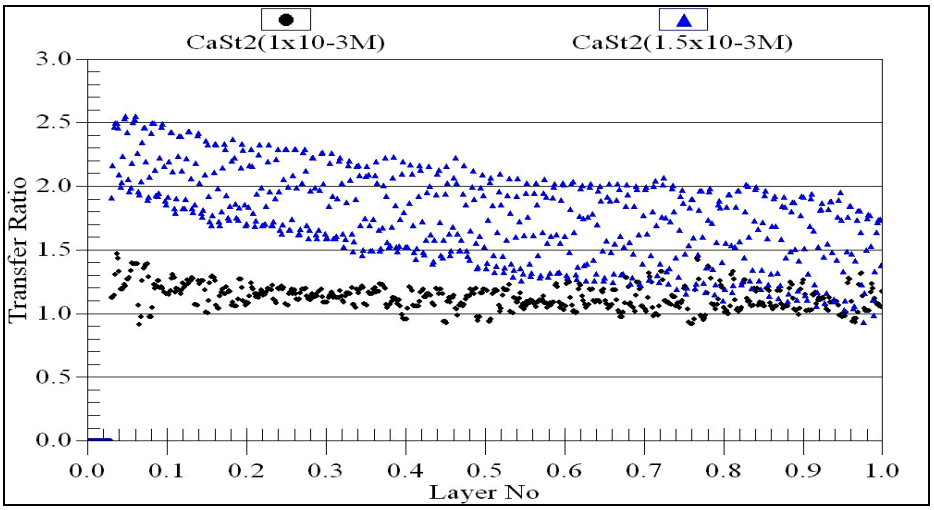


Figure 10.30. $CaCl_2$ subphase concentration effect on $CaSt_2$ layer transfer at pH 9.5 and 20°C.

The surface calcium stearate micelles tend to aggregate into large clusters when they become sufficiently numereous (Figure 10.31.). The incomplete juxtaposition of these clusters during compression gives rise to less dense regions, which are either monolayer free or contain film molecules in some other phase, being interspersed throughout the surface film. With continued micelle formation, the monolayer becomes increasingly nonuniform. This nonuniformity leads to varying transfer ratios.

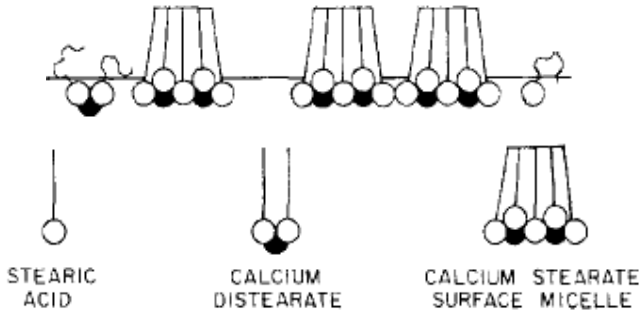


Figure 10.31. The representative picture of formation of $CaSt_2$ surface micelles.

The same behaviour was also observed for zinc stearate layer transfer at 30 mN/m surface pressure. If $ZnCl_2$ concentration is increased from $1\times10^{-3}$ M to $1.5\times10^{-3}$ M, transfer ratio is directly influenced by this increase as in Figure 10.32. Therefore, transfer surface pressure should have been lessened to obtain good tranfer ratio.

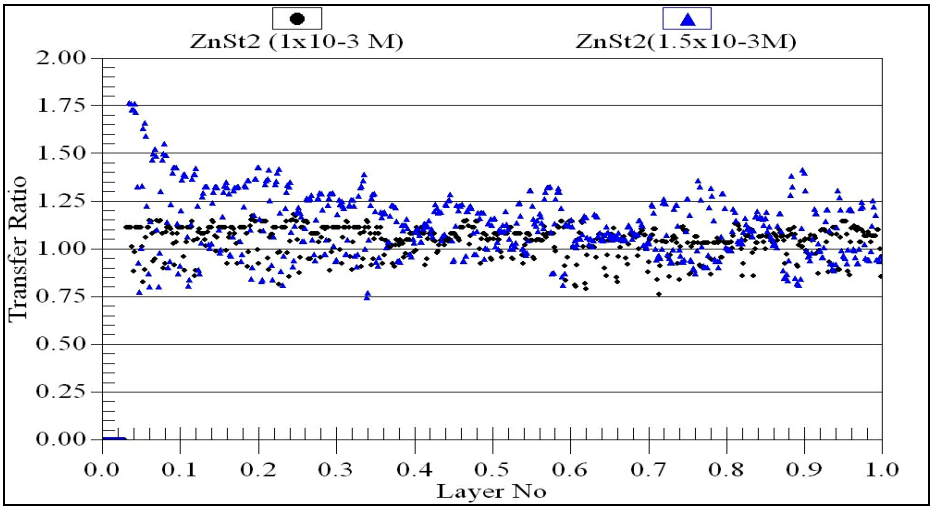


Figure 10.32. $ZnCl_2$ subphase concentration effect on $ZnSt_2$ layer transfer at pH 6.5 and 20°C.

Bukreeva reported that as pH increases, the monolayer is saturated with metal ions at lower concentrations. This could be the reason why better transfer ratios were obtained for both metal salt concentrations. Namely, if subphase pH is 9.5, the calcium stearate monolayer is formed at a metal salt concentration of C = $1\times10^{-3}$ M. On the other hand, at lower pH values, such as 9.2 is enough to obtain calcium stearate monolayer at the higher concentration of metal salt $1.5\times10^{-3}$ M in the subphase. Using high metal concentration caused instability in monolayer transfer (Bukreeva et al. 2002).

Yazdanian also found that alkaline earth metals, magnesium, calcium, barium appear to interact with fatty acids electrostatically by screening the negative charges, as demonstrated by an increase in the surface potential as the concentration of these ions in the subphase is increased. Cadmium, cobalt and lead, (zinc can be added to this group as well) significantly decreased surfcae potential and appear to interact more strongly via covalent bonding, thus ordering the molecules in the monolayer more effectively. This could be the answer why more scattered transfer ratios were obtained for $CaSt_2$ layers (Yazdanian et al. 1990).

### 10.3.2.3. Buffer Concentration Effect on Metal Stearate Deposition

The formation of $CaSt_2$ monolayers is achieved at high surface pH. To obtain completely converted calcium stearate, pH should be stable. Therefore, importance of buffer usage and its concentration come forth. Figure 10.33. depicts the transfer ratio results of calcium stearate layers prepared at two different concentration of borax ($Na_2B_4O_7$) buffer. Using higher concentration of buffer narrowed the distribution of transfer ratio.

Neuman reported that carbon dioxide adsorption and bicarbonate buffer influence monolayer properties and may play some role in the observed film behaviour. The rise of concentration of borax does not lead to sodium stearate layer formation because the calcium binding had a much more covalent character than the sodium. Bagg found the very marked specificity for calcium over sodium. There is a pronounced selectivity for calcium over sodium ions in the competitive adsorption to a stearic acid monolayer, provided that the concentration of $Na^+$ is no more than 100 times higher than that of $Ca^{2+}$ (Neuman 1975, Bagg et. al 1964, Dutta et al. 1990).

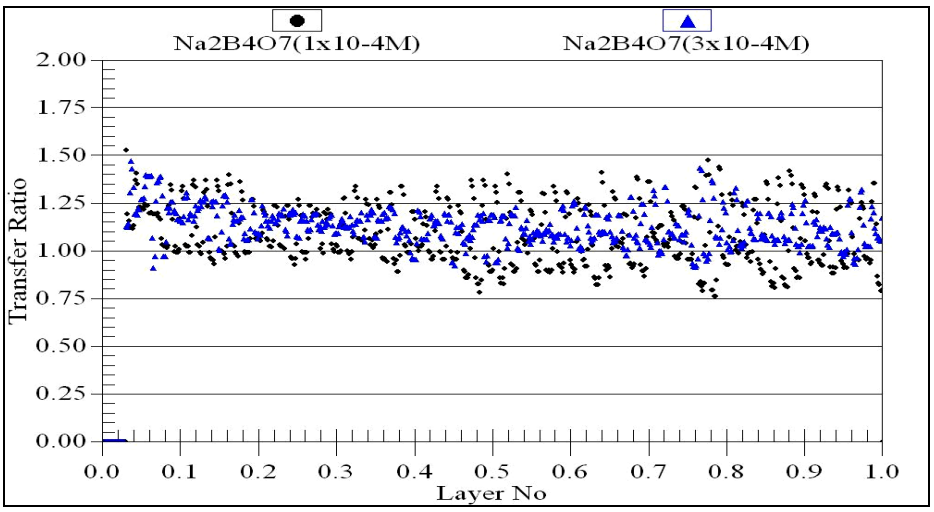


Figure 10.33. $Na_2B_4O_7$ (buffer) concentration effect on $CaSt_2$ layer transfer at pH 9.5 and 20°C.

Changing the type of anion present and possibly causing complexes to form with metal cations appears to reduce the interaction between these ions and the fatty acid monolayer. In contrast, in the presence of calcium ions, no counterion effects were noted confirming the results of Yazdanian (Yazdanian et al. 1990).

### 10.3.2.4. Temperature Effect on Metal Stearate Deposition

The deposition of zinc stearate layer from different subphase temperature revealed that a strong dependence of the layered structure and molecular packing on the subphase temperature. The results are shown in Figure 10.34. $ZnSt_2$ monolayers at 30 mN/m transfer surface pressure were transferred onto Marienfeld bare glass slide from subphase containing $5\times10^{-4}$ M $ZnCl_2$ at pH 6.3.

Monolayer studies revealed that when the $ZnSt_2$ film is compressed, the domains are packed more densely and coalesce each other. Finally, the domains become homogeneous monolayers at the onset point of surface pressure. Upon compression, the morphology remains unchanged at low temperature, while at high temperature, the morphology might change from monolayers into circular domains due to bilayers accompanying the phase transition. Further compression results in the growth of many large circular domains. Therefore in transfer ratio results more deviation from ideality is observed.

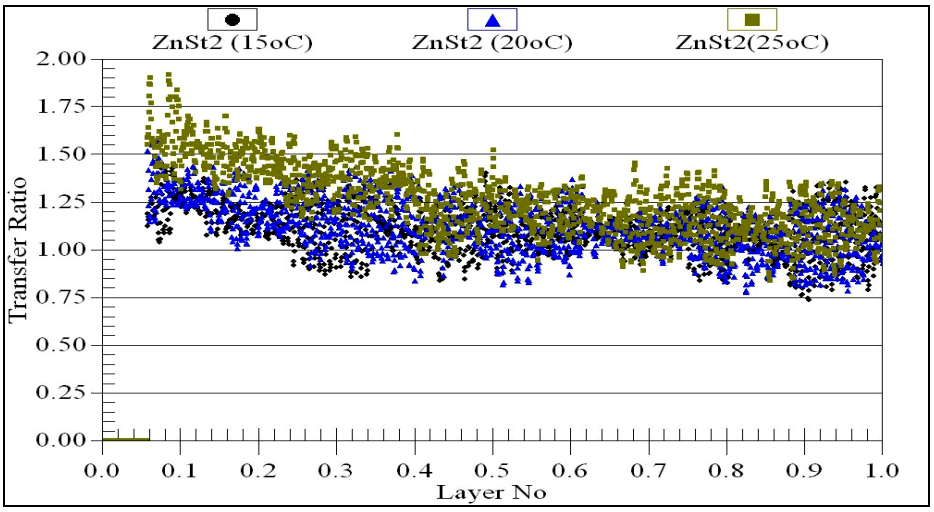


Figure 10.34. Temperature dependency of $ZnSt_2$ layer transfer at pH 6.3.

### 10.3.2.5. pH Effect on Metal Stearate Deposition

The ordered, charged surface of the Langmuir monolayer appears to be a factor causing the ordering of counterion complexes and the distribution of polar molecules in the aqueous phase near the interface and so initiating the formation of new surface connected structures. Therefore to obtain dissociated fatty acid monolayer and formation of bond between metal cations, the importance of pH should be reconsidered.

The range of conditions for the formation of good LB films of metal stearates is fairly narrow and depends on many factors. pH is one of these factors. The transfer ratio results of $ZnSt_2$ monolayers transferred at 30 mN/m from different subphase pH seen in Figure 10.35. confirm these expression.

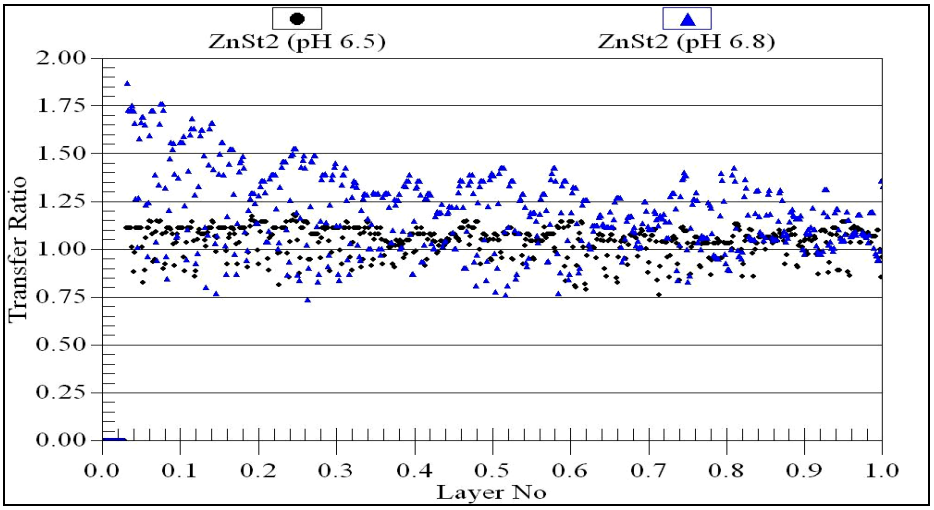


Figure 10.35. pH dependency of $ZnSt_2$ layer transfer at 20$^{o}$C.

It is noteworthy that at pH 6.5, better transfer ratio results with close to one were obtained for $ZnSt_2$ monolayer transfer operations. Peng reported that above pH 6.6 the zinc arachidate monolayer exhibits a complex pattern of instability (Peng et al. 2001). Here at pH 6.8, same instability due to complex pattern of hydrolysis for $Zn^{2+}$ in solution.

Kutscher also confirmed for $ZnSt_2$ monolayers on water subphase, slight changes of the pH value may give rise to dramatic modifications of the monolayer (Kustcher et al. 1996).

It has been suggested that the precursor Langmuir monolayer molecules are of two distinct types. One species consists of a dissociated fatty carboxylate molecule bound with one divalent cation from the subphase. This positively charged species is then neutralized by pairing with another negatively charged fatty carboxylate molecule. Overall monolayer charge neutrality is maintained, therefore via a network of $(ZnSt)^+$ and $(St)^-$ pairs where St denotes a dissociated carboxylate amphiphile. The monolayer molecules do not form the more energetically favorable, neutral $ZnSt_2$ complexes as the structure of the monolayer does not allow the surfactant molecules to get close enough. The head groups of the charged species might be highly solvated, and this high degree of solvation might thus be taken up in the deposition process leading to a greater amount of entrained subphase at higher surface pH than in lower pH samples. This microscopic entrainment process is thus an intrinsic property of the LB film material and deposition process.

### 10.3.2.6. Dipping Speed Effect on Metal Stearate Deposition

Transfer ratio values fluctuate between 0.75 and 1.5 by increasing the dipping rate of substrate from 1 to 10 mm/min as depicted in Figure 10.36. When the dipping speed was decreased from 10 mm/min to 1 mm/min, the randomized data points were approached each other and the better transferred LB films could be obtained at this low speed. This is consistent with the report by Ariga that the lower transfer speed was favorable to obtain higher quality LB films (Ariga et al. 1994). Faster dipping speeds dramatically increased the amount of water taken into the film. The amount of water incorporated into the film during first layer deposition was greater while using hydrophilic substrates due to presence of more hydrophilic headgroups.

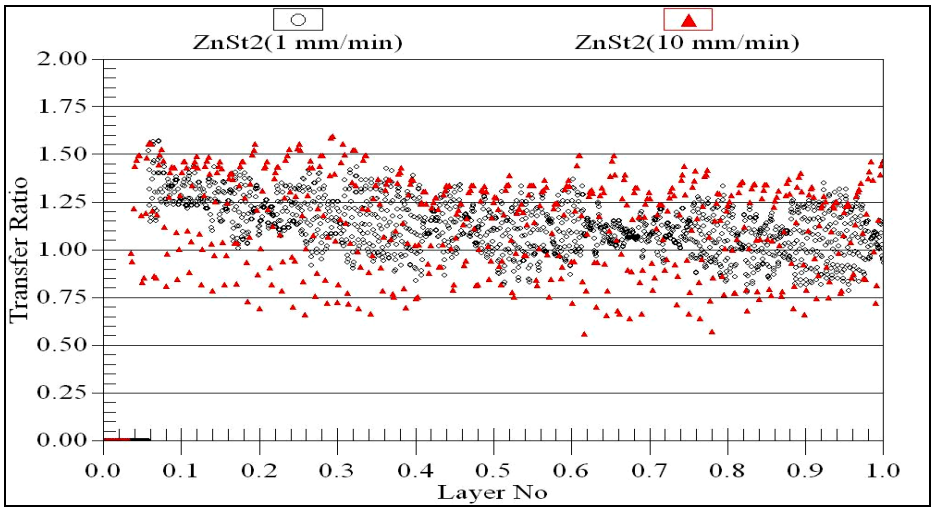


Figure 10.36. Transfer ratios taken for $ZnSt_2$ layer at 20°C and pH 6.2 with different dipping speed.

Lovell found that at relatively high speeds of substrate withdrawal (e.g.> 1.5 cm/min for behenic acid deposition), either a film or small droplets of macroscopic water taken up on the QCM surface (Lovell and Roser 1996). However, at slower speeds of withdrawal they have not observed any macroscopic water.

### 10.3.2.7. Transfer Surface Pressure Effect on Metal Stearate Deposition

The transfer process was repeated several times at different surface pressures (35 and 30 mN/m) and the deposition behaviour of $CaSt_2$ monolayer at 20°C and pH 9.5 was seen in Figure 10.37. The metal salt concentration was $1\times10^{-3}$ M for both cases. At the high surface pressure of 35 mN/m, the transferred layer through substrate surface was not in proper distribution for all 4 successive layers. The transfer ratio values are random. The barrier motion on the surface can not compensate the disappeared area of the transferred monolayer sufficiently at high surface pressure. The presence of collapsed layer due to high surface pressure might also be responsible from this result.

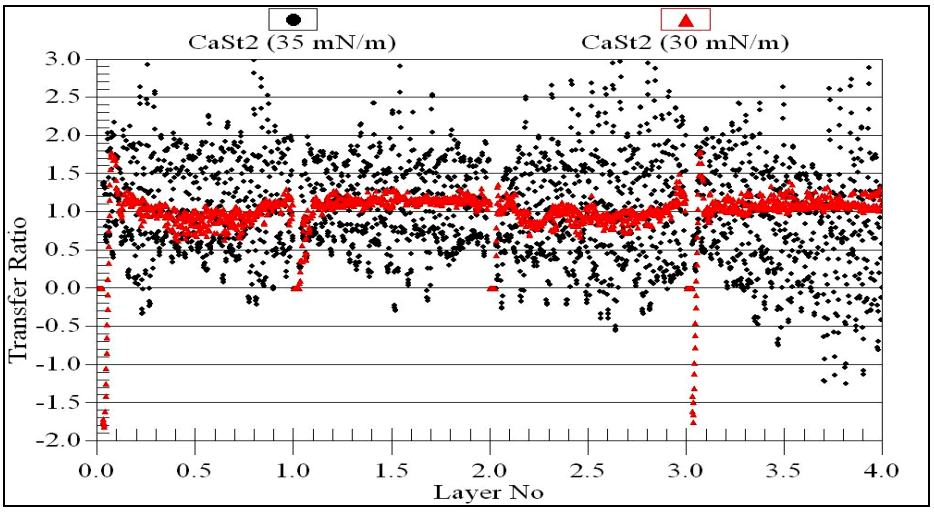


Figure 10.37. Transfer ratios taken for successive 4 layer of $CaSt_2$ at different transfer surface pressure.

Metal soap monolayers are quite stable and in condensed form. In isotherm passage to LS phase is directly occurred and there would be no problem to study at lower transfer surface pressure. It has been generally accepted that monolayers are homogeneous at high surface pressures. However, the close packed $CaSt_2$ films are nonuniform above pH 9. It could not be easy to predict its behaviour.

### 10.3.2.8. Drying Effect on Metal Stearate Deposition

In Figure 10.38., the deposition distributions of $CaSt_2$ monolayer from a $1x10^{-3}$ M $CaCl_2.2H_2O$ subphase at 30 mN/m successively after one layer were depicted. Without drying the first layer, the transfer of next monolayer onto this water contained layer, decreased the transfer ratio. This undesired transfer continued for coming next layers. However, after drying first layer in $P_2O_5$ desiccator and then transfer of next layers onto this dried layer was done successfully. Transfer ratio closed to unity in this way.

During deposition onto the glass substrate, there is a thin layer of water present between the film and the substrate, which likely remains if it is not dried. This hydration layer allows the monolayer to retain more of the character of the monolayer at the original air/water interface, in particular its packing density.

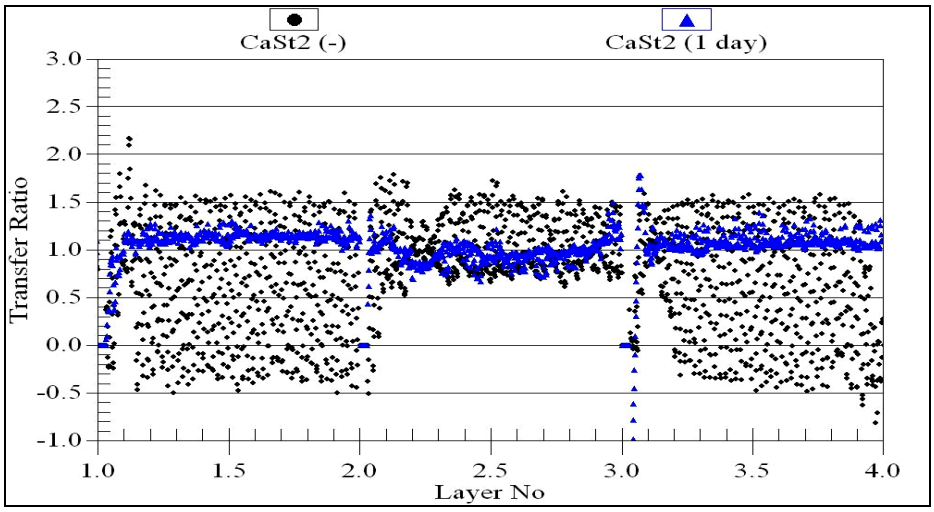


Figure 10.38. Drying period effects on transfer ratio for multilayer $CaSt_2$ layers at 20°C and pH 9.5.

Viswanathan showed that the presence of a thin water layer between the substrate and the headgroups of the monolayer increases the lateral diffusivity of the molecules in the monolayer (Viswanathan et al. 1992). This additional mobility of the monolayer might allow defects that would otherwise form to anneal more rapidly than in the absence of the water film, especially in the case of the less homogeneous $CaSt_2$ LB films. Lovell showed that during the deposition process a small amount of water molecules are entrained with each of polar head groups due to favorable hydrogen bonding interactions (Lovell and Roser 1996). Increasing the subphase pH to a relatively high value may lead to the deposition of dissociated charged amphiphilic molecules with their associated charged divalent metal cations as seen in behenic acid on $CaCl_2$ subphases.

### 10.3.3. The Significance of the Factors Affected on the Deposition of Stearic Acid and Metal Stearates

From the experiments conducted so far, it can be summarized that experimental conditions affect the transfer ratio. They can be varied as such as:

- Nature and composition of the monolayer,
- The composition of the aqueous subphase, especially the nature and concentration of ionic components in the case of ionic monolayers,
- The (constant) surface pressure, $\pi$, of the monolayer,

- The temperature, T,
- The velocity of the solid substrate through the monolayer upward, V↑ and downward, V↓,
- The time, above and under water, between two successive trips,
- The nature of the solid substrate, comprising, besides the chemical nature, such factors as surface roughness and porosity.

Many of the peculiarities associated with the deposition of stearic acid and metal stearates haven't been fully understood. Honig and coworkers expressed that the transfer ratio is not equal for upward and downward trips in the case of Y-type films and reported various deviations from ideality: a) the transfer ratio is constant for succeeding trips, but not equal to 1, b) the transfer ratio depends on the number of previous dipping cycles, c) the transfer ratio is not equal for upward and downward trips in the case of Y-type films, d) the transfer ratio (defined as a differential quantity) varies with the height on the slide (Honig et al. 1973).

One of these is that X type films usually are not formed on the first immersion-withdrawal cycle, but the film gradually develops X type behaviour as fewer molecules transfer to the emerging slide during deposition as seen in Table 10.5. for transfer onto silver coated glass slides. Stearic acid was transferred at 20$^{o}$C, pH 6.8 and 25 mN/m surface pressure. Metal stearates were transferred at 20$^{o}$C, pH 9.8 and 10 mN/m surface pressure.

Table 10.5. The transfer ratios of 13 layer StAc, $CaSt_2$ and $ZnSt_2$ onto silver coated glass surfaces.

| | *Transfer ratios* | | | | | | | | | | | | |
|---|---|---|---|---|---|---|---|---|---|---|---|---|---|
| *Transferred compound* | *1* | *2* | *3* | *4* | *5* | *6* | *7* | *8* | *9* | *10* | *11* | *12* | *13* |
| Stearic acid | 0.95 | 0.7 | 0.1 | 0.9 | 0.1 | 0.9 | 0.3 | 0.9 | 0.4 | 0.9 | 0.5 | 0.9 | 0.7 |
| Calcium stearate | 1.1 | 0.96 | 0.7 | 1 | 0.6 | 1 | 0.6 | 0.97 | 0.5 | 0.96 | 0.4 | 0.9 | 0.3 |
| Zinc stearate | 1 | 0.9 | 0.9 | 0.95 | 0.8 | 0.93 | 0.7 | 0.92 | 0.62 | 0.93 | 0.59 | 0.9 | 0.55 |

In these deposition experiments, first deposited layers with the transfer ratios are close to unity and further deposition tended to XY-type decreased transfer ratios. The transfer ratio begins to decrease after the deposition of a certain number of layers indicating that the transfer efficiency of the monolayer is deteriorating beyond a certain film thickness. This shows that the film structure may be changing (Table 10.5.). Here the importance of studied pH comes out once more.

Besides, some researchers has observed the similar phenomenon for fatty acids deposited at different subphase pH (6-8). They found a transfer ratio of about unity only for the first upstroke and then a steady drop in transfer ratio for subsequent upstrokes (Schwartz 1997). Neuman also found that perfect Y type deposition occurs below pH 6.4, whereas the films gradually develop more X type characteristics with increasing subsolution pH for $CaSt_2$ (Neuman et al. 1980).

During the downward passage transfer ratio is always approximately close to unity for both the cations. Interactions between the ends of the hydrocarbon chains only are involved. The bond energy is always sufficient for the transfer because the polar groups of the transferred molecules remain in the water and the change in the free enthalpy is always negative. Moreover, owing to the condensed state of the layer at the transfer surface pressure (10 mN/m) used, the molecules are strongly laterally bound and the film can be transferred as a whole even if each molecule of the film does not interact with those of the preceding layer of the multilayer. However, the polar groups which account for the binding during the upward passage differ according to the cation.

The some research groups proposed different mechanisms for evolution from Y to XY deposition such as rearrangement mechanism under water, the model of differing structure with mixed species and peel-off mechanism (Schwartz 1997).

The decrease in the withdrawal transfer ratio might be attributed to the incomplete transfer of metal stearate surface micelles. Another probability is the monolayer not depositing on the water filled interstices existing within the surface of the immersed multilayer.

In particular, the decrease in transfer ratio with number of layers may be due to an increasing density of defects in the preceding monolayer especially for stearic acid monolayer. Because generally there was no observed X type deposition for stearic acid layers in the literature.

Nevertheless, not all the molecules which leave the regular monolayer state during the deposition process might be deposited on the silver glass slide but rather

some film molecules simultaneously disappear from the water surface by dissolution, evaporation, or monolayer collapse mechanisms.

For zinc and calcium ions, studied pH is so different from each other. Monolayer binds calcium and zinc in a quantity exceeding that necessary for 100% formation of calcium and zinc stearate ($CaSt_2$ and $ZnSt_2$).

On the other hand, the acceptance of unity transfer ratio as ideal, however reflects a strongly ingrained implicit assumption that the deposition process consists of simply transferring the molecules from water surface to the substrate-creating a sort of replica. It is seen in our experiments and the studies done in the literature (Schwartz 1997), this assumption is often incorrect. Because LB transfer is a complicated process in which the amphiphiles; here stearic acid molecules generally attempt to reach a new thermodynamic minimum as they experience interactions with the solid substrate. If the molecular packing density changes during transfer, then TR = 1 might not be the indicator of a defect free film. In spite of these facts, at least transfer ratio gave the information about the success of transfer.

While it is true that extreme care should have been taken in the fabrication of LB films, it is not practical -but rather very expensive- to have, for example, controlled atmosphere, temperature, pH and humidity in the laboratory. Therefore, their influence on our experimental results were inevitable.

## 10.4. Characterization of the LB Films

### 10.4.1. Crystal Structure of Stearic Acid and Metal Stearates

Grazing incidence X-ray diffraction was used in studying the microscopic molecular structure films. The possible packing arrangements in LB films were investigated in this way. Figure 10.39. presents the XRD patterns of the thirteen layers of StAc, $CaSt_2$ and $ZnSt_2$ LB films covered onto bare glass slides.

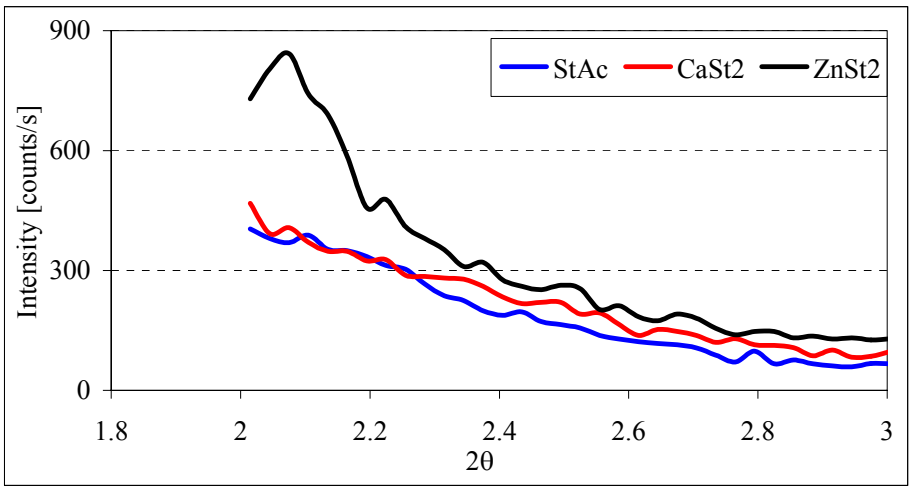


(a)

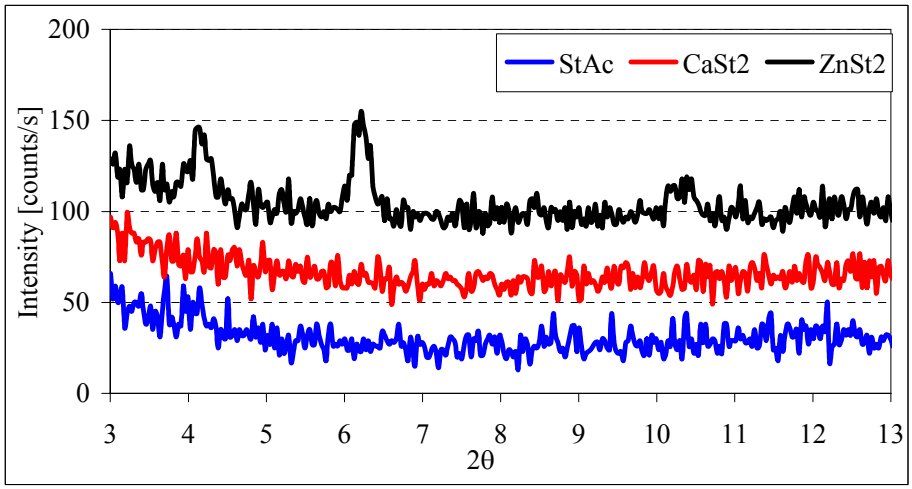


(b)

(cont. on next page)

Figure 10.39. XRD patterns of StAc, $CaSt_2$ and $ZnSt_2$ LB films on glass (a) at interval $2\theta$ = 2-3, (b) at interval $2\theta$ = 3-13, (c) at interval $2\theta$ = 2-28.

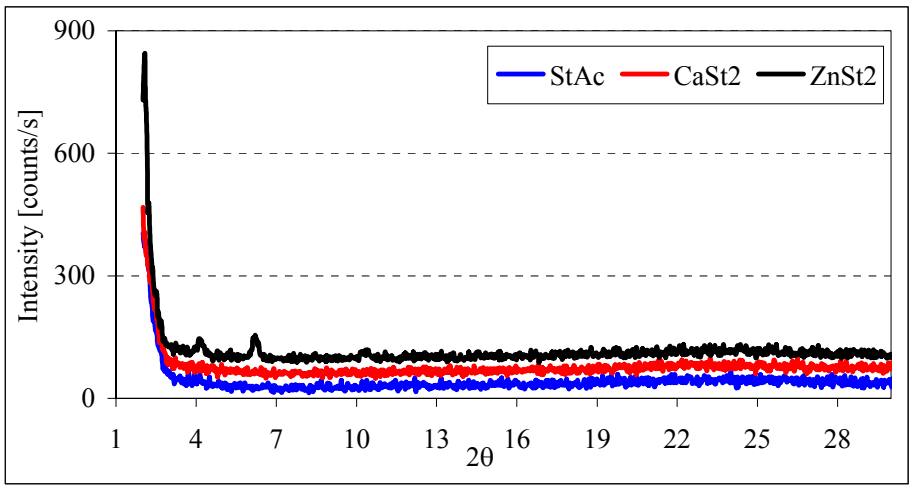


(c)

Figure 10.39.(cont.)

In all cases, several Bragg reflections were observed. The layer spacing, *d* can be determined according to the Bragg formula:

$$n\lambda = 2d\sin\theta \qquad (10.1)$$

where n is the order of the reflection peak, λ denotes the wavelength and θ the maxima of the Bragg peaks.

Stearic acid and calcium stearate layers' patterns exhibited only very weak and broad diffraction peaks. They were not crystalline since no sharp diffraction peaks were observed. Moreover, in long range order, for stearic acid and calcium stearate at less than $2\theta = 2^{o}$ corresponding to 4.42 nm interplanar distance could not be observed due to limitations of the instrument. Low angle X ray diffraction instrument is needed for that purpose. It can be said that the distance between succesive planes are larger than 4.42 nm.

On the other hand, for zinc stearate a peak at $2\theta = 2.075^{o}$ corresponding to 4.269 nm was observed. This corresponds to bilayer distance in zinc stearate. A second peak at $2\theta = 4.205^{o}$ corresponding to 2.07 nm belongs to monolayer distance in zinc stearate.

The strongest peak in zinc stearate diffraction diagram is at $2\theta = 6.406^{o}$ (diffraction data library of Philips Xpert-Pro (PCPDFWIN v.2.1.)). In Figure 10.39., a peak at $2\theta = 6.2^{o}$ is observed and close to the value given in database. A second peak at 10.609 is also observed in Figure 10.39. which is one of the characteristic peak of the zinc stearate. Thus, it can be concluded that zinc stearate film on glass is in crystal form.

Zinc stearate LB films exhibited a set of more sharp and intense diffraction peaks. $ZnSt_2$ LB film exhibited a set of diffraction peaks with a bilayer distance of 4.269 nm. The bilayer spacing of ~4.269 nm corresponds to a chain axis tilt angle of $31^o$ assuming the height of the zinc stearate molecule to be 2.5 nm similar to cadmium stearate reported in Umemura's work (Umemura et al. 1990). The same tilt angle was observed for zinc arachidate LB films in Dhanabalan's study (Dhanabalan et al. 1998). The arrangement under the orthorhombic (R) subcell with chain tilt angle of $31^o$ may be identified as R(111) packing.

The size of the cyrstals causing diffraction peak at $2\theta = 6.2^o$ for zinc stearate is found from using Scherrer equation (Equation 10.2.) from the width of the peak at half peak height as 88.7 nm.

$$B = \frac{0.9\lambda}{LCos\theta} \qquad (10.2)$$

where $\lambda$ denotes the wavelength and $\theta$ is the angle of the maximum of the peak, L is the width of the peak at half peak height.

The passage from neutral pH to alkaline pH for $CaSt_2$ formation may lead to a transition from a crystallized state to a more amorphous state of the monomolecular layer, resulting probably from the binding of water molecules.

The comparison of XRD patterns of LB films formed in these conditions with solid powder diffraction peaks might not be correct. Because here for $ZnSt_2$ and $CaSt_2$ LB films were formed at 10 mN/m and stearic acid LB films were formed at 25 mN/m. These values are much lower than collapse points given in monolayer studies section as 50 mN/m for StAc and $ZnSt_2$ and 53 mN/m for $CaSt_2$ where 3-D crystals start to form. Thus, the peaks are at lower intensities.

## 10.4.2. Functional Groups in LB Films

One of most reliable method for determination of film characteristics on solid substrates is FTIR spectroscopy. FTIR measurements were carried out with the aim to correlate the differences in composition and structure between the LB films deposited from different subphases. The question then arises as to whether the film is actually stearic acid or metal soap ($CaSt_2$ or $ZnSt_2$).

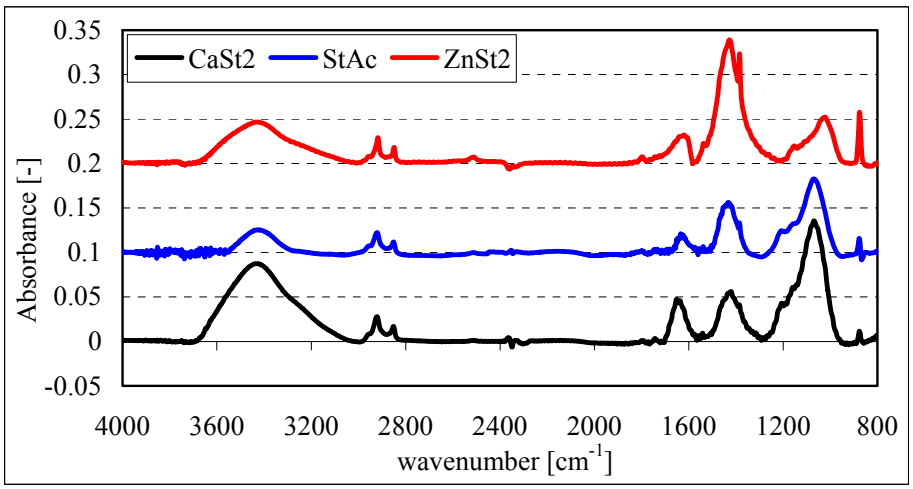


Figure 10.40. FTIR transmission spectra of prepared KBr pellets of $CaSt_2$, $ZnSt_2$ and StAc collected from surface at collapse point.

The IR spectra of stearic acid, calcium and zinc stearate pellets prepared by KBr (2 mg / 200 mg) in Figure 10.40. are given between 4000 and 800 $cm^{-1}$. These pellets were prepared from collapse layers of these compounds which are collected from surface. Therefore, the intensity of water peaks are very high and dominant. The bands near 3460 and 1630 $cm^{-1}$ in IR spectra are due to the OH stretching and HOH bending modes of hydroxide and lattice water. The presence of these peaks made unable to see the peaks around 1600-1500 $cm^{-1}$ which indicate metal stearate formation. Besides, in StAc, $CaSt_2$ and $ZnSt_2$ spectra, $CH_2$ asymmetric and symmetric stretching bands at around 2920 $cm^{-1}$ and 2850 $cm^{-1}$ were observed. Strong symmetric $COO^-$ band for $ZnSt_2$ at 1433 $cm^{-1}$, for $CaSt_2$ at 1436 $cm^{-1}$ and for StAc at 1446 $cm^{-1}$ appears. This is the indication of unionized stearic acid was ionized due to high pH media. $pK_A$ of stearic acid is 5.6 and the studied pH range is 6.8, 6.7 and 9.8 respectively. For StAc, C=O stretching band at 1700 $cm^{-1}$ was not observed. This indicated that preparation of KBr pellets from wet films affected the state of the films. Rather than KBr technique, in situ measurement of IR spectrum should be preferred.

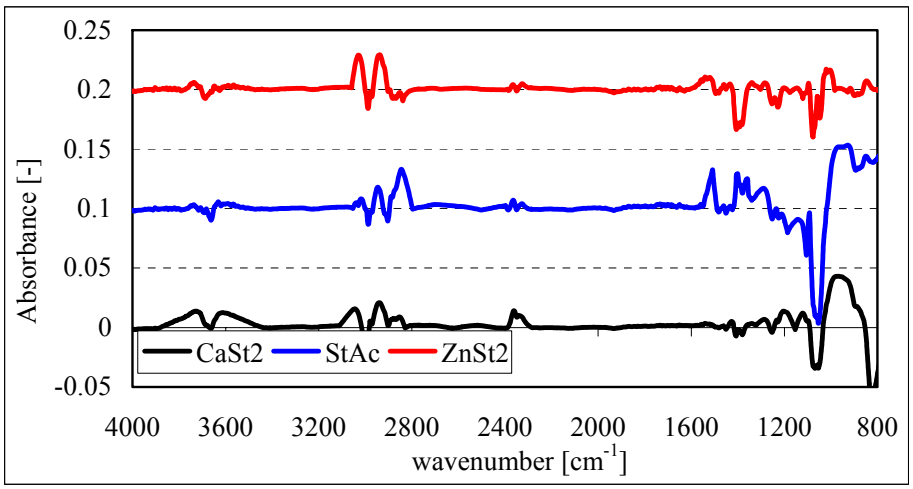


Figure 10.41. StAc, $CaSt_2$ and $ZnSt_2$ LB films on bare glass taken with ATR.

Figure 10.41. illustrates FTIR-ATR spectra of 4-layer LB films composed of stearic acid, calcium and zinc stearate on bare glass between 4000 and 800 $cm^{-1}$. Although produced film were kept in $P_2O_5$ desiccator, water peaks were still observed and a clear interpreatation was not easily done in spectra taken with ATR due to working principles of ATR measurements. Because to get representative peaks of substances, the film should have been covered onto ATR Germanium plate (Umemura et al. 1986). However, this is not pratical and films were coated onto bare glass slide and these slides were put onto Germanium plate. As a result, some peaks were missaligned.

In StAc, $CaSt_2$ and $ZnSt_2$ spectra, antisymmetric (2952 $cm^{-1}$) and symmetric (2877 $cm^{-1}$) methyl stretching bands ($\nu_aCH_3$ and $\nu_sCH_3$) were seen respectively. In StAc spectra, the band that should be 1702 $cm^{-1}$ assigned to the C = O stretching vibration is very weak. In StAc, also at 1440 $cm^{-1}$, there is a $COO^-$ stretching peak may be representing ionized acid. The band progression which is due to coupling of the $CH_2$ wagging vibrations of the trans zig zag alkyl chain is seen in the range from 1380 and 1180 $cm^{-1}$. In the spectrum of $ZnSt_2$, The antisymmetric COO stretching band at 1543 $cm^{-1}$ strongly appears, but the symmetric $COO^{-1}$ stretching band at 1433 $cm^{-1}$ is very weak.

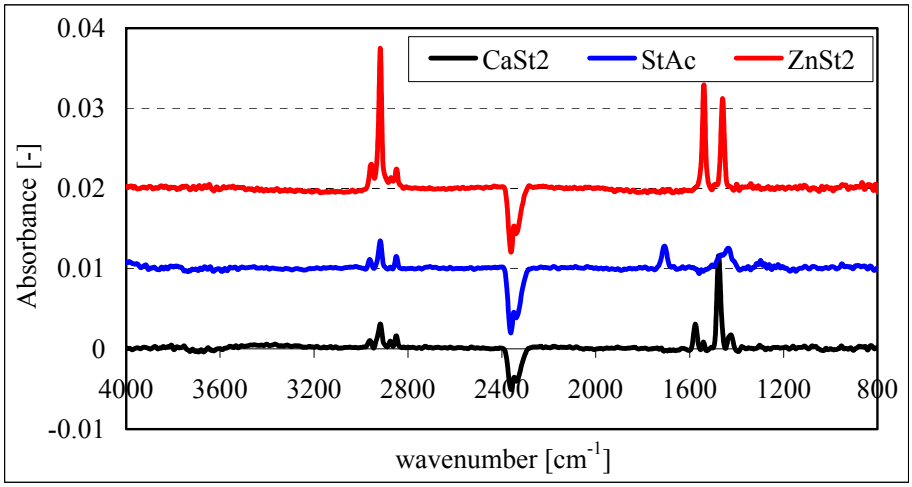


Figure 10.42. IR spectra of StAc, $CaSt_2$ and $ZnSt_2$ LB films on silver glass taken with 80 degree specular reflectance attachment.

IR spectra of 13-layer LB films of stearic acid, calcium and zinc stearate on silver coated glass in Figure 10.42. taken with 80 degree specular reflectance device are given between 4000 and 800 $cm^{-1}$. These spectra are meaningful and although the fluctuations in transfer ratio (between 0.7 to 1) dropped the intensities of peaks observed, it gives important informations about our LB films. Therefore, all spectra are interpreted separately.

The high intensity of asymmetric and symmmetric stretching vibrations of $CH_2$ groups (at around 2920 and 2850 $cm^{-1}$, respectively) especially for $ZnSt_2$ layers might be indicator of $CH_2$ groups in the LB films are arranged almost parallel to the substrate surface, whereas hydrocarbon chains are oriented vertically. It is certain that the water bands near 3460 and 1630 $cm^{-1}$ due to the OH stretching and HOH bending modes of hydroxide and lattice water are not observed in the spectras. These substrates were kept in $P_2O_5$ desiccator prior to characterization for longer periods. Therefore, possible entrained water were gone out.

### *Stearic acid (StAc)*

Antisymmetric and symmetric methylene stretching bands ($\nu_aCH_2$ and $\nu_sCH_2$) at about 2922 and 2850 $cm^{-1}$, which are comparable with those of antisymmetric (2962 $cm^{-1}$) and symmetric (2875 $cm^{-1}$) methyl stretching bands ($\nu_aCH_3$ and $\nu_sCH_3$) were seen respectively. The band observed at 1706 $cm^{-1}$ is undoubtedly assigned to the C=O stretching vibration in the unionized carboxylic group not shown by calcium and zinc

stearate spectra. The broadened $CH_2$ scissoring vibration near 1465 $cm^{-1}$ for the solution is indicative of a "liquid-disordered" subcell packing (Li et al. 2001). Another peak at 1404 $cm^{-1}$ might be ascribed to symmetric $COO^-$ stretching vibration of silver stearate at the interface (Umemura et al. 1987).

At the same time, the band progression especially seen in StAc layers on silver coated glass from 1400 to 1200 $cm^{-1}$ which is due to the $CH_2$ wagging mode and is characteristics of the all- trans conformation of the hydrocarbon chain. The bands near 1300 $cm^{-1}$ assigned to a coupled mode of the C-O stretching and OH in plane bending vibrations indicate the trans configuration is preferable with respect to the C=O and $C_\alpha$-$C_\beta$ bonds in LB films (Li et al. 2001).

### *Zinc stearate ($ZnSt_2$)*

Antisymmetric and symmetric methylene stretching bands ($\nu_aCH_2$ and $\nu_sCH_2$) at about 2917 and 2852 $cm^{-1}$, which are comparable with those of antisymmetric (2956 $cm^{-1}$) and symmetric (2872 $cm^{-1}$) methyl stretching bands ($\nu_aCH_3$ and $\nu_sCH_3$) were seen respectively. Kutscher indicated that wavenumbers of the asymmetric $CH_2$ vibration are conformation sensitive and they can be emprically correlated with the conformational order (i.e. with the trans/gauche ratio) of the hydrocarbon chain as follows: lower wavenumbers are characteristic of highly ordered conformations with preferential all-trans characteristics while the number of gauche conformers increases with increasing wavenumbers and width of the band (Kutscher et al. 1996). According to this expression, $ZnSt_2$ LB films are highly ordered conformations with all trans characteristics.

If carboxylic group is ionized and metal ions are introduced into the film absorption bands at 1540 $cm^{-1}$ and 1398 $cm^{-1}$ are assigned to asymmetrical and symmetrical stretching vibrations of the $-COO^-$ group appear in the spectra. A methylene scissorring band $CH_2$ at about 1460 $cm^{-1}$.

Note that only the C= O stretching band of stearic acid at about 1700 $cm^{-1}$ do not appear in both $ZnSt_2$ and $CaSt_2$ layers. These observations suggested that the proton exchange between carboxylic and metal salt has completely proceeded.

Kutscher reported that the bonding type of anhydrous carboxylates and in acetates in aqueous solution can be classified by the difference ($\Delta$) between the antisymmetric and symmetric $COO^-$ stretching frequencies (Kutscher et al. 1996).

Therefore the $\Delta$ = 142 $cm^{-1}$ value of the present study can be safely assigned to the bidentate structure where two different metal atoms bind covalently to each of the oxygen atoms of the carboxylate group as described in Figure 10.40.

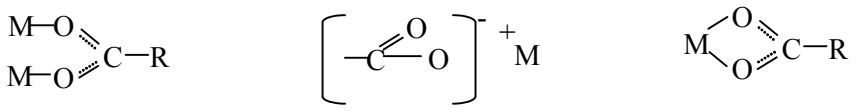

*Bridging bidentate ligand* *Ionic (1544 $cm^{-1}$)* *Chelating ligand (1579 $cm^{-1}$)*

Figure 10.43. Coordination type between carboxylates and $Ca^{2+}$ and $Zn^{2+}$ metals. (Source: Benavides et al. 1994)

## *Calcium stearate ($CaSt_2$)*

Antisymmetric and symmetric methylene stretching bands ($\nu_aCH_2$ and $\nu_sCH_2$) at about 2919 and 2852 $cm^{-1}$, which are comparable with those of antisymmetric (2962 $cm^{-1}$) and symmetric (2876 $cm^{-1}$) methyl stretching bands ($\nu_aCH_3$ and $\nu_sCH_3$) were seen respectively. Asymmetric $CH_2$ band at 2919 $cm^{-1}$ also showed the increased gauche conformers and less ordered conformations with respect to zinc stearate.

The thick films of calcium stearate shows a well-splitted doublet at 1577 and 1544 $cm^{-1}$ assignable to the antisymmetric $\nu_aCOO^-$ stretching vibration and relatively weak symmetric carboxylate stretching $\nu_sCOO^-$ appears at around 1477 and 1423 $cm^{-1}$. This is characteristic of the calcium stearate monohydrate (Umemura et al. 1994).

Nevertheless, the intensity ratios of the ($\nu_aCH_2$) band to the ($\nu_sCOO^-$) band reflects the overall orientation of the zinc stearate with trans zig zag alkyl chain (Umemura et al. 1990). The fact that the ratio is the smaller for calcium stearate than zinc stearate reveals that the tilting angle of the molecules increases in order of Ca< Zn salts at 20$^oC$. Indeed, a tilt angle of 31$^o$ was found for zinc stearate by X ray diffraction and calcium stearate and stearic acid were expected to have lower tilt angles since no X ray peak above $2\theta = 2^o$ was observed.

$CaSt_2$ is considered to possess both chelating with characteristic absorption at 1579 $cm^{-1}$ and ionic groups with characteristic absorption at 1544 $cm^{-1}$ (Benavides et al. 1994). The coordination types are given in Figure 10.40. Yazdanian mentioned about chelating in calcium arachidate as well (Yazdanian et al. 1990). Such difference between $ZnSt_2$ and $CaSt_2$ may be attributed to Lewis acid/base character, size and the states of hydration of these groups of ions in the monolayer states.

### 10.4.3. Contact Angle Measurements on Several Substrates

For any substrate prior to LB film deposition, contact angle measurements were done. This measurements are very important to decide whether substrate surface hyrdrophobic or hydrophilic. The result of this measurement determined the side where coating start; outside of the subphase or inside of the subphase. Table 10.6. shows the measurements done with KRÜSS G10 contact angle measurement device using deionized water as dropping compound. Imperfect cleaning stage and handling steps might have affected our measurement results.

Table 10.6. Contact angle measurements done on several substrates.

| *Material* | | *Measured contact angle($^o$)* |
|---|---|---|
| Glass substrates | Isolab | 28-32 |
| | Marienfeld | 26-29 |
| | Matsunami | 25-27 |
| Silver coated glass substrates | Isolab | 78-80 |
| | Marienfeld | 79-81 |
| | Matsunami | 80-82 |
| Silver coated glass substrates, (after rinse with water) | Isolab | 20-22 |
| | Marienfeld | 20-24 |
| | Matsunami | 19-23 |
| One layer LB film (upward) coated glass | Isolab | 77-82 |
| | Marienfeld | 79-81 |
| | Matsunami | 80-82 |
| Two layer LB film (up+down ward) coated glass | Isolab | 30-35 |
| | Marienfeld | 32-34 |
| | Matsunami | 29-33 |

Above table, it is seen that the clean glass slide is fully hydrophilic, because glass contains $SiO_2$, but the surface group is mainly SiOH which is wet with water. After rinsing water, silver surface behaves as hydrophilic instead of hydrophobic behaviour. The reason is that the silver surface can act hydrophobic or hydrophilic

depending on the surface treatment. The clean silver surface after coating in evaporator acts in a hydrophobic manner. It is important not to wait after coating process. On the other hand, when the silver coated glass substrate is immersed in the water, because of possible surface oxidation, it becomes hydrophilic.

On the other hand, Table 10.6. also illustrates the difference in contact angle after one layer of LB film transfer and then second layer of LB film. The glass surface was coated with organic layer after first layer transfer and surface behaves as hydrophobic (where head groups were towards substrate and tail groups were towards outside). The measured contact angles therefore were high. However, another organic layer transfer onto first layer (where head groups were towards outside and tail groups were towards the tail groups of inner layer in this case) made surface hydrophilic as expected due to the low contact angle measurements.

### 10.4.4. Topographic Images of Different Substrate Surfaces

2-D topographic image of glass, chrome coated glass, silver+chrome coated glass zinc stearate multilayer LB films on silver+chrome coated glass and bare glass are given in Figure 10.44.

AFM could nondestructively determine LB film quality with good resolution. One can see substantial differences in the morphology between these material surface AFM images. Random disordered structure of the glass surface were turned into uniform fine structure by first coating with chrome and then silver. Surface morphologies of 13 layer of zinc stearate LB film on glass and silver coated glass are also different.

The glass surface showed inhomogeneous regions and relatively homogeneous regions. After first chrome coating, the inhomogeneity of the film decreased due to presence of thin (10 nm) chrome layer with smaller crystals. An ordered and smooth surface structure was then obtained with silver layer at a thickness of 60-70 nm.

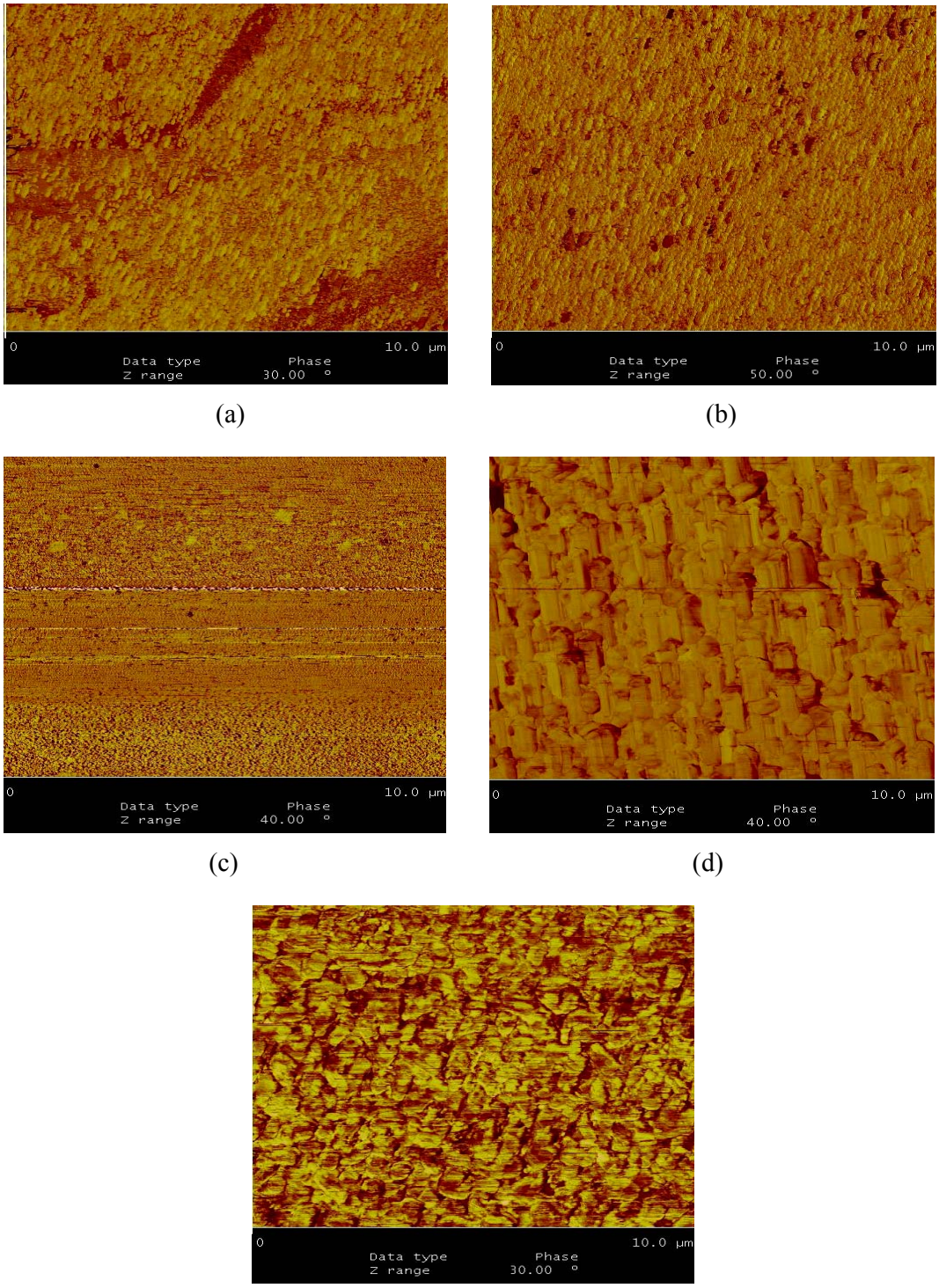


Figure 10.44. AFM tapping mode top view phase images ( 10x10 $\mu m^2$ ). (a) Glass (Marienfeld), (b) Chrome coated glass, (c) Chrome + Silver coated glass, (d) 13 layer $ZnSt_2$ LB film coated onto chrome + silver coated glass, (e) 13 layer $ZnSt_2$ LB film coated glass.

As it is visible from the image, many holes and grains especially for LB film coated surfaces are present in the film. The holes correspond to the dark areas of the images, with the lighter “background” being the surface of the films. Unlike other films, for silver films almost smaller holes and grains are visible and the silver film appears relatively flat and featureless.

The larger patches and grains are especially dominant for $ZnSt_2$ LB film coated surfaces. It is not easy to know whether patches and grains are formed during deposition or if they form upon “drying” of the film in air. The large crystallic structures might be a kind of island. Because the zinc stearate may begin to associate to form islands of an ordered phase. The size of these islands is much bigger than zinc stearate layers.

### 10.4.5. Surface Morphology of Coated Films

With scanning electron microscopy, the surface image of glass, chrome coated glass, silver+chrome coated glass, thirteen layers of $ZnSt_2$ coated onto glass and silver+chrome coated glass were taken and presented in Figure 10.45.

SEM micrographs for surfaces corroborate with AFM results as well. Glass surface topography is substantially different from all other images. The surface inhomogeneites observed in glass bare surface was removed by first coating chrome and then silver. It looks like the chrome coated glass surface is slightly rougher than silver +chrome coated one but no large defects.

The image belongs to thirteen layer $ZnSt_2$ LB film in Figure 10.45. give information about the crystal size of the molecules; as 80-90 nm-scale approximately. This crystal size is in agreement with the crystal size calculated from X-ray diffraction data according to Scherrer equation. The 50 nm-scale "hollows" seen in the $ZnSt_2$ coated SEM photographs may mean that at least part of the acid in the monolayer separates into aggregates (perhaps crystals). Grainy structures observed with different colors ranging from bright to darker might be due to different phases as well.

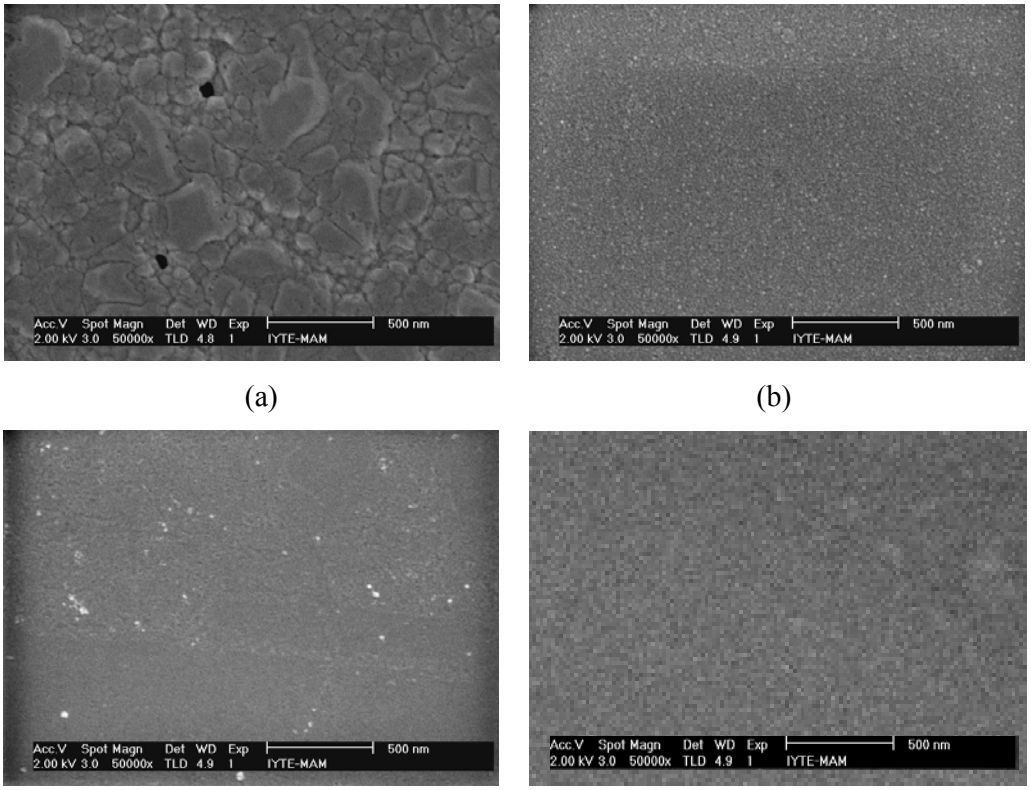


Figure 10.45. Surface morphology in plane structural data ( scale bar shows 500 nm). (a) Glass (Marienfeld), (b) Chrome coated glass, (c) Chrome + Silver coated glass, (d) 13 layer $ZnSt_2$ LB film coated onto silver + chrome coated glass.

### 10.4.6. Water Vapor Adsorption on StAc, $CaSt_2$ and $ZnSt_2$ Solid Powders

Water vapour adsorption studies were done to realize the water adsorption and desorption behaviour of $ZnSt_2$, $CaSt_2$ and StAc. The used amount for each compound was 1 g. The change in the weight of substance as a weight percentage with humidity is given below in the related Figures 10.46., 10.47., 10.48.

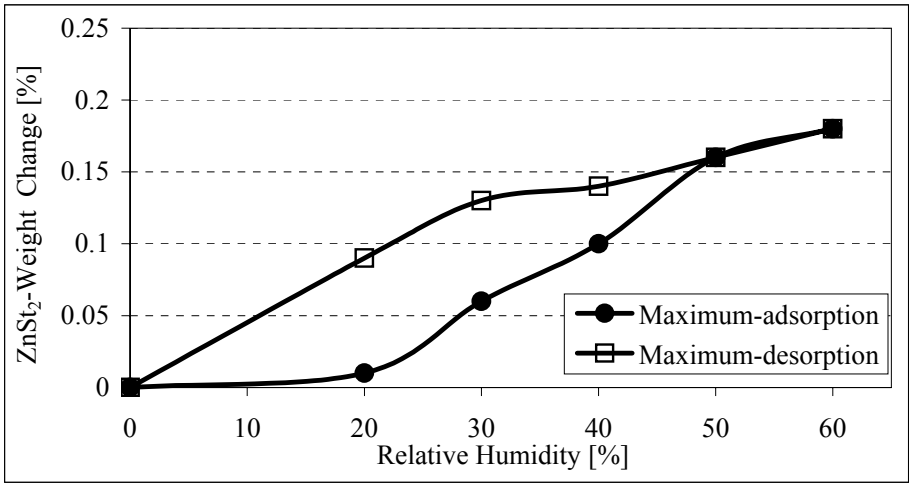


Figure 10.46. Adsorption and desorption of water vapor on $ZnSt_2$ at 25°C.

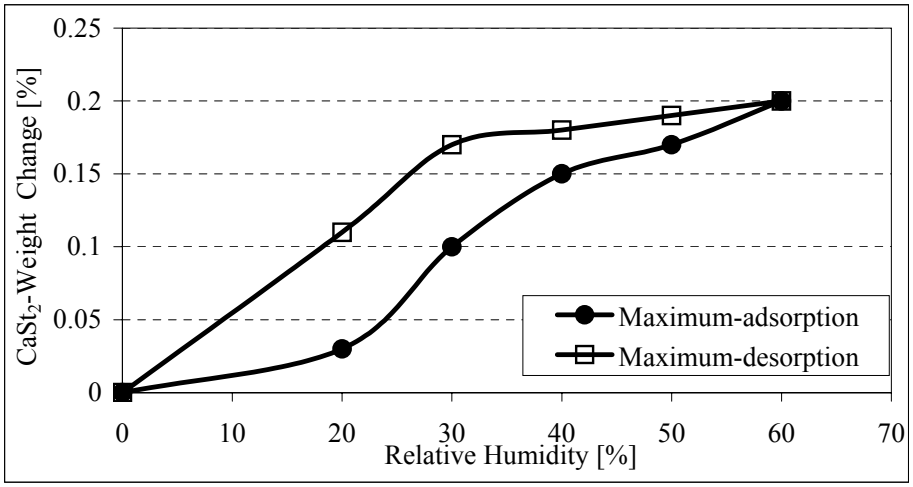


Figure 10.47. Adsorption and desorption of water vapor on $CaSt_2$ at 25°C.

It is clearly seen that the weight change is very small with respect to humid atmosphere. The weight increase for maximum relative humidity (60 %) is just 0.2 % for $ZnSt_2$ and $CaSt_2$. They adsorb water vapour faster but releases slowly. This might be a problem for humidity sensor applications because it is well known that response to any change for a sensor material is very crucial although the comparison of bulk material with thin film might not be correct. On the other hand, StAc weight change with relative humidity is unpredictable and water vapor adsorption was in the error limit of determination method for both adsorption and desorption cases.

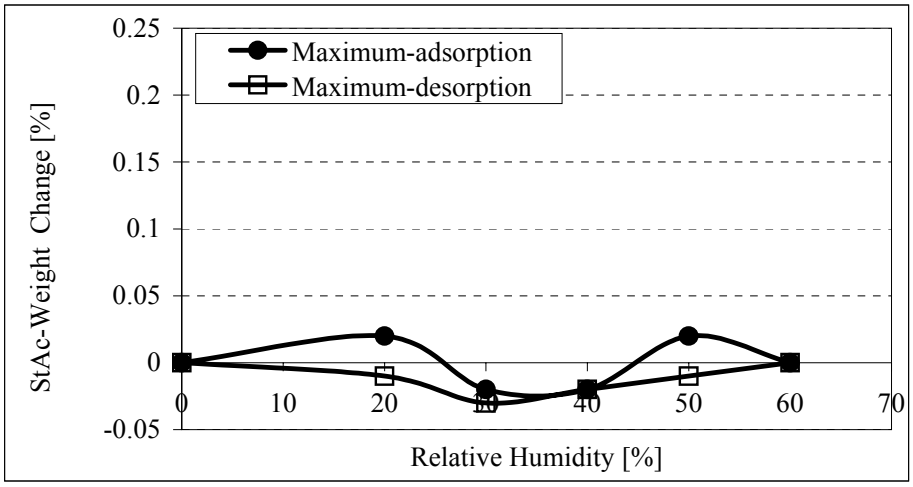


Figure 10.48. Adsorption and desorption of water vapor on StAc at 25°C.

## 10.4.6.1. Adsorption Isotherms and Adsorption Models

Different models were applied to each equilibrium data. As indicated from Figure 10.49. and Figure 10.50., as well as from regression coefficient values, Chung-Pfost model showed considerable superiority to others. This model were applied to water sorption characteristics of substances (Barreiro et al. 2005). It is given by;

$$\ln a_W = A\exp(BV) \qquad (10.3)$$

where A: regression constant for the isotherm model, $a_w$: water activity (dimensionless), V: moisture content, B: regression constant for the isotherm model. It gave better correlation for both $CaSt_2$ and $ZnSt_2$. There is no adsorption model suitable for stearic acid. Because StAc do not easily adsorp and desorp water vapour as it is seen from water vapour adsorption-desorption graphic.

Kusano in their study reported that number of water molecules increased with increasing the number of palmitoyl cellulose organic layers. However, this increase may not be in the same degree. The twofold increase in layer number did not give twofold increase in number of water molecules adsorbed.

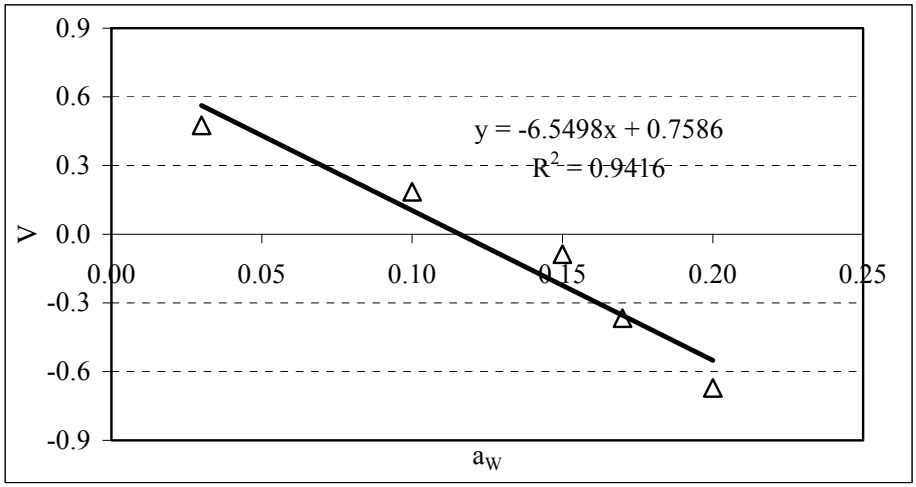


Figure 10.49. Chung-Pfost adsorption model applied to adsorption of water vapour by $CaSt_2$ solid particles at 25°C.

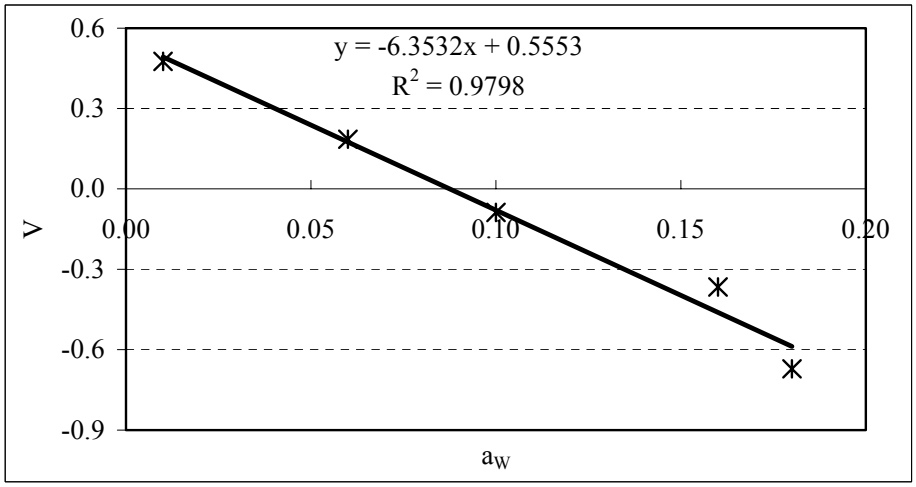


Figure 10.50. Chung-Pfost adsorption model applied to adsorption of water vapour by $ZnSt_2$ solid particles at 25°C.

Our results showed that in the low relative humidity region, desorption/adsorption was observed to be slow, whereas in the high relative humidity region it was more rapid. Kusano interpreted this behaviour as using two different adsorption model Freundlich and Polanyi. In low relative humidity region, Freundlich adsorption model were applied and it is explained as sorption onto the hydrophilic sites in the glucose units in the monolayer. In high relative humidity region, another model (Polanyi) dominated sorption characteristics and sorption process is controlled by the free condensation of water molecules onto the film surface (Kusano et al. 1997).

## 10.4.7. Electrical Conductivity of the $ZnSt_2$ LB Films

Electrical measurements on LB layers (particularly monolayers) are a stringent test of film quality and possibly the most difficult of all the available characterization tools. Although there have been many reports on the structural and optical properties of LB layers, it is not easy to obtain reproducible and reliable electrical data. This is almost certainly due to film preparation and handling techniques.

The results of LB film deposition processes, and characteristics of LB films showed that $ZnSt_2$ films were easily formed and have good ordered structure in comparison to $CaSt_2$. For molecular electronic applications, calcium soaps have been reported in some studies to be unstable (Peterson 1990). The water vapour adsorption results also suppported the usage of this compound and $ZnSt_2$ was chosen to study humidity sensor characteristics.

Before studying humidity sensor characteristics of $ZnSt_2$ LB films, electrical properties of this metal soap LB films were investigated. The films were in direct contact with two solid electrodes (silver). Two types of arrangement were studied; through plane and in plane. However, electrodes were established by hand (e.g., using a fine paint brush), the dimensions of the electrodes were not well defined and the electrical conductivity was only approximate. The current values were measured after 5 sec of voltage supply.

### 10.4.7.1. Through Plane Conductivity

The application of a small voltage to the junctions of monolayer assemblies between evaporated silver electrodes produces a current due to the tunnelling of electrons through $ZnSt_2$ multilayer as presented in Figure 10.51. The measurements were done with two terminal connections at $20^oC$ and RH 45%. The measurements made between the points indicated in the legend and shown in the Figure 9.3. The voltage applied to 0 connection point. The current values are taken from 1, 2 and 3 connection points respectively. The current values rised with the increase of voltage values.

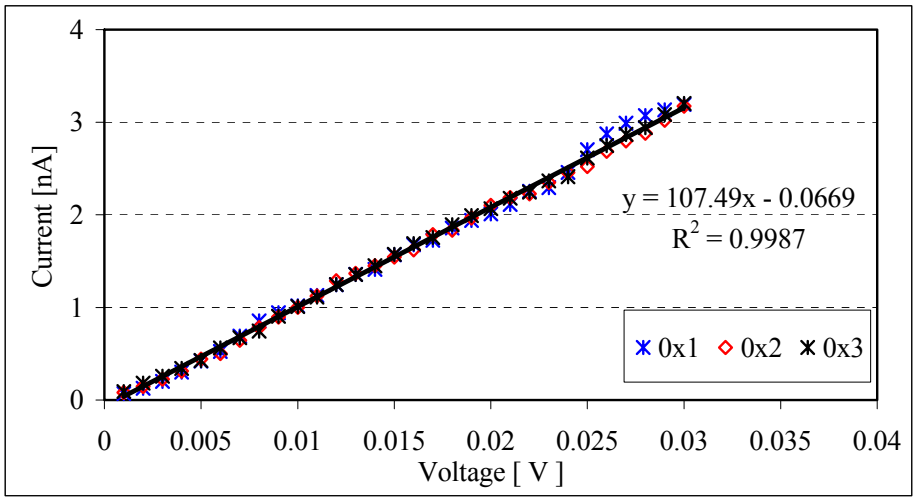


Figure 10.51. Current-voltage plots of 9 layers $ZnSt_2$ LB film at ambient conditions.

In LB film deposition process, before first monolayer was transferred, the substrate is normally exposed to the atmosphere and then dipped into the water solution in the Langmuir trough. The oxide layer which is unavoidably present added another semi-insulating region in series with insulating organic film and thus complicated the interpretation of the experimental data. Roberts also reported that the oxide layer influences current-voltage characteristics in $CdAd_2$ tunnelling structures (Roberts et al. 1978).

The electrical conductivity is calculated from the values of the applied voltage V and current I using the equation given in (Petty 1996);

$$\sigma = \frac{I \times t}{V \times A} = \frac{t}{A \times R} \qquad (10.4)$$

where t is the film thickness taken as nine layers $ZnSt_2$ film $(2\pm0.2)\times10^{-8}$, A is the area of electrode overlap $(0.25\times10^{-6})$ $m^2$ and R is the resistance taken as V/I at each data point. Conductivity versus voltage data was calculated for each experiment data point using equation above is plotted in Figure 10.52.

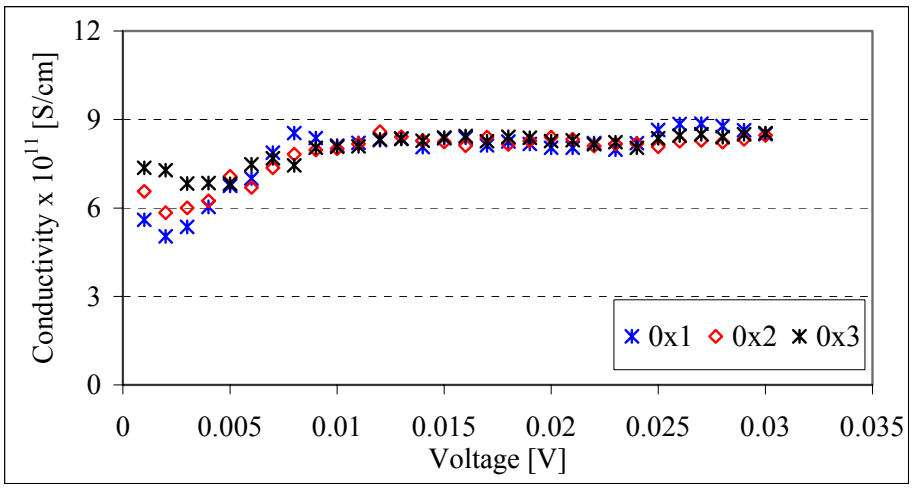


Figure 10.52. Conductivity change with voltage properties of $ZnSt_2$ LB film with 9 layers at ambient conditions.

At low voltages, conductivity values contained experimental fluctuation, but in 0.008-0.03 mV range, conductivity was nearly constant at $7.2\times10^{-11}$ S/cm. The conductivity through LB multilayers can be described by a combination of two mechanisms: a) electron tunnelling through each LB bilayer and b) Thermally activated hopping within the plane of carboxylic head groups (Nabok et al. 2002).

In these measurements, the several effects of different factors could not be omitted. The presence of pin holes might increase the conductivity values. The currents measured whilst being largely due to tunnelling might not be through organic layer but rather via defects in it. This is confirmed with Tredgold (Tredgold et al. 1981). Water molecules from the interstices between the molecules, progressive oxidation of silver and hence thickening of AgO layer; annealing out of defects in the monolayer also could affect conductivity.

It can be suggested that the evidence here shows that some defects (grain boundaries or pin holes), characterised by the σ-V and I-V curves presented, might be slowly annealed from the film and higher voltages force the organic molecules reorganization. Above 0.008 volt, this reorganization stops and leads to the constant conductivity.

### 10.4.7.2. In Plane Conductivity

Typical room temperature I–V characteristics of the 13 layer $ZnSt_2$ monolayer assemblies between silver electrodes are presented in Figure 10.53. The measurements were done with two terminal connections at 20°C and RH 40 %. The voltage applied to points; firstly to 1 and then 2, the current values are taken from firstly from 4, 5, and 6 and then only 6 respectively depicted in Figure 10.53.

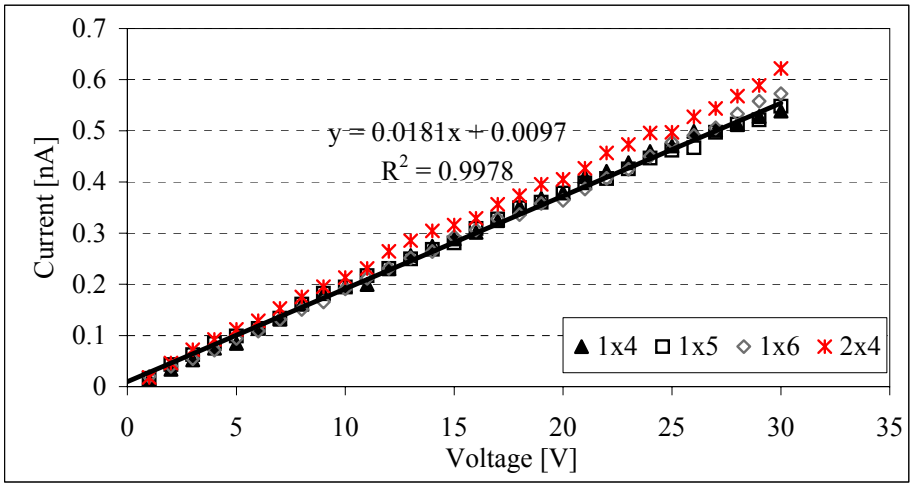


Figure 10.53. Current-voltage plots of 13 layer $ZnSt_2$ LB film at ambient conditions.

In plane measurements, same relationship between voltage and current seen in through plane measurements is valid. The measured current increased with applied voltage linearly.

To evaluate the in-plane conductivity from the current and voltage measurements using the equation given in (Petty 1996);

$$\sigma = \frac{I \times d}{V \times l \times t} \qquad (10.5)$$

where d is the distance between the electrodes taken as $80\times10^{-6}$ m confirmed by AFM image in Figure 10.54., l is the total length of their overlap measured as 0.36 cm and t is the thickness taken as 13 layer $ZnSt_2$ layer $(3\pm0.2)\times10^{-8}$ m.

Conductivity versus voltage data was calculated for each experiment data point using equation 10.5 and plotted in Figure 10.55. Although there was a fluctuation at smaller voltages, after 10 V, the conductivity values were stabilized.

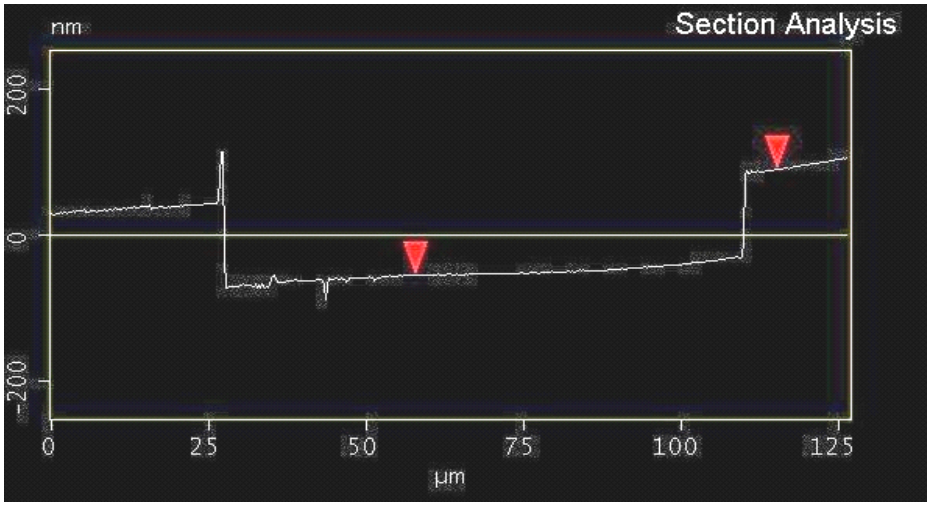


(a)

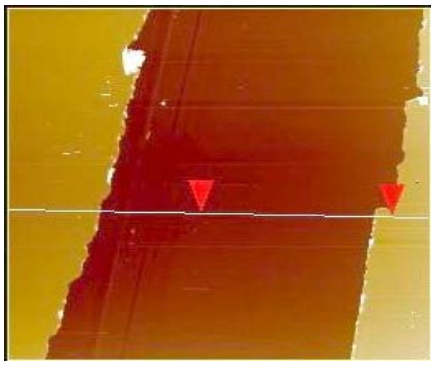

(b)

Figure 10.54. (a) Section analysis, (b) AFM image of related channel showing the distance between two silver electrodes for in plane measurements.

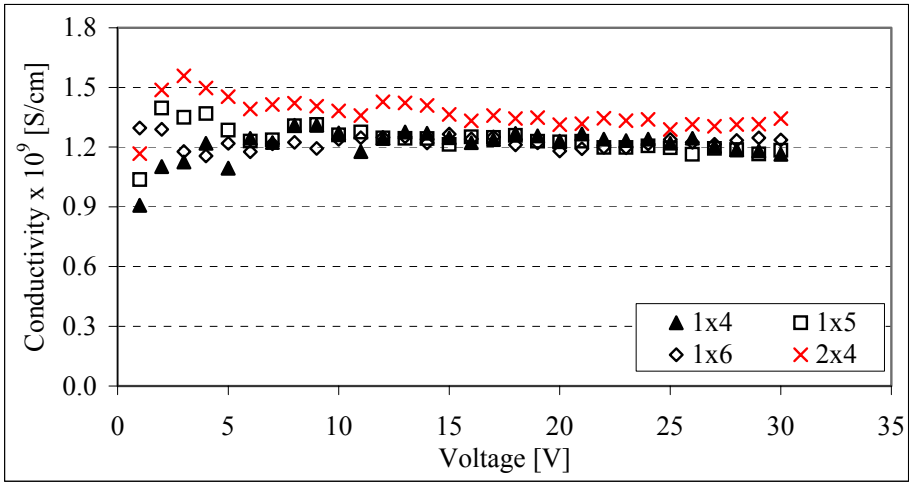


Figure 10.55. Conductivity change with voltage properties of $ZnSt_2$ LB film with 13 layers at ambient conditions.

The electrical characteristics of LB films has been found by many workers to depend on the ambient (Roberts 1990). Therefore, current voltage characteristics of thirteen layers of $ZnSt_2$ LB film were characterized by $N_2$ atmosphere as well (Figure 10.56.). The same trend; linear dependency of the current on voltage were obtained.

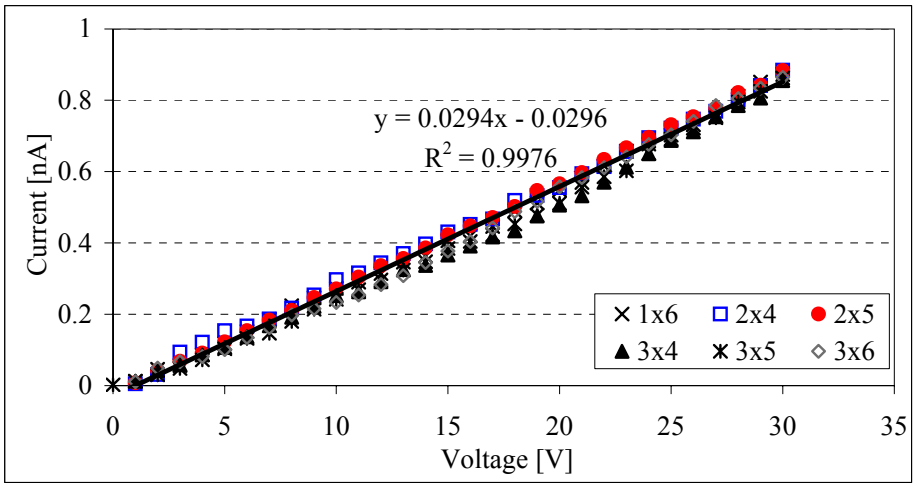


Figure 10.56. Current-voltage plots of 13 layer $ZnSt_2$ LB film at $N_2$ atmosphere at 25°C .

If the conductivities measured $N_2$ atmosphere and ambient condition were compared, the relatively higher conductivities were observed for $N_2$ atmospere as seen in Figure 10.57. Higher conductivities are invariably found if the measurements are made in air, probably due to the presence of moisture (Roberts 1990). However, our results showed opposite of this behaviour. This could be attributed to inevitable presence of water coming from outside during handling in layers.

Some of our data for zinc stearate LB films on silver coated glass substrates are similar to those reported by previous authors but our results also indicate that $ZnSt_2$ LB films may well have different electrical behaviour. It seems very likely that the presence of water of hydration in the zinc stearate multilayer is in part responsible for the electrical conductance observed. Because water content must affect the electrical and the optical properties of LB films (Ariga et al. 1994). This is unsuprising as the polar nature of water molecules may attract them to the head group regions of the multilayer structure. This result is also confirmed with the measurements done in humid atmosphere. This may be cause of why observed conductivities are higher than the values corresponding stearic acid measured by Kim (Kim et al. 1998). Moreover, it is

certain that $ZnSt_2$ layers are in ionic character this can give also higher conductivity values. Now, it is quite complicated to rationalize reasons of the difference revealed.

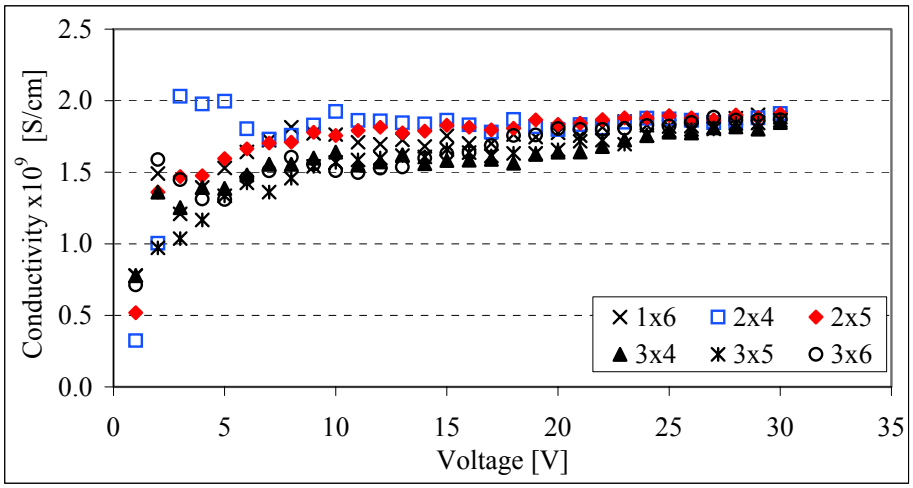


Figure 10.57. Conductivity change with voltage properties of $ZnSt_2$ films with 13 layers at $N_2$ atmosphere.

Figure 10.58. and 10.59. show change of current at specific voltages with respect to relative humidity. The measured current increased with the applied voltage especially higher than 9 V.

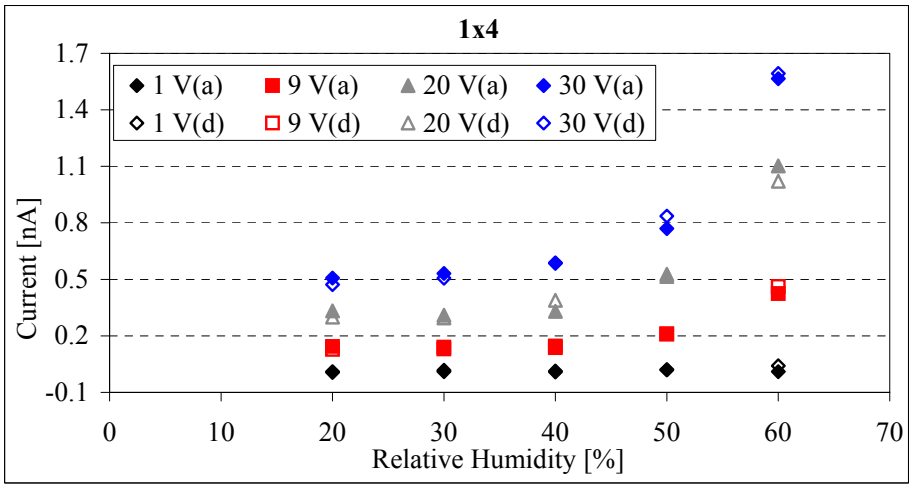


Figure 10.58. Effect of relative humidity on measured current at specific applied voltage ( a:adsorption, d:desorption) on connection points 1 and 4.

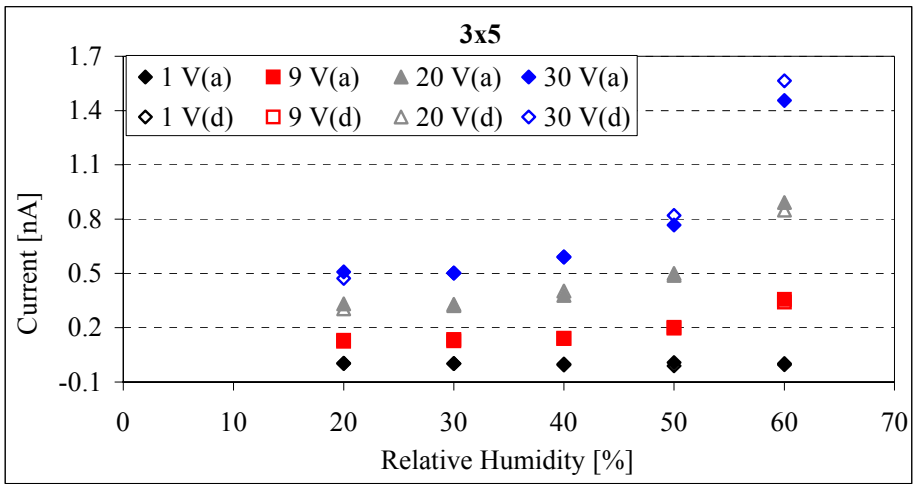


Figure 10.59. Effect of relative humidity on measured current at specific applied voltage (a:adsorption, d:desorption) on connection points 3 and 5.

There are two region behaviours in these graphs; low relative humidity region and high relative humidity region. In low relative humidity region (20% to 40%), the effect of water vapour in humid atmosphere to current values is relatively small. However, in high relative humidity region (40% to 60%), the strong dependency of current values on relative humidity is clearly seen.

Conductivity change of $ZnSt_2$ LB films after exposure to humid atmosphere is given in Figure 10.60. and 10.61. for different connections. The conductivity of $ZnSt_2$ layers for an in-plane was distributed in the range of $10^{-9}$ S/cm in humid air which close to the range of semiconductor (around at $10^{-8}$ S/cm). The conductivity values increased in higher humid atmospheres. This phenomena occurred by surface adsorption and penetration of humid air molecules into organic $ZnSt_2$ layers. Especially at higher voltages (>9V) and higher relative humidity values (>40%), sharp increase in conductivity with voltage was observed.

If the behaviour of conductivity in Figures 10.60. and 10.61. with respect to relative humidity at definite applied voltages is represented by third degree equation; $y=ax^3+bx^2+cx+d$, high R-square values are obtained. Because it is clear that the relation between conductivity and voltage was not linear. The R-square values and coefficients of applied third degree equation are given in Table 10.7. for connection points 1 and 4, and in Table 10.8. for connection points 3 and 5. Moreover, power law variation of D.C. conductivity is observed in a wide variety of amorphous materials but zinc stearate provides one of the examples of such behaviour in an ordered system.

During adsorption and desorption of water vapour, no hysteresis was observed for conductivity-voltage measurements but moisture adsorption-desorption curve of $ZnSt_2$ solid powder showed hysteresis as seen in Figure 10.46. Thus, the increase in conductivity with moisture should not be attributed to only moisture adsorption. There could be another mechanism effective. On the other hand, the thin film might come to the equilibrium quickly different from the bulk phase present in powder substances because it is very thin and open to the humid atmosphere present in the chamber. It can be readily influenced from the exposure to humidity.

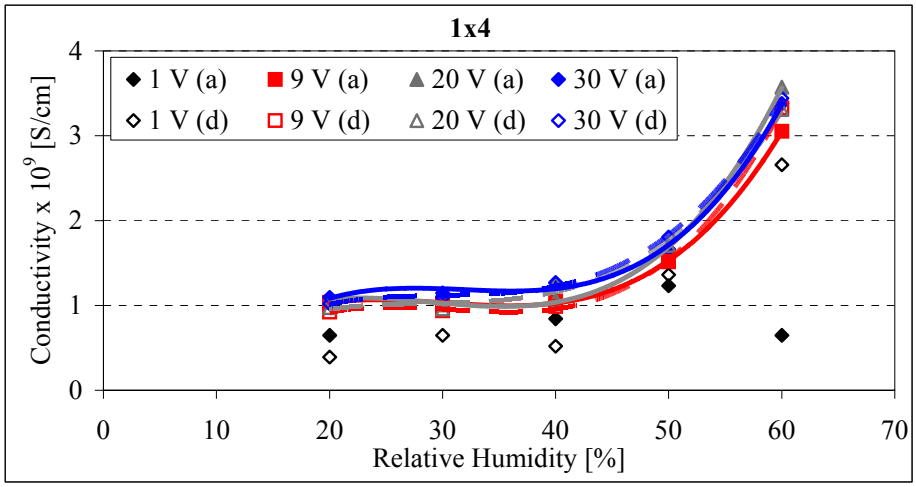


Figure 10.60. Effect of relative humidity on measured conductivity at specific applied voltage (a:adsorption, d:desorption) on connection points 1 and 4.

Table 10.7. Equation constants and R square values for conductivity versus relative humidity measurements done at connection points 1 and 4.

| | *Voltage* | *a* | *B* | *c* | *d* | $R^2$ |
|---|---|---|---|---|---|---|
| *Adsorption* | *1 V* | $-2\times10^{-5}$ | 0.0016 | -0.0136 | 0.5056 | 0.5475 |
| | *9 V* | $9\times10^{-5}$ | -0.0077 | 0.2225 | -1.0226 | 0.9996 |
| | *20 V* | $1\times10^{-4}$ | -0.0084 | 0.2324 | -0.9787 | 0.9996 |
| | *30 V* | $1\times10^{-4}$ | -0.01 | 0.3108 | -1.9851 | 0.9972 |
| *Desorption* | *1 V* | $7\times10^{-5}$ | -0.0063 | 0.1916 | -1.4778 | 0.9857 |
| | *9 V* | $1\times10^{-4}$ | -0.0095 | 0.2818 | -1.7529 | 0.9996 |
| | *20 V* | $7\times10^{-5}$ | -0.006 | 0.1734 | -0.6786 | 0.9949 |
| | *30 V* | $8\times10^{-5}$ | -0.0075 | 0.226 | -1.1852 | 0.9993 |

The conductivities measured for through and in plane arrangements are very different. Because the pathway which electrons follow is different. The way followed for in plane is much longer than through plane. The presence of cations on the pathway increased the measured conductivity values much higher (100 times).

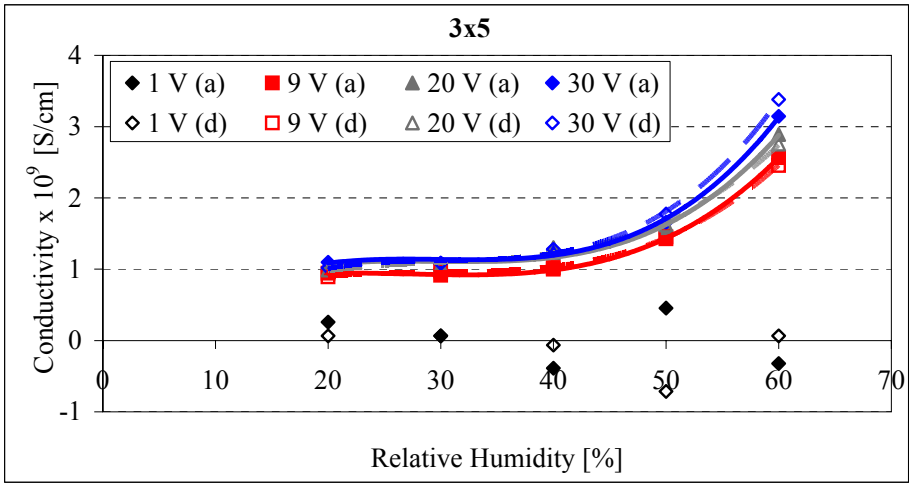


Figure 10.61. Effect of relative humidity on measured conductivity at specific applied voltage (a:adsorption, d:desorption) on connection points 3 and 5.

Table 10.8. Equation constants and R square values for conductivity versus relative humidity measurements done at connection points 3 and 5.

| | *Voltage* | *a* | *b* | *c* | *d* | $R^2$ |
|---|---|---|---|---|---|---|
| *Adsorption* | *1 V* | $-1\times10^{-4}$ | 0.0137 | -0.5211 | 6.1704 | 0.4636 |
| | *9 V* | $5\times10^{-5}$ | -0.0041 | 0.107 | 0.0302 | 0.9998 |
| | *20 V* | $6\times10^{-5}$ | -0.0058 | 0.1691 | -0.5308 | 0.9968 |
| | *30 V* | $7\times10^{-5}$ | -0.0067 | 0.198 | -0.7938 | 0.9961 |
| *Desorption* | *1 V* | $1\times10^{-4}$ | -0.0148 | 0.5111 | -5.3019 | 0.8298 |
| | *9 V* | $5\times10^{-5}$ | -0.0044 | 0.1311 | -0.3687 | 0.9996 |
| | *20 V* | $5\times10^{-5}$ | -0.0045 | 0.1424 | -0.4634 | 0.9942 |
| | *30 V* | $8\times10^{-5}$ | -0.0074 | 0.2243 | -1.1814 | 0.9984 |

### 10.4.8. The Application of $ZnSt_2$ LB Films as Humidity Sensor

By measuring conductivity and applying known voltage in humid atmosphere, humidity could be determined from equation $y=ax^3+bx^2+cx+d$. The root of this equation in expected humidity range will give the humidity. Thus it can be used as a humidity sensor. However, as it is seen from related figures, the applicable humidity range was between 40% and 60% RH. Besides voltage should be higher than 9 V. At voltages lower than 9 V and lower relative humidity values (20-40%), response to change in ambient humidity was out of practice.

$ZnSt_2$ LB multilayer is anisotropic with different head and tail parts. This property of $ZnSt_2$ give different sorption capacity to sorbents as here in water vapour. Although it is assumed that stearic acid molecules well packed into planar structures and individual lamallae are readily and strongly "glued" together with $Zn^{2+}$ cations, to form well ordered, stable multilayered films. They might harbor nanoscopic regions of disorder or "pockets" with corresponding high and/or selective absorption affinities. Water molecules may "fill the molecular gaps" without introducing much or any expansion of the film or or come into contact with polar head groups of $ZnSt_2$ LB film. Therefore, with more sophisticated set-up, humidity sensor applicability of $ZnSt_2$ LB films can be understood well.

# CHAPTER 11

# CONCLUSIONS

This study is about the preparation and characterization of metal soap (calcium and zinc stearate) nanofilms. The preparation of nanofilms was done with Langmuir-Blodgett deposition technique by sequentially transferring monolayers from a liquid subphase onto a solid substrate in a predefined, controllable way.

The solid or solid-liquid phases obtained by compressing stearic acid layer were chosen to transfer. Surface pressure relaxation studies showed that a fast decrease of area at the beginning, and after some time, a constant area is probably a rearrangement of molecules in the monolayer takes place (promotion of crystallization within the two dimensional space) or collapse of monolayer. The mechanism of nucleation is instantaneous with hemispherical nuclei formed and growth through the edges for stearic acid layer. Moderate pH close to 6 and low temperature were ideal conditions for stearic acid layer because of better packing confirmed by surface compression moduli values. The change of mean molecular area of stearic acid with compression speed may be related to the compression of a meta-stable monolayer under non-equilibrium conditions.

To form zinc and calcium stearate LB films, these cations were incorporated into the subphase by metal salts. In the stearic acid monolayer, the liquid condensed $L_2$ phase and the super-liquid LS phase (more correctly solid phase) were observed while there was only an LS phase in zinc stearate and calcium stearate monolayers. The "plateau" at $\pi_C$ for metal stearates has been associated with the irregular fracture of the ionized monolayers. The bonding between the metal ion and the fatty acid carboxylate ion is covalent character for zinc stearate and ionic character for calcium stearate due to the electronegativity difference between zinc and calcium ions. Nucleation process modelling results depicted that the progressive nucleation mechanism where hemisperical nuclei formed and grow from the edges were observed for both metal stearates.

The monolayer studies revealed that as monolayer stability behaviour and molecular packing arrangement in metal salt multilayers were significantly affected by subphase pH and temperature. The critical pH value for zinc stearate 6.1 and for

calcium stearate around 9. The low temperature decreased thermal motion and led to condensed layers for zinc and calcium stearates.

The formation of films characterized by transfer ratio are dramatically influenced by the subphase and substrate properties such as pH, temperature, concentration of metal and buffer ions, hydrophobicity or hydrophilicity of substrate, dipping speed, transfer surface pressure and drying period. For instance, the excess metal concentration caused higher transfer ratio. In particular, the decrease in transfer ratio with number of layers may be due to an increasing density of defects in the preceding monolayer especially for stearic acid monolayer and XY deposition for metal stearates. The dissolution, evaporation, or monolayer collapse mechanisms were other dominant factors.

It was concluded from XRD patterns that zinc stearate crystallinity was higher with respect to calcium stearate and stearic acid and measured cyrstal size was around 90 nm confirmed by SEM micrographs. The zinc stearate arrangement may be identified as under the orthorhombic (R) subcell with chain tilt angle of $31^{o}$. Our FTIR results were also in aggreement with XRD so that zinc stearate molecules have tilting angle due to high intensity ratios of the ($\nu_a CH_2$) band to the ($\nu_s COO^-$) band. IR spectra of calcium stearate and zinc stearate LB films on silver coated surface indicated that zinc ion forms bridging bidantate type bonding and calcium cation forms chelating bidentate type and ionic type bonding with carboxylate ion of stearic acid. On the other hand, preparation of KBr pellets from wet films affected the state of the films. Rather than KBr technique, in situ measurement of IR spectrum should be preferred.

AFM and SEM images showed that surface roughness of glass slides was decreased firstly chrome coating and then silver coating. Zinc stearate coated surfaces have large crystal size and contained grains and defects.

The adsorption desorption behaviour of water vapour on zinc and calcium stearate and stearic acid solid powders was different. Metal stearates did not give easily the adsorbed water causing the hysteresis. The proper model for water vapor adsorption on zinc and calcium stearate was Chung-Pfost model. There was no clear weight change observed for stearic acid indicating that water vapour was not adsorbed.

The results of LB film deposition processes and characteristics of produced LB films showed that $ZnSt_2$ films were easily formed and had good ordered structure in comparison to $CaSt_2$. Thus, $ZnSt_2$ was chosen to study humidity sensor characteristics.

It has been investigated for the first time, the electrical properties of $ZnSt_2$ LB films deposited onto a silver coated glass surface. The current values were increased with voltage increment for the through plane and the in plane measurements done on $ZnSt_2$ LB films. The conductivity versus voltage curves taken at different environmental conditions strongly emphasized the dependency of electrical characteristics of $ZnSt_2$ LB films on humidity. The effects of humid air on the measurements done in the room and $N_2$ atmosphere can be minimized for by storing the samples in a dry environment in $P_2O_5$ desiccator to understand the better electrical behaviour of $ZnSt_2$ LB films.

Although moisture adsorption-desorption curve of $ZnSt_2$ solid powder showed hysteresis, no hysteresis during adsorption and desorption conductivity-voltage measurements was observed for zinc stearate LB films. Thus, the increase in conductivity with moisture should not be attributed to only moisture adsorption. There could be another mechanism effective. On the other hand, the thin film might come to the equilibrium quickly different from the bulk phase present in powder substances because it is very thin and open to the humid atmosphere present in the chamber. It can be readily influenced from the exposure to humidity.

The following conclusions were drawn from the conducitivity measurements done on $ZnSt_2$ LB films. The relation between conductivity and voltage was not linear. By measuring conductivity and applying known voltage in humid atmosphere, humidity could be determined from equation $y = ax^3+bx^2+cx+d$. The root of this equation in expected humidity range will give the humidity. Thus it can be used as a humidity sensor. However, the applicable humidity range was limited to 40-60% RH and when voltage was higher than 9 V.

Data obtained in the course of this study makes it possible to control the cationic composition of LB films of zinc and calcium stearates by varying aqueous subphase properties. After grasping the fundamentals of monolayer formation and film deposition, metal stearate LB films with decreased content of micro- and macrodefects will be produced and applied for more sophisticated purposes. With preparation of electrode structure using nanolithography technique, these films can be utilized in gas sensing circuit and organic Josephon tunnel barrier between superconductive electrodes such as $MgB_2$ or YBCO to get better tunnelling characteristics.

# REFERENCES


Adamson, A.W., 1990. *Physical Chemistry of Surfaces*, (Wiley-Interscience, New York), pp. 131-141.

Ariga K. and Okahata, Y., 1994. "In Situ Characterization of Langmuir-Blodgett Films During a Transfer Process. Evaluation of Transfer Ratio and Water Incorporation by Using a Quartz Crystal Microbalance" *Langmuir*. Vol. 10, pp. 3255-3259.

Avila, L.V.N., Saraiva, S.M., Oliveira, J.F., 1999. "Stability and Collapse of Monolayers of Stearic Acid and the Effect of Electrolytes in the Subphase," *Colloids and Surfaces A: Physicochemical and Engineering Aspects*. Vol. 154, pp. 209-217.

Bagg. J., Abramson, M.B., Fichman, M., Haber M.D., Gregor, H.P., 1964. "Composition of Stearic Acid Monolayers from Calcium-containing Substrates," *Journal of the American Chemical Society*. Vol. 86, pp. 2759-2763.

Barreiro, J.A., Fernandez, S., Sandoval, A.J., 2003. "Water Sorption Characteristics of Six Row Barley Malt (Hordeum Vulgare)", *Lebensm.-Wiss. U.-Technol.* Vol. 36, pp. 37-42.

Benavides, R., Edge, M., Allen, N.S., 1994. "The Mode of Action of Metal Stearate Stabilisers in Poly (vinyl chloride). I. Influence of Pre-heating on Melt Complexation", *Polymer Degradation and Stability*. Vol. 44, pp. 375-378.

Blachford, J., *U.S. Patent*, 4,316,852, 1982.

Braun, R.D., 1983. *Introduction to Chemical Analysis,* (McGraw Hill Inc., Singapore), p. 441.

Bukreeva, T.V., Arslanov, V.V., Gagina, I.A., 2003. "Langmuir-Blodgett Films of Fatty Acid Salts of Bi- and Trivalent Metals: Y, Ba, Cu Stearates," *Colloid Journal*. Vol. 65-2, pp. 134-140.

Cao, C., Zhu, H., Wang, H., 2000. "Electrodeposition Diamond-like Carbon Films from Organic Liquids", *Thin Solid Films*. Vol. 368, pp. 203-207.

Chen, Y.L., Israelachvili, J.N., 1992. "Effects of Ambient Conditions on Adsorbed Surfactant and Polymer Monolayers" *J. Phys. Chem.* Vol. 96, pp. 1152-1160.

Çapan, R., Richardson, T.H., Lacey D., 2004. "Pyroelectric Effect in Langmuir-Blodgett Films Incorporating Ions", *Thin Solid Films.* Vol. 468, pp. 262-267.

Datta, A., Kmetko, J., Yu, C-J., Richter, A.G., Chung, K-S., Bai, J-M., Dutta, P., 2000. "pH-dependent Appearance of Chiral Structure in a Langmuir Monolayer", *J. Phys. Chem. B.* Vol. 104, pp. 5797-5802.

Dhanabalan, A., Kumar, N.P., Major, S., Talwar, S.S., 1998. "Variation of Monolayer Behaviour and Molecular Packing in Zinc-arachidate LB films with Subphase pH," *Thin Solid Films*. Vol. 327-329, pp. 787-791.

Dote, J.L. and Mowery, R.L., 1988. "Infrared Reflectance-Absorption Spectra of Langmuir-Blodgett Stearic Acid Monolayers on Gold and Aluminum. Influence of Substrate" *J. Phys. Chem.* Vol. 92, pp. 1571-1575.

Dreuth, H., Heiden, C., 1998. "A Method for Local Application of Thin Organic Adhesive Films on Micropatterned Structures," *Materials Science and Engineering C.* Vol. 5, pp. 227-231.

Dupres, V., Cantin, S., Benhabib, F., Perrot, F., Fontaine, P., Goldmann, M., Daillant J. and Konovalov, O., 2003. "Superlattice Formation in Fatty Acid Monolayers on a Divalent Ion Subphase: Role of Chain Length, Temperature, and Subphase Concentration", *Langmuir.* Vol. 19, pp. 10808-10815.

Elvers, B., Hawkins, S. and Schulz, G., 1990. "Ullmann's Encyclopedia of Industrial Chemistry", Vol. A16, 5th Edition, pp. 361-371.

Gaines, G.L.; 1966. *Insoluble Monolayers at Liquid-Gas Interfaces*, (Intersciences, New York), pp. 30-40.

Girard, K.P., Quinn, J.A. and Vanderlick, T.K., 1999. "The Directional Dependence of Water Penetration into Langmuir–Blodgett Multilayers", *Journal of Colloid and Interface Science.* Vol. 217, pp. 146-153.

Girard, K.P., Quinn, J.A., Vanderlick, T.K., 2002. "Vapor Sorption into Pure and Mixed Fatty Acid Multilayers", *Langmuir*. Vol. 18, pp. 5830-5834.

Gönen, M., Process Development for Metal Soaps, *M.S. Thesis*, İzmir Institute of Technology, 2003.

Hansma, H.G., Gould, S.A.C. and Hansma, P.K., 1991. "Imaging Nanometer Scale Defects in Langmuir-Blodgett Films with Atomic Force Microscope", *Langmuir*. Vol. 7, pp. 1051-1054.

Hasegawa, T., Umemura J., Kamata, T., Takenaka T., 1990. "Thermal Stability of Metal Stearate LB Films Studied by Infrared Reflection-Absorption Spectroscopy," *Japan Chemistry Letters*. pp. 1543-1546.

Hasmonay H., Vincent, M., Dupeyrat, M., 1980. "Composition and Transfer Mechanism of Langmuir-Blodgett Multilayers of Stearates", *Thin Solid Films*. Vol. 68, pp.21-31.

Hiroshi S., Umemura, J., 1997. "Molecular Orientation Change in Langmuir Films of Stearic Acid and Cadmium Stearate upon Surface Compression as Studied by Infrared External-Reflection Spectroscopy", *Bull. Chem. Soc. Jpn*. Vol. 70, pp. 1027-1032.

Honig, E.P., Hengst, J.H., Engelsen, D.D., 1973. "Langmuir-Blodgett Deposition Ratios", *Journal of Colloid and Interface Science.* Vol. 45, pp. 92-102.

Howe-Grant, M., 1990. "Kırk-Othmer Encyclopedia of Chemical Technology", Vol. 8, 4th Edition, pp. 433-445.

Ito, T., Okayama, Y., Shiratori, S., 2001. "The Fabrication of Organic-Inorganic Multilayer by Wet Process and Sequential Adsorption Method", *Thin Solid Films*. Vol. 393, pp. 138-142.

Kamata, T., Kato, A., Umemura, J., Takenaka, T., 1987**. "**Intensity Enhancement of Infrared Attenuated Total Reflection Spectra of Stearic Acid Langmuir-Blodgett Monolayers with Evaporated Silver Island Films", *Langmuir.* Vol. 3-6, pp. 1150-1154.

Kanicky, J.R. and Shah, D.O., 2002. "Effect of Degree, Type, and Position of Unsaturation on the p*Ka* of Long-Chain Fatty Acids", *Journal of Colloid and Interface Science,* Vol. 256, pp. 201–207.

Khomutov, G.B., Yakovenko, S.A., Yurova, T.V., Khanin, V.V., Soldatov, E.S., 1997. "Effect of Compression of a Stearic Acid Monolayers on Interfacial Binding of Copper Ions and Cluster Formation", *Supramolecular Sci*. Vol. 4, pp. 349-355.

Khomutov, G.B., Antipina, M.N., Bykov, I.V., Dembo, K.A., Klechkovskaya, V.V., Yurova, T.V., Bohr, J., Gainutdinov, R.V., Tolstikhina, A.L., 2002. "Structural Studies of Langmuir-Blodgett Films Containing Rare-Earth Metal Cations", *Colloids and Surfaces A: Physicochemical and Engineering Aspects*. Vol. 198-200, pp. 261-274.

Kim, D.K., Choi, Y.S., Chang, J.S., Kwon, Y.S., 1998. "A Study on Gas Sensor Using Electrical Properties of Fatty Acid Langmuir–Blodgett Films" *Thin Solid Films*. Vol. 327–329, pp. 612-615.

Kmetko, J., Datta, A., Evmenenko, G., Dutta, P., 2001. "The Effects of Divalent Ions on Langmuir Monolayer and Subphase Structure: A Grazing-Incidence Diffraction and Bragg Rod Study" *J. Phys. Chem. B.* Vol. 105, pp. 10818-10825.

Kondrashkina, E.A., Hagedorn, K., Vollhardt, D., Schmidbauer, M., Köhler, R., 1996. "Structure of Relaxed Monolayers of Arachidic Acid Studied by X-ray Reflectometry and Atomic Force Microscopy", *Langmuir*. Vol. 12, pp. 5148-5155.

Kusano, H., Kimura, S., Kitagawa, M., Kobayashi, H., 1997. "Application of Cellulose Langmuir-Blodgett Films as Humidity Sensors, and Characteristics of the Sorption of Water Molecules into Polymer Monolayers", *Thin Solid Films*. Vol. 295, pp. 53-59.

Kutscher, J.S., Gericke, A., Hühnerfuss, H., 1996. "Effect of Bivalent Ba, Cu, Ni, and Zn Cations on the Structure of Octadecanoic Acid Monolayers at the Air-Water Interface As Determined by External Infrared Reflection-Absorption Spectroscopy", *Langmuir.* Vol. 12*,* pp. 1027-1034.

Leonard, M., Morelis, R.M., Coulet, P.R., 1995. "Linked Influence of pH and Cations on Fatty-Acid Monolayer Integrity Related to High-Quality Langmuir-Blodgett Films", *Thin Solid Films*. Vol. 260, pp. 227-231.

Li, C., Zhao, B., Lu, Y., Liang, Y., 2001. "Microstructure and Ion Exchange in Stearic Acid Langmuir-Blodgett Films Studied by Fourier Transform Infrared-Attenuated Total Reflection Spectroscopy"*, Journal of Colloid and Interface science*. Vol. 235, pp. 56-65.

Lin, B., Bohanon, T. M., Shih, M.C., Dutta, P., 1990. "X-ray Diffraction Studies of the Effects of $Ca^{2+}$ and $Cu^{2+}$ on Langmuir Monolayers of Heneicosanoic Acid", *Langmuir*. Vol. 6, pp. 1665-1667.

Lovell, M.R. and Roser, S.J. 1996. "Dependence of the Rate of Diffusion of Entrained Water on the Degree of Ion Incorporation in Langmuir-Blodgett Films" *Langmuir*. Vol. 12, pp. 2765-2773.

Markley, K.S., 1961. *Salts of fatty acids*, (Interscience Publishers, New York), pp. 739-752.

Marshbanks, T.L., Ahn, D.J., Franses, E.I., 1994. "Transport and Ion Exchange in Langmuir-Blodgett Films: Water Transport and Film Microstructure by Attenuated Total Reflectance Fourier Transform Infrared Spectroscopy" *Langmuir*. Vol. 10, pp. 276-285.

Moriizumi, T., 1988. "Langmuır-Blodgett Films as Chemical Sensors", *Thin solid films*. Vol. 160, pp. 413-429.

Nabok, A.V., Iwantono, B., Hassan, A.K., Ray, A.K., Wilkop, T., 2002. "Electrical Characterisation of LB Films Containing CdS Nanoparticles", *Materials Science and Engineering C*. Vol. 22, pp. 355-358.

Neuman, R.D., Swanson, J.W., 1980. "Multilayer Deposition of Stearic Acid-Calcium stearate Monomolecular Films", *Journal of Colloid and Interface science.* Vol. 74-1, pp. 245-258.

Neuman, R.D., 1975. "Calcium Binding in Stearic Acid Monomolecular Films", *Journal of Colloid and Interface Science.* Vol. 74-2, pp. 161-171.

Nieto-Su´arez, M., Vila-Romeu, N., Dynarowicz-Latka, P., Prieto, I., 2004. "The Influence of Inorganic Ions on the Properties of Nonionic Langmuir Monolayers", *Colloids and Surfaces A: Physicochem. Eng. Aspects*. Vol. 249, pp. 11-14.

Peng, J.B., Barnes, G.T., Gentle, I.R., 2001. "The Structures of Langmuir-Blodgett Films of Fatty Acids and Their Salts", *Advances in Colloid and Interface Science*. Vol. 91, pp. 163-219.

Peterson, I.R., 1990. "Langmuir-Blodgett Films", *J. Phys. D: Appl.Phys.* Vol. 23, pp. 379-395.

Petty, M.C., 1996. *Langmuir-Blodgett Films-An introduction*, (Cambridge University press, Cambridge), pp. 25-37.

Pignataro, B., Consalvo, C., Compagnini, G., Licciardello, A., 1999. "Barium stearate Langmuir–Blodgett Films Investigated by Mapping Adhesion Forces With Atomic Force Microscopy," *Chemical Physics Letters*. Vol. 299, pp. 430-436.

Rajagopal, A., Dhanabalan, A., Major, S.S., Kulkarni, S.K., 1998. "The Effect of Different Metal Cation Incorporation in Arachidic Acid Langmuir-Blodgett (LB) Monolayer Films", *Applied Surface Sci.* Vol. 125, pp. 178-186.

Rashid, Ali N., Gunter, P., 2004. "Self-Assembled Organic Supramolecular Thin Films for Nonlinear Optics", *Organic Electronics.* Vol. 5, Issues 1-3, pp. 147-155.

Roberts, G., 1990. *Langmuir-Blodgett films*, (Plenum Press, New York), pp. 113-120.

Roberts, G.G., Vincett, P.S, Barlow, W.A., 1978. "AC and DC Conduction in Fatty Acid Langmuir Films", *J. Phys. C: Solid State Phys.* Vol. 11, pp. 2077-2085.

Sakai, H., Umemura, J., 2002. "Evaluation of Molecular Structure in Langmuir Monolayers of Zinc stearate and Zinc-12-hydroxystearate by IR External Reflection Spectroscopy," *Colloid Polym. Sci*., Vol. 280, pp. 316-321.

Schwartz, D.K., 1997. "Langmuir-Blodgett Film Structure," *Surface Science Reports*. Vol. 27, pp. 241-334.

Scott, L.F., Strachan, H.D., McCloskey, C.M., U.S. Patent 3,803,188, 1974.

Shih, M.C., Bohanon, T.M., Mikrut, J.M., Zschack, P., Dutta, P., 1992. "Pressure and pH Dependence of the Structure of a Fatty Acid Monolayer with Calcium Ions in the Subphase" *J. Chem. Phys.* Vol. 96, pp. 1556-1559.

Sigiyama N., Shimizu, A., Nakamura, M., Nakagawa, Y., Nagasawa, Y., Ishida, H., 1998. "Molecular-scale Structures of Langmuir-Blodgett Films of Fatty Acids Observed by Atomic Force Microscopy (II)-Cation Dependence," *Thin Solid Films*. Vol. 331, pp. 170-175.

Srivastava, V.K., Verma, A.R., 1966. "Interferometric and X-ray Diffraction Study of "Built-up" Molecular Films of Some Long Chain Compounds", *Solid State Communications*. Vol. 4, pp. 367-371.

Stuart, R.V., 1983. *Vacuum Technology, Thin Films, and Sputtering-An Introduction,* (Academic press, Orlando), pp. 1-19.

Taylor, D.M., Oliveria, O.N., Morgan, H., 1989. "The Effect of Water Quality on the Electrical Characteristics of Langmuir Monolayers" *Thin Solid Films*. Vol. 173, pp. L141-L147.

Tredgold, R.H., Winter, C.S., 1981. "Tunnelling Currents in Langmuir-Blodgett Monolayers of Stearic Acid", *J. Phys. D: Appl. Phys.* Vol. 14, pp. L185-8.

Tredgold, R.H., Vickers, A.J., Allen, R.A., 1984. "Structural Effects on the Electrical Conductivity of Langmuir-Blodgett Multilayers of Cadmium Stearate", *J. Phys. D: Appl. Phys.* Vol. 17, pp. L5-LX.

Ulman, A., 1991. *An Introduction Ultrathin Organic Films from Langmuir-Blodgett to Self-Assembly*, (Academic Press, London), pp. 117-130.

Ulman, A., 1996. "Formation and Structure of Self-Assembled Monolayers", *Chem. Rev*. Vol. 96, pp. 1533-1554.

Umemura, J., Kamata, T., Kawai, T., Takenaka, T., 1990. "Quantitative Evaluation of Molecular Orientation in Thin Langmuir-Blodgett Films by FT-IR Transmission and Reflection-Absorption Spectroscopy", *J. Phys. Chem.* Vol. 94, pp. 62-67.

Umemura, J., Takeda, S., Hasegawa, T., Kamata, T. and Takenaka, T., 1994. "Effect of Thickness and Monolayer Location on Thermostability of Metal stearate LB Films Studied by FT-IR Reflection-Absorption Spectroscopy," *Spectrochimica Acta*. Vol. 50A, No.8/9, pp. 1563-1571.

Umemura, J., Takeda, S., Hasegawa, T., Takenaka, T., 1993. "Thickness and Temperature Dependence of Molecular Structure in Stearic Acid LB Films Studied by FT-IR Reflection-Absorption Spectroscopy," *Journal of Molecular Structure.* Vol. 29, pp. 57-62.

Umemura, J., Takenaka, T., Kimura, F., 1986. "FTIR-ATR Studies on Langmuir-Blodgett Films of Stearic Acid with 1-9 Monolayers", *Langmuir*. Vol. 2, pp. 96-101.

Umemura, J.; Toshihide, K.; Kato, A., Takenaka, T., 1987. "Intensity Enhancement of Infrared Attenuated Total Reflection Spectra of Stearic Acid Langmuir-Blodgett Monolayers with Evaporated Silver Island Films", *Langmuir*. Vol. 3, pp. 1150-1154.

Viswanathan, R., Schwartz, D.K., Garnaes, J., Zasadzinski, J.A.N., 1992. "Atomic Force Microscopy Imaging of Substrate and pH Effects on Langmuir-Blodgett Monolayers", *Langmuir*. Vol. 8, pp. 1603-1607.

Vollhardt, D. and Retted, U., 1992. "Nucleation in Insoluble Monolayers. 3. Overlapping Effect of the Growing Centers", *Langmuir*. Vol. 8, pp. 309-312.

Wagendristel, A., Yuming, W., 1994. *An introduction to Physics and Technology of Thin film,* (World Scientific, Singapore), pp. 3-15.

Wolthaus, L., Schaper, A. and Möbius, D., 1994. "Microcrystallinity of Solid-state Langmuir-Blodgett Films of Saturated Fatty Acids Studied by Scanning Force Microscopy and Brewster Angle Microscopy", *J. Phys. Chem*. Vol. 98, pp. 10809-10813.

Yazdanian, M., Yu, H., Zografi, G., 1990. "Ionic Interactions of Fatty Acid Monolayers at the Air/Water Interface", *Langmuir*. Vol. 6, pp. 1093-1098.

# APPENDIX A

# pH RANGE CALCULATIONS FOR STUDIED METAL CATIONS

Both the studied pH and the presence of divalent cations; $Ca^{2+}$ and $Zn^{2+}$ in the subphase are important variables which must also be optimized to achieve high quality LB films. Their influence on the homogeneity of either the monolayer or the films after transfer has been investigated separately.

Many weakly soluble ionic compounds have solubilities which depend on the pH of the solution. A direct example is hydroxides since the $OH^-$ ion is directly involved in the equilibrium constant. Other cases of pH dependence may not be quite so simple. To decide the pH range for each cations, it is necessary to consider solubility equilibrium;

$$Ca(OH)_2 \leftrightarrow Ca_{aq}^{2+} + 2OH_{aq}^{-}$$

$$Zn(OH)_2 \leftrightarrow Zn_{aq}^{2+} + 2OH_{aq}^{-}$$

Solubility products ($K_{sp}$) of slightly soluble ionic compounds in the subphase at $20^oC$ are given as $5.5\times10^{-6}$ for $Ca(OH)_2$ and $2\times10^{-17}$ for $Zn(OH)_2$ (Braun 1982).

According to this table, if any $M(OH)_x$ precipitate, there would be no $M^{+x}$ ion in aqueous solution. In general, many metal ions precipitate as $M(OH)_x$ at pH higher than a certain pH. In that sense, it is similar to metal stearate that has less solubility than metal hydroxide.

For $Ca(OH)_2$,

$$K_{sp} = \left[Ca^{2+}\right]\left[OH^-\right]$$

$$5.5\times10^{-6} = \left[Ca^{2+}\right]\times\left[2\times10^{-5}\right]^2 \text{ for pH = 9}$$

$$13750M = \left[Ca^{2+}\right]$$

$$5.5\times10^{-6} = \left[Ca^{2+}\right]\times\left[2\times10^{-4}\right]^2 \text{ for pH =10}$$

$$137.5M = \left[Ca^{2+}\right]$$

and for $Zn(OH)_2$,

$$K_{sp} = \left[Zn^{2+}\right]\left[OH^{-}\right]$$

$$2\times10^{-17} = \left[Zn^{2+}\right]\times\left[2\times10^{-9}\right]^2 \text{ for pH = 5}$$

$$5M = \left[Zn^{2+}\right]$$

$$2\times10^{-17} = \left[Zn^{2+}\right]\times\left[2\times10^{-7}\right]^2 \text{ for pH = 7}$$

$$5\times10^{-4}M = \left[Zn^{2+}\right]$$

$Ca(OH)_2$ does not precipitate between pH 9 and 10 because studied concentrations are much lower than the concentration causes precipitation. Above pH 13, it only precipitates. For $Zn(OH)_2$, pH 8.5 is the equilibrium pH resulting from dissolving the zinc hydroxide in pure water. By changing the pH, the equilibrium will shift to reduce the stress; above pH 8.5, solubility decreases and below pH 8.5 it increases. $Zn(OH)_2$ does not precipitate between pH 5 and 7 because studied concentrations are again lower than the concentration which causes precipitation. Besides, precipitation is also related to the concentration of metal ions in the solution. If the concentration is lower, pH at which metal hydroxide start to precipitate becomes higher.